NUREG/CR-5136
MEA-2289

Fatigue Strength of Smooth and Notched Specimens of ASME SA 106-B Steel in PWR Environments

Prepared by J.B. Terrell

Materials Engineering Associates, Inc.

Prepared for
U.S. Nuclear Regulatory
Commission

NUREG/CR-5136
MEA-2289
RF, R5

Fatigue Strength of Smooth and Notched Specimens of ASME SA 106-B Steel in PWR Environments

Manuscript Completed: August 1988
Date Published: September 1988

Prepared by
J.B. Terrell

Materials Engineering Associates, Inc.
9700-B Martin Luther King, Jr. Highway
Lanham, MD 20706-1837

Prepared for
Division of Engineering
Office of Nuclear Regulatory Research
U.S. Nuclear Regulatory Commission
Washington, DC 20555
NRC FIN B8900

ABSTRACT

Fatigue strain-life tests were conducted on ASME SA 106-B piping steel base metal and weld metal specimens in 288°C (550°F) pressurized water reactor (PWR) environments as a function of strain amplitude, strain ratio, notch acuity, and cyclic frequency. Notched base metal specimens tested at 0.017 Hz in 1.0 part per billion (ppb) dissolved oxygen environments nearly completely used up the margins of safety of 2 on stress and 20 on cycles incorporated into the ASME Section III design curve for carbon steels, whereas smooth specimen tests from base and weld metal under similar conditions showed considerably less degradation. Tests conducted with specimens having theoretical notch concentration (K_t) values ranging from 2 to 6 showed virtually no effect of notch acuity on fatigue life. Tests conducted with smooth base and weld metal specimens at 1.0 Hz showed virtually no degradation in cycles to failure when compared to 288°C air test results. In all cases, however, the effect of temperature alone reduces the margin of safety offered by the design curve in the low cycle regime for the test specimens. Comparison between the fatigue life results of smooth and notched specimens suggests that fatigue crack initiation is not significantly affected by 1.0 ppb dissolved oxygen, and that most of the observed degradation may be attributed to crack growth acceleration. These results suggest that the ASME Section III methodology should be revised to account for PWR environment variables which degrade fatigue life of pressure-retaining components.

CONTENTS

LIST OF FIGURES

LIST OF FIGURES

LIST OF TABLES

FOREWORD

The work reported here was performed at Materials Engineering Associates (MEA) under the program Structural Integrity of Water Reactor Pressure Boundary Components, F. J. Loss, Program Manager. The program is sponsored by the Office of Nuclear Regulatory Research of the U. S. Nuclear Regulatory Commission (NRC). The technical monitor for the NRC is Alfred Taboada.

Prior reports under the current contract are listed below:

1. J. R. Hawthorne, "Significance of Nickel and Copper to Radiation Sensitivity and Postirradiation Heat Treatment Recovery of Reactor Vessel Steels," USNRC Report NUREG/CR-2948, Nov. 1982.

2. "Structural Integrity of Water Reactor Pressure Boundary Components, Annual Report for 1982," F. J. Loss, Ed., USNRC Report NUREG/CR-3228, Vol. 1, Apr. 1983.

3. J. R. Hawthorne, "Exploratory Assessment of Postirradiation Heat Treatment Variables in Notch Ductility Recovery of A 533-B Steel," USNRC Report NUREG/CR-3229, Apr. 1983.

4. W. H. Cullen, K. Torronen, and M. Kemppainen, "Effects of Temperature on Fatigue Crack Growth of A 508-2 Steel in LWR Environment," USNRC Report NUREG/CR-3230, Apr. 1983.

5. "Proceedings of the International Atomic Energy Agency Specialists' Meeting on Subcritical Crack Growth," Vols. 1 and 2, W. H. Cullen, Ed., USNRC Conference Proceeding NUREG/CP-0044, May 1983.

6. W. H. Cullen, "Fatigue Crack Growth Rates of A 508-2 Steel in Pressurized, High-Temperature Water," USNRC Report NUREG/CR-3294, June 1983.

7. J. R. Hawthorne, B. H. Menke, and A. L. Hiser, "Notch Ductility and Fracture Toughness Degradation of A 302-B and A 533-B Reference Plates from PSF Simulated Surveillance and Through-Wall Irradiation Capsules," USNRC Report NUREG/CR-3295, Vol. 1, Apr. 1984.

8. J. R. Hawthorne and B. H. Menke, "Postirradiation Notch Ductility and Tensile Strength Determinations for PSF Simulated Surveillance and Through-Wall Specimen Capsules," USNRC Report NUREG/CR-3295, Vol. 2, Apr. 1984.

9. A. L. Hiser and F. J. Loss, "Alternative Procedures for J-R Curve Determination," USNRC Report NUREG/CR-3402, July 1983.

10. A. L. Hiser, F. J. Loss, and B. H. Menke, "J-R Curve Characterization of Irradiated Low Upper Shelf Welds," USNRC Report NUREG/CR-3506, Apr. 1984.

11. W. H. Cullen, R. E. Taylor, K. Torronen, and M. Kemppainen, "The Temperature Dependence of Fatigue Crack Growth Rates of A 351 CF8A Cast Stainless Steel in LWR Environment," USNRC Report NUREG/CR-3546, Apr. 1984.

12. "Structural Integrity of Light Water Reactor Pressure Boundary Components -- Four-Year Plan 1984-1988," F. J. Loss, Ed., USNRC Report NUREG/CR-3788, Sep. 1984.

13. W. H. Cullen and A. L. Hiser, "Behavior of Subcritical and Slow-Stable Crack Growth Following a Postirradiation Thermal Anneal Cycle," USNRC Report NUREG/CR-3833, Aug. 1984.

14. "Structural Integrity of Water Reactor Pressure Boundary Components: Annual Report for 1983," F. J. Loss, Ed., USNRC Report NUREC/CR-3228, Vol. 2, Sept. 1984.

15. W. H. Cullen, "Fatigue Crack Growth Rates of Low-Carbon and Stainless Piping Steels in PWR Environment," USNRC Report NUREG/CR-3945, Feb. 1985.

16. W. H. Cullen, M. Kemppainen, H. Hanninen, and K. Torronen, "The Effects of Sulfur Chemistry and Flow Rate on Fatigue Crack Growth Rates in LWR Environments," USNRC Report NUREG/CR-4121, Feb. 1985.

17. "Structural Integrity of Water Reactor Pressure Boundary Components: Annual Report for 1984," F. J. Loss, Ed., USNRC Report NUREG/CR-3228, Vol. 3, June 1985.

18. A. L. Hiser, "Correlation of C_v and K_{Ic}/K_{Jc} Transition Temperature Increases Due to Irradiation," USNRC Report NUREG/CR-4395, Nov. 1985.

19. W. H. Cullen, G. Gabetta, and H. Hanninen, "A Review of the Models and Mechanisms For Environmentally-Assisted Crack Growth of Pressure Vessel and Piping Steels in PWR Environments," USNRC Report NUREG/CR-4422, Dec. 1985.

20. "Proceedings of the Second International Atomic Energy Agency Specialists' Meeting on Subcritical Crack Growth," W. H. Cullen, Ed., USNRC Conference Proceeding NUREG/CP-0067, Vols. 1 and 2, Apr. 1986.

21. J. R. Hawthorne, "Exploratory Studies of Element Interactions and Composition Dependencies in Radiation Sensitivity Development," USNRC Report NUREG/CR-4437, Nov. 1985.

22. R. B. Stonesifer and E. F. Rybicki, "Development of Models for Warm Prestressing," USNRC Report NUREG/CR-4491, Jan. 1987.

23. E. F. Rybicki and R. B. Stonesifer, "Computational Model for Residual Stresses in a Clad Plate and Clad Fracture Specimens," USNRC Report NUREG/CR-4635, Oct. 1986.

24. D. E. McCabe, "Plan for Experimental Characterization of Vessel Steel After Irradiation," USNRC Report NUREG/CR-4636, Oct. 1986.

25. E. F. Rybicki, J. R. Shadley, and A. S. Sandhu, "Experimental Evaluation of Residual Stresses in a Weld Clad Plate and Clad Test Specimens," USNRC Report NUREG/CR-4646, Oct. 1986.

26. "Structural Integrity of Water Reactor Pressure Boundary Components: Annual Report for 1985," F. J. Loss, Ed., USNRC Report NUREG/CR-3228, Vol. 4, June 1986.

27. G. Gabetta and W. H. Cullen, "Application of a Two-Mechanism Model for Environmentally-Assisted Crack Growth," USNRC Report NUREG/CR-4723, Oct. 1986.

28. W. H. Cullen, "Fatigue Crack Growth Rates in Pressure Vessel and Piping Steels in LWR Environments," USNRC Report NUREG/CR-4724, Mar. 1987.

29. W. H. Cullen and M. R. Jolles, "Fatigue Crack Growth of Part-Through Cracks in Pressure Vessel and Piping Steels: Air Environment Results, USNRC Report NUREG/CR-4828.

30. D. E. McCabe, "Evaluation of Surface Cracks Embedded in Reactor Vessel Cladding Unirradiated Bend Specimens," USNRC Report NUREG/CR-4841, May 1987.

31. H. Hanninen, M. Vulli, and W. H. Cullen, "Surface Spectroscopy of Pressure Vessel Steel Fatigue Fracture Surface Films Formed in PWR Environments," USNRC Report NUREG/CR-4863, July 1987.

32. A. L. Hiser and G. M. Callahan, "A User's Guide to the NRC's Piping Fracture Mechanics Data Base (PIFRAC)," USNRC Report NUREG/CR-4894, May 1987.

33. "Proceedings of the Second CSNI Workshop on Ductile Fracture Test Methods (Paris, France, April 17-19, 1985)," F. J. Loss, Ed., USNRC Conference Proceeding NUREG/CP-0064, (in publication).

34. W. H. Cullen and D. Broek, "The Effects of Variable Amplitude Loading on A 533-B Steel in High-Temperature Air and Reactor Water Environments," USNRC Report NUREG/CR-4929 (in publication).

35. "Structural Integrity of Water Reactor Pressure Boundary Components: Annual Report for 1986," F. J. Loss, Ed., USNRC Report NUREG/CR-3228, Vol. 5, July 1987.

36. F. Ebrahimi et al., "Development of a Mechanistic Understanding of Radiation Embrittlement in Reactor Pressure Vessel Steels: Final Report," USNRC Report NUREG/CR-5063, Jan. 1988.

37. J. B. Terrell, "Fatigue Life Characterization of Smooth and Notched Piping Steel Specimens in 288°C Air Environments," USNRC Report NUREG/CR-5013, May 1988.

ACKNOWLEDGMENTS

The author wishes to express his appreciation to the following people who helped make this work possible: Greg Baker for his experience in test systems and for conducting the tests, Bob Taylor for his useful suggestions, Gray Carlson and Leah Gelzer-Cargill for their efforts in assembling the manuscript, the students who assisted in conducting the tests, and Dr. William H. Cullen and Dr. Frank J. Loss for their support and direction of this effort.

Sincere thanks are also extended to Milt Vagins and Al Taboada of the Nuclear Regulatory Commission for their support and direction of this effort.

1. INTRODUCTION

The likelihood of fatigue failure of primary cooling water loop reactor piping components is minimized by conservative component design. The designer of pressure-retaining components must meet the requirements of Section III of the ASME Boiler and Pressure Vessel Code (Ref. 1), insuring that the cumulative fatigue usage does not exceed unity over the projected design life of the component. Using the Code, designers construct components such that the operating stresses do not exceed the design life; i.e., the region above the design curve for the particular class of materials.

Section III includes a set of design rules which require a rigorous analysis and classification of all the major stresses and loading conditions which may take place in the component. This has been called a "design by analysis" approach, and categorizes the stresses into primary, secondary, and peak stresses (Ref. 2). A "hopper" diagram (Fig. 1) groups the stress categories for the purpose of applying limits to the stress intensities (Ref. 1). The end result of stress intensity determination is a calculation of a value for the alternating stress intensity (S_{alt}), which is the maximum difference between the principle stresses acting on the component. If the component is subject to constant amplitude loading, the design life is determined by entering the value of S_{alt} into the applicable fatigue curve given in Section III. If the component is subject to variable amplitude loading, the Palmgren-Miner linear cumulative damage rule is employed. This rule assumes that, for example, if N_1 cycles would produce failure at a stress level $S_{alt(1)}$, then n_1 cycles at the same stress level would use up the fraction n_1/N_1 of the total life. The design life, as specified for each stress level by the design curve, is used up when the cumulative usage factor (the sum of n_i/N_i fractions) is equal to 1.0.

Efforts toward construction of the design curves were put forth some twenty-five years ago by Coffin (Ref. 3), Langer (Refs. 4 and 5), and other researchers. The data for these design curves were originally acquired for carbon, low alloy, and stainless steels through the testing of small, polished, stress-life (S-N) specimens utilizing completely-reversed bending rotating fatigue tests in the presence of air environments. These tests were performed in strain control, because fatigue damage in the plastic region was known to be a function of plastic strain, and because the material found at structural discontinuities is strain cycled as a result of constraint from the adjacent material. Most of these tests, particularly those for carbon steels, were performed at room temperature. Fictitious stress (or pseudostress) quantities were incorporated into the ordinate axes of the design curves instead of more conventional stress or strain quantities (pseudostress is the product of total strain and elastic modulus), because the Section III design philosphy was based on the assumption that all calculations should be made assuming cyclic strain hardening and subsequent shake down to elastic action for most constructional metals.

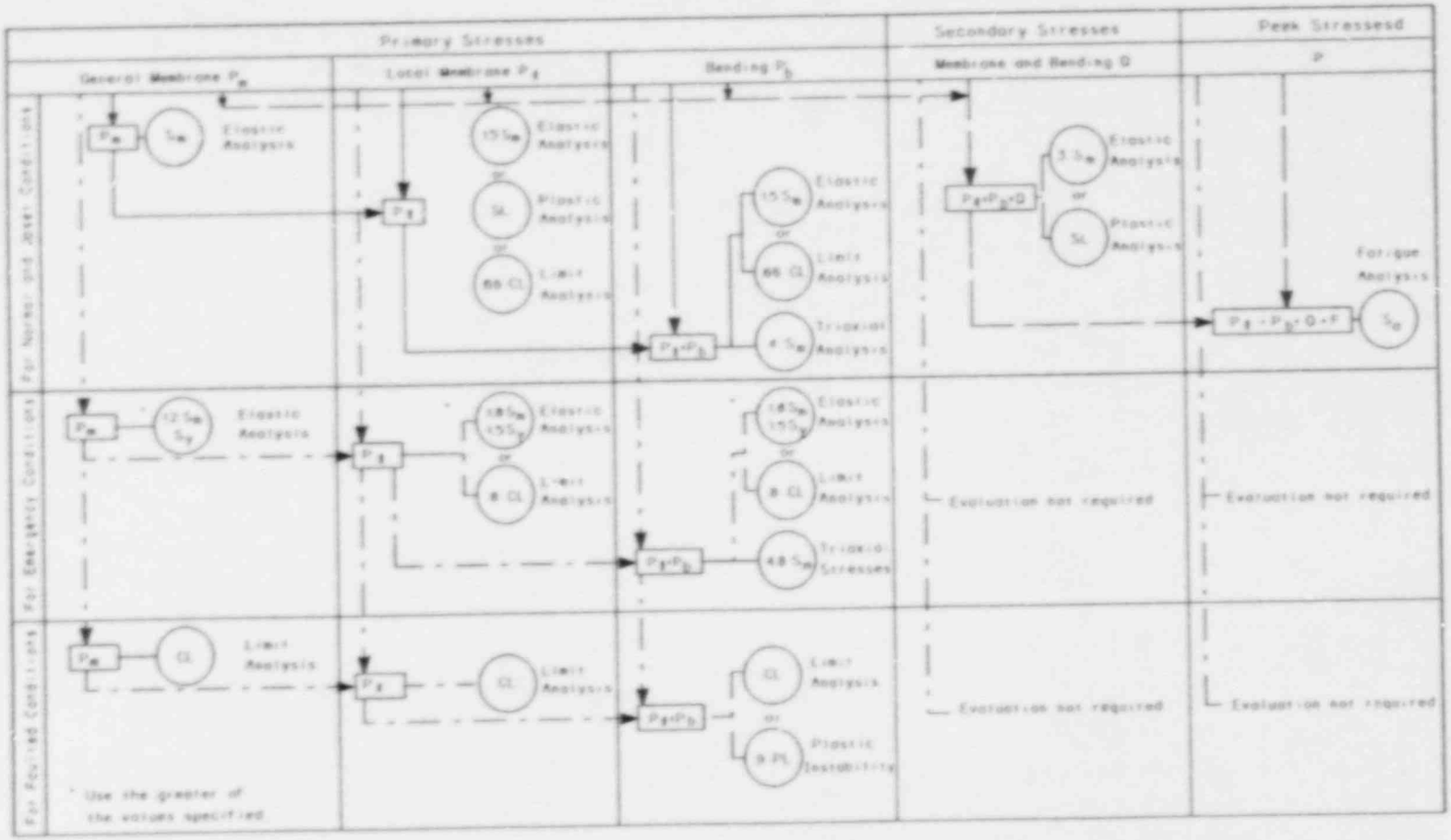

Fig. 1 "Hopper" diagram used for applying limits to the stress intensities in ASME Section (Ref. 1).

The validity of the design curves, when subjected to LWR environmental conditions, has become an important concern to both the public and the power generation industry in recent years, especially since some nuclear plants are nearing the ends of their 40 year design lives. The prohibitively high costs of building new plants has also spurred the willingness to extend the lives of existing plants, provided that public safety is not compromised. When the design curves were put into service, they were constructed by imposing margins of 2 on stress or 20 on life, whichever was greater, to the mean data curves. These margins were not "safety factors," but were margins which were intended to cover unknowns which may result in the fatigue life of pressure vessels in actual service to be shorter than the fatigue life of smooth specimens tested in laboratory air. These unknowns may include environment, size effects, residual stresses, and data scatter. Even though verification tests were performed on full-scale pressure-containing structures, none of these tests were performed in the presence of light water reactor (LWR) environments (Refs. 6 and 7). Clearly, there was a need to establish a data base for nuclear materials subjected to LWR environments.

The first LWR environment tests were performed by General Electric, and were sponsored by the Electric Power Research Institute (EPRI) (Ref. 8). These tests were performed using compact tension (C(T)) and pipe specimens in boiling water reactor (BWR) environments. The oxygen levels in the test environments varied between 0.2 and 8.0 parts per million (ppm) dissolved oxygen, and the simulated BWR environment test temperature was 288°C (550°F). The results showed that the environment and possibly other variables imposed a dramatic detrimental effect on the life of the specimens (Fig. 2). Many of the data points fell well below the design curve, which suggests that the ASME Section III design curves for carbon steels failed to account for unknown variables which degrade the fatigue life of piping steel when subjected to BWR envoronments. These results have shown that significant reductions in the fatigue strength of notched specimens correlate with both an increase in dissolved oxygen content and temperature or decreases in cyclic frequency.

The fatigue life response of carbon piping steels in pressurized water reactor (PWR) environments has been an unknown quantity even though many PWR plants have been in service throughout the world for a number of years. The effect of the PWR environment, loading sequence, cyclic frequency, material variability, and even temperature on the cyclic response of piping steels is little understood and has not been addressed until very recently (Ref. 9). The PWR environment, which typically contains 1.0 ppb (parts per billion) dissolved oxygen, is generally thought to not pose an immediate threat to the structural integrity of PWR piping systems. To date, there have apparently been no fatigue failures, nor any discovered cracks, in coolant piping as a result of a corrosive PWR environment (Ref. 10). This does not suggest that such problems will not surface in the future, because the effects of long-term exposure to reactor water are not fully understood and may possibly be detrimental to fatigue life. However, the issue of plant life extension has required that the structural integrity of PWR components be more quantitatively addressed.

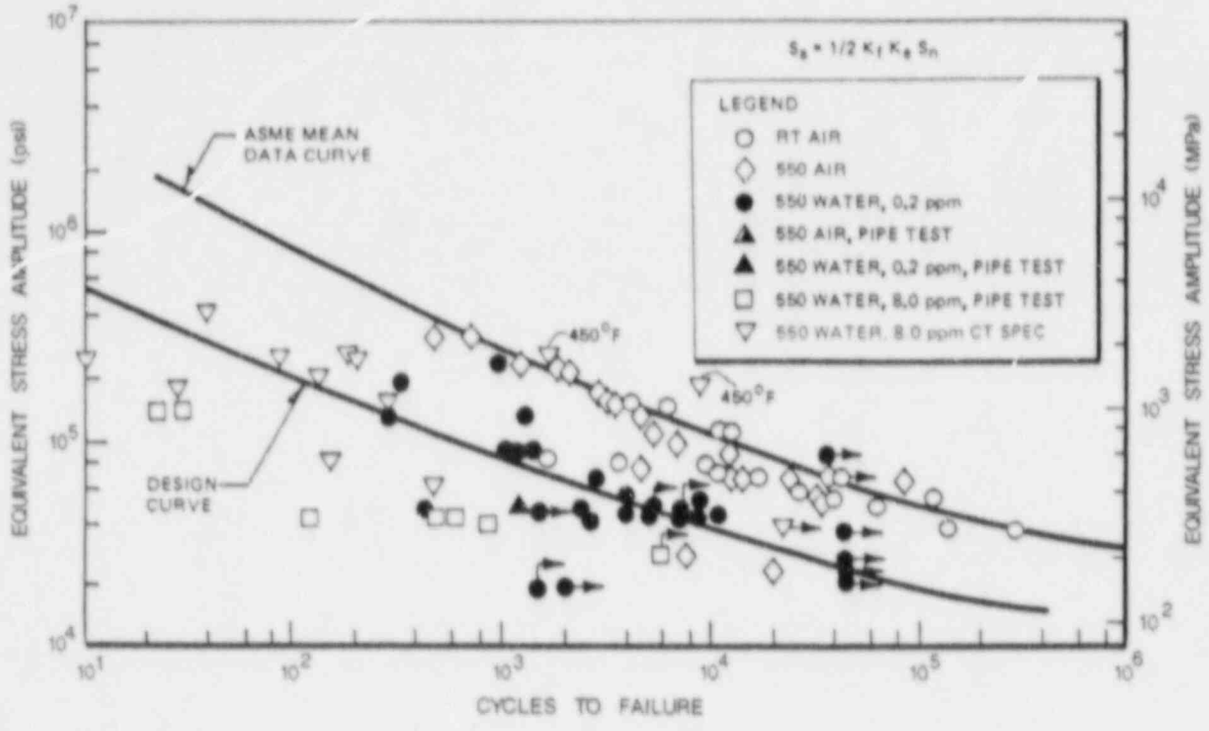

Fig. 2 Pseudostress-life plot of nuclear steel specimens tested in BWR environments. The data, generated by General Electric, shows the detrimental effect of 0.2 and 8.0 ppm dissolved oxygen on the fatigue life of nuclear steels (Ref. 8).

The primary purpose of this investigation is to characterize the strain-life behavior of ASME SA 106-B piping steel using small specimens (a) in air at both room and PWR environment temperatures so that the effect of temperature can be quantified, and (b) in simulated PWR environments so that any detrimental effects of the environment will be revealed. The results of fatigue life tests conducted in air environments have been reported in Ref. 9. A number of variables, such as cyclic frequency, strain ratio, stress level, and notch acuity, were investigated. The results constitute the first known data base which quantifies the cyclic response of carbon piping steels in simulated PWR environments. These results also constitute the basis for possible revisions to the ASME Section III design curve for carbon steels.

2. BACKGROUND

Since the inception of the current program, additional studies involving BWR environments (Refs. 11, 12, and 13) have been completed. These results have shown that significant reductions in fatigue strength of notched specimens correlate with both an increase in dissolved oxygen content and temperature or decreases in cyclic frequency. Prater and Coffin (Ref. 11) fatigue cycled notched C(T) specimens of SA 333-6 steel in 288°C, 10.34 MPa (1500 psi), water having dissolved oxygen contents of 0.2 ppm and 8.0 ppm. At cyclic frequencies of 0.00021 Hz, crack initiation life (defined in Ref. 11 as the number of cycles required to initiate and grow a crack of length 7.6×10^{-2} mm (0.003-in.)) was severely degraded. At cyclic frequencies of 0.021 Hz, (1.25 cpm), the number of cycles to initiation approached that of 288°C air tests. Figure 3 compares pseudostress amplitude vs. cycles to initiation with the Section III mean data curve for carbon steels. Clearly, the test results for the 8.0 ppm dissolved oxygen BWR environment tests fall well below both the Section III mean data curve and data points generated from tests in air at the same temperatures. More recently, Prater and Coffin (Ref. 12) have completed additional tests with SA 333-6 steel in BWR environments and showed that degradation of fatigue initiation life was most pronounced at 288°C, 8.0 ppm dissolved oxygen, and at 0.00021 Hz with a notch radius of 0.051 mm (0.002 in.).

In order to account for the effect of the environment, GE investigatiors suggested that the equation for S_{alt} be modified to include an environmental correction factor (K_{en}) (Ref. 8). GE also recommended correction factors to account for local notch yielding and mean stress. However, the data base of tests conducted in BWR environments is not large and comprehensive enough to integrate these correction factors into Section III.

Studies recently carried out by Iida et al. (Ref. 13) in LWR environments has shown that decreases in low cycle fatigue life of smooth specimens of SA 333-6- and SA 508-3-equivalent steels correlate with (a) decreases in strain rate when the dissolved oxygen content is 8 ppm and (b) dissolved oxygen contents higher than 100 ppb. Figure 4 shows the results for the SA 333-6-equivalent steel specimen tests in 8.0 ppm dissolved oxygen water at 250°C (482°F) as compared to the ASME Section III curves. Strain rates less than 0.0001 yielded results which fell below the Section III curve for carbon steels. Figure 5 shows the results for the SA 508-3-equivalent steel specimen tests in both 8.0 and 0.2 ppm water at 288°C. Tests in 0.2 ppm water showed virtually no effect of the environment on fatigue life.

Studies by Shack et al. (Ref. 14) are currently addressing the effect of BWR environments on the fatigue behavior of Type 316 NG stainless steels. Thus far, only baseline room temperature tests have been completed. Their results show agreement with the ASME mean data curve in the low cycle regime, but show a trend for nonconservative cycles to failure in the high cycle regime.

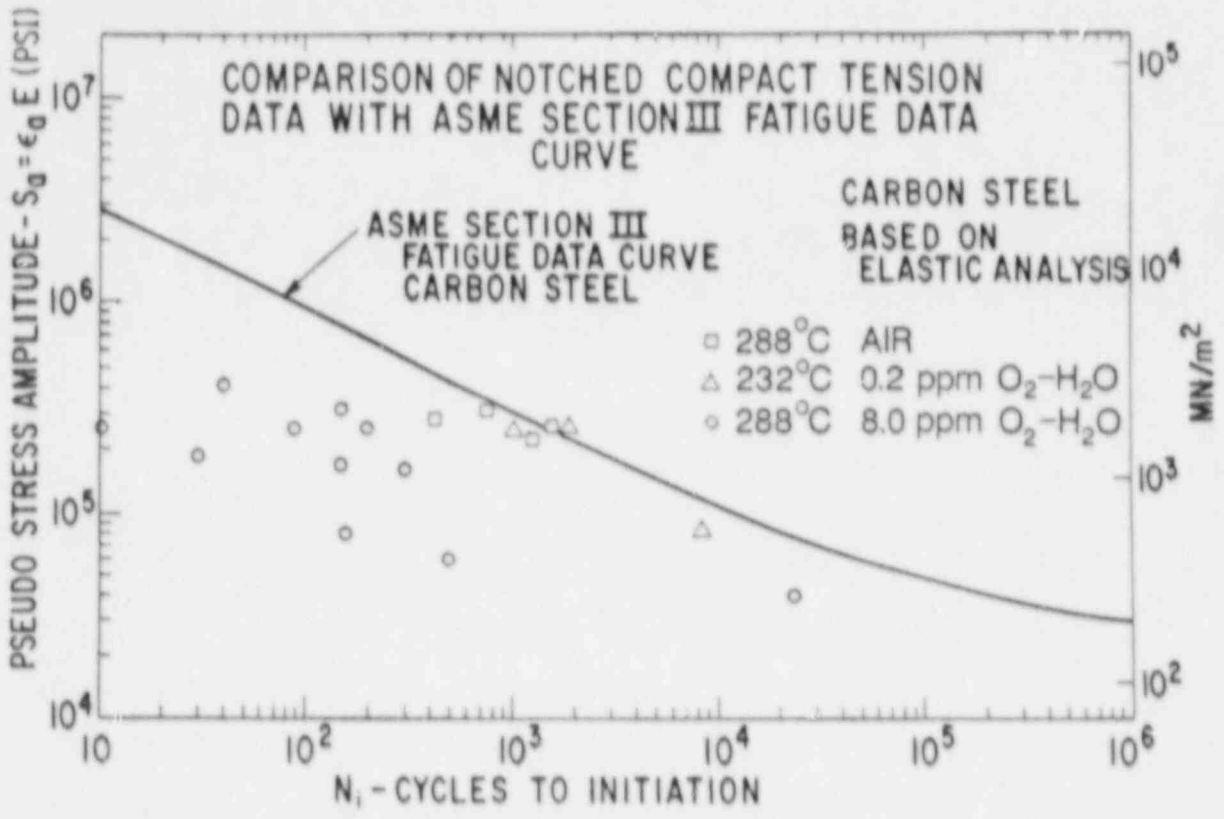

Fig. 3 Comparison of notched C(T) fatigue life data for tests conducted in 8.0 and 0.2 ppm dissolved oxygen BWR environments at 288°C with (a) tests conducted in air and (b) the ASME Section III mean data curve for carbon steels. Pseudostress amplitude was determined by combining Neuber notch analysis, fracture mechanics, and "worst case" notch concepts (Ref. 11).

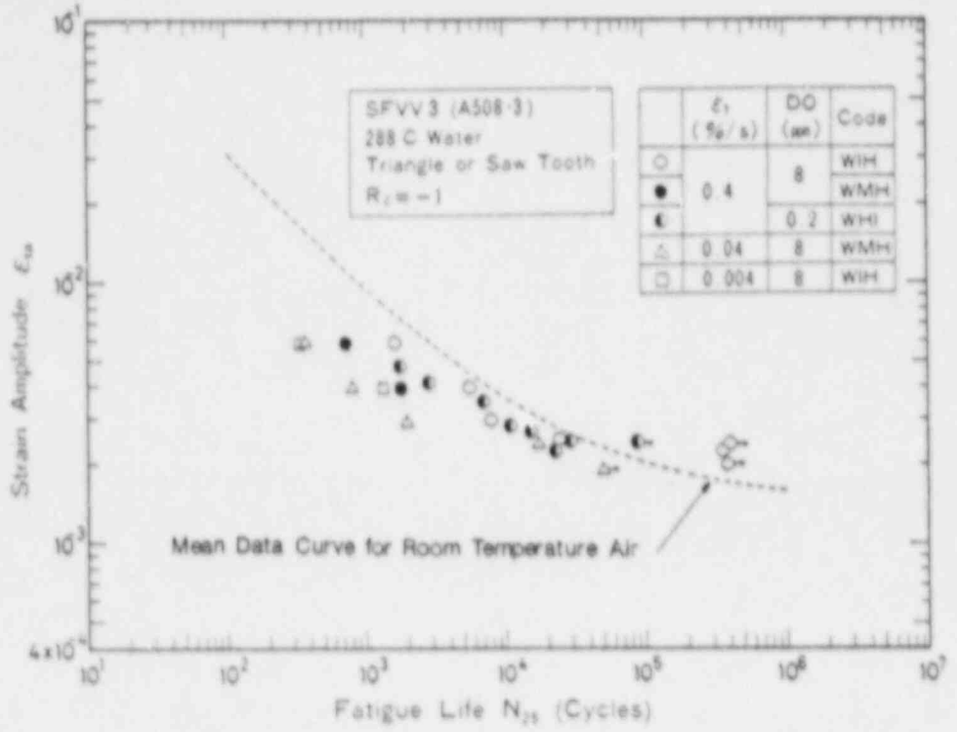

Fig. 4 Strain-life plot of SA 333-6-equivalent steel in 250°C, 8.0 ppm dissolved oxygen water, showing fatigue life degradation due to changes in strain rate (Ref. 13).

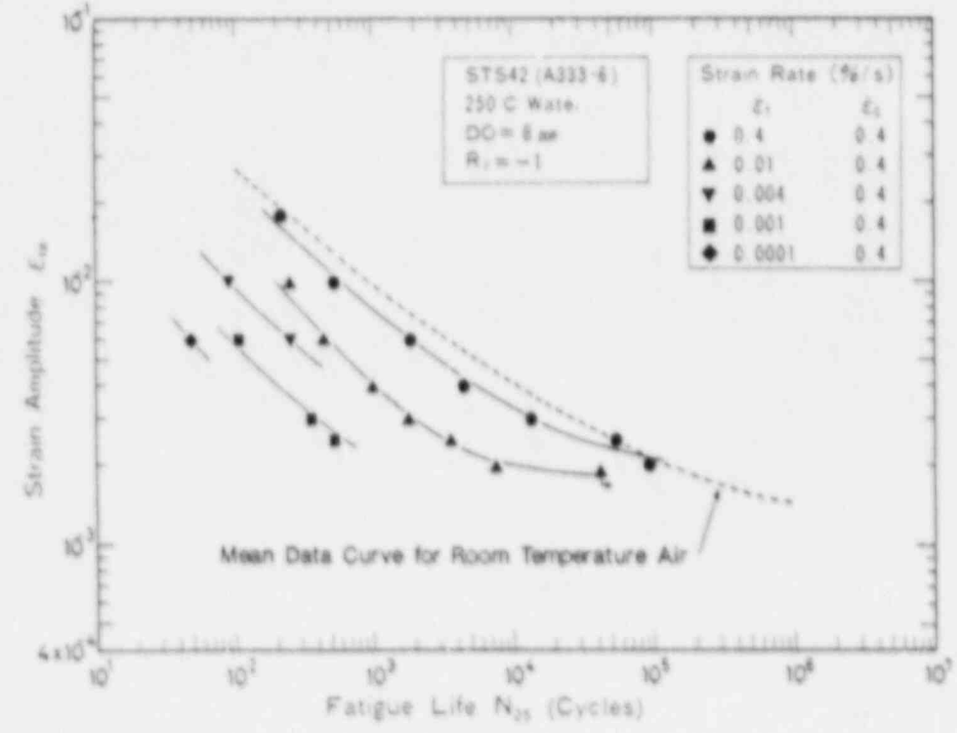

Fig. 5 Strain-life plot of SA 508-3-equivalent steel in 288°C water having a dissolved oxygen content of either 0.2 ppm or 8.0 ppm (Ref. 13).

Since PWR environments typically exhibit dissolved oxygen levels lower than 100 ppb, the results in Ref. 13 for smooth S-N-type specimens suggest a reduced prospect of finding a significant environmental effect on smooth specimens of SA 106-B steel. These findings directed more attention to the fatigue life response of notched specimens in PWR environments. It was concluded that a study to determine the sensitivity of fatigue life to frequency should include notched specimens as well as smooth specimens. The logic supporting this approach is based on the results of extensive studies of fatigue crack initiation of notched components and fatigue crack growth frequency sensitivity of piping and pressure vessel steels. A number of investigators have found, for both inert and corrosive environments, that fatigue crack initiation not only occurs earlier in the life of notched specimens, but is also a function (to a certain extent) of notch root radius (Refs. 11, 12, and 15 - 22). Specimens having sharply-notched cross sections often undergo crack initiation immediately after cycling has begun (Refs. 16, 18, and 21), as shown in Fig. 6. Studies of fatigue crack growth rates in PWR environments have shown that a maximun in crack growth rate occurs near 0.017 Hz for tests conducted with load ratios (R) of 0.2 (Refs. 23 and 24), as shown in Fig. 7. Therefore, it is logical to assume that the environmental effect on notched specimens in PWR water containing less than 100 ppb dissolved oxygen may be more pronounced than for smooth specimens because notched specimens will undergo crack initiation early in their lifetimes. It appears that the low dissolved oxygen of a PWR environment is more detrimental to cracked specimens than to smooth, uncracked specimens. In addition, notched specimens may exhibit the shortest lives when tested at a frequency of 0.017 Hz at low R values simply because these test conditions have been shown to be the most detrimental to specimens which contain cracks.

In this study, a matrix of strain-life tests of both smooth base and weld metal and notched base metal specimens of SA 106-B piping steel were carried out in 24°C and 288°C air environments and in PWR environments at 13.8 MPa (2000 psi) utilizing various strain ratios (R_ε) and notch aquities. Part of the matrix included a cyclic frequency sensitivity study which included the testing of both smooth and sharply-notched specimens in PWR environments. A modified Neuber's rule was used to correlate test results from notched specimens with test results from smooth specimens.

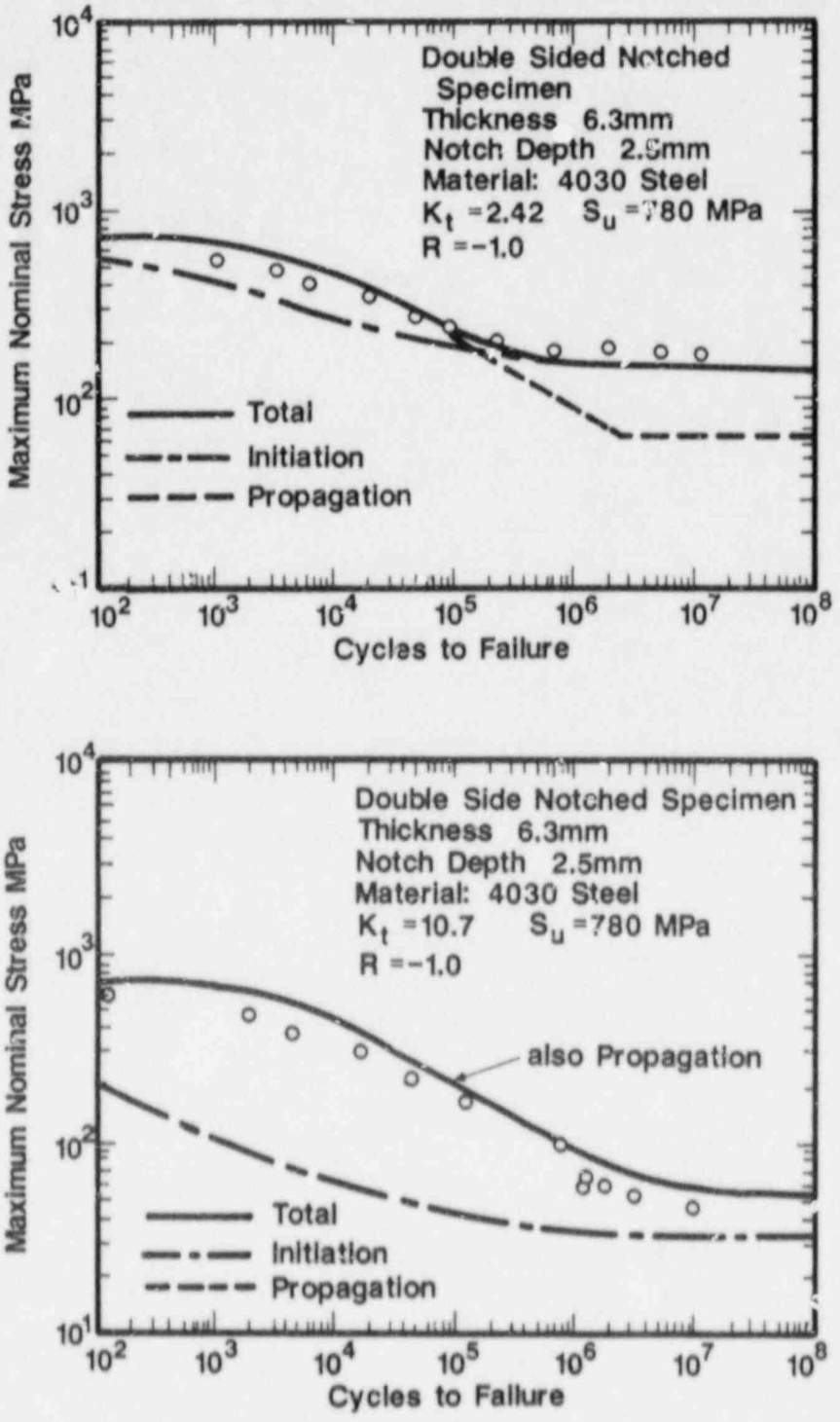

Fig. 6 Fatigue-life estimations, showing crack initiation and propagation lives for alloy steel specimens having either blunt or sharp notches (Ref. 21).

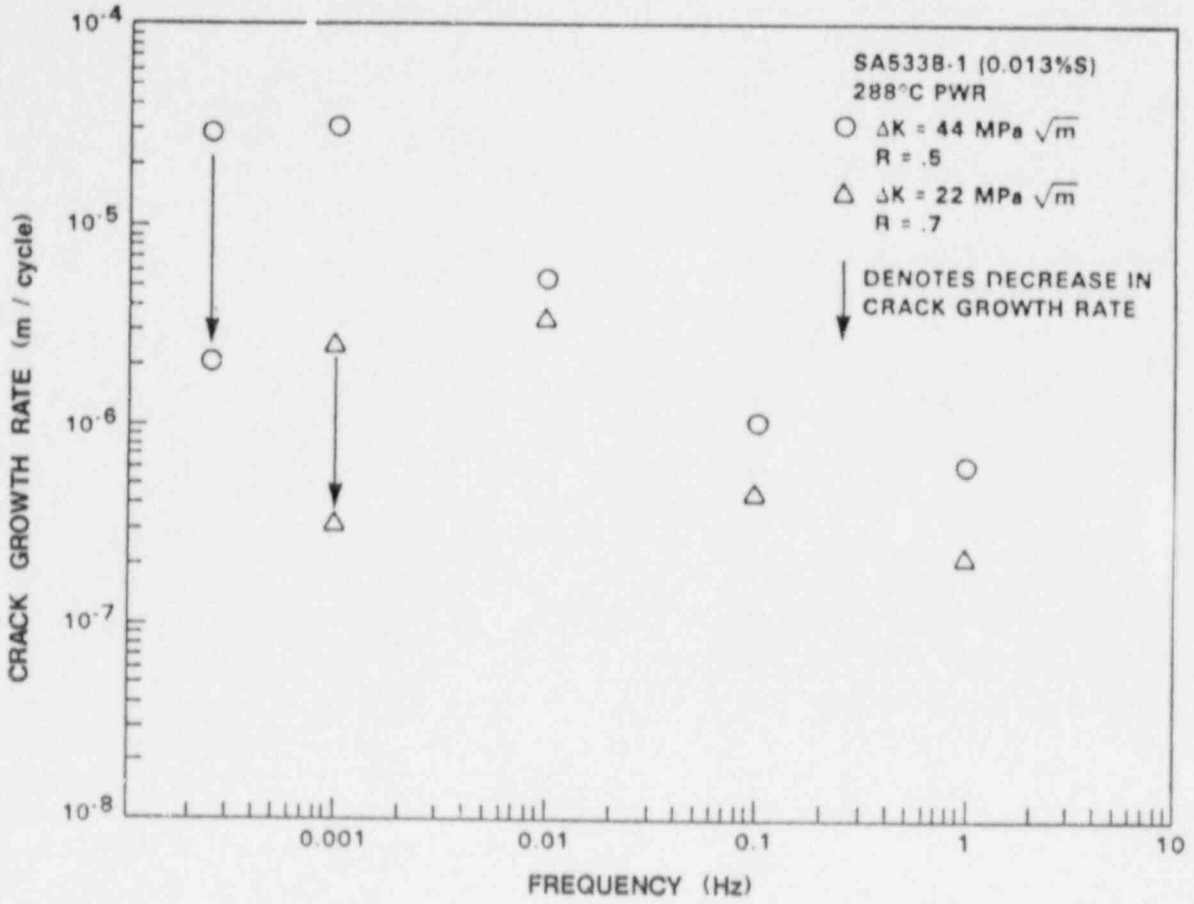

Fig. ' Effect of frequency on cyclic crack growth rate of SA 533 steel in PWR environments (Ref. 24).

3. EXPERIMENTAL PROCEDURE

3.1 Test Materials

3.1.1 Base Metal Specimens

The base metal material used in this investigation is SA 106-B 203-mm (8-in.) Schedule 100 steel pipe having the chemical composition given in Table 1 and the room temperature mechanical properties as given in Table 2. Metallographic studies indicated that the base metal microstructure consisted primarily of elongated grains of free ferrite and grains consisting of finely-spaced lamellar pearlite (Fig. 8). ASTM grain size was from 7 to 8 and the inclusion count was 1.5 for silicates.

Table 1 Chemical Composition (in wt.%) of SA 106-B Steel Used in This Investigation

C	S	Si	Mo	Cr	Ni	Mn	P	N
0.26	0.020	0.28	0.003	0.015	0.002	0.92	0.008	0.0069

Table 2 Average Mechanical Properties of SA 106-B Steel Test Temperature: 24°C (76°F)

Yield Strength (MPa)	Yield Strength (ksi)	Ultimate Strength (MPa)	Ultimate Strength (ksi)	Elongation (%)	Reduction in Area (%)
300	43.5	522.6	75.8	36.6	66.3

Base metal specimen blanks were sawed from the pipe wall as shown in Fig. 9. Smooth specimens were machined in compliance with ASTM E 606-85 (Ref. 25) according to Fig. 10. All of the notched specimens were machined according to Fig. 11. The nominal (net section) diameter (d) for both smooth and all notched specimens was 6.35 mm (0.250 in.). The major (gross) diameter (D) and the notch root radius were specimen dimensions which were modified in order to achieve K_t values of 2, 3, and 6. The notch geometries were obtained from Peterson's handbook of stress concentration factors (Ref. 26) and are also shown in Fig. 11.

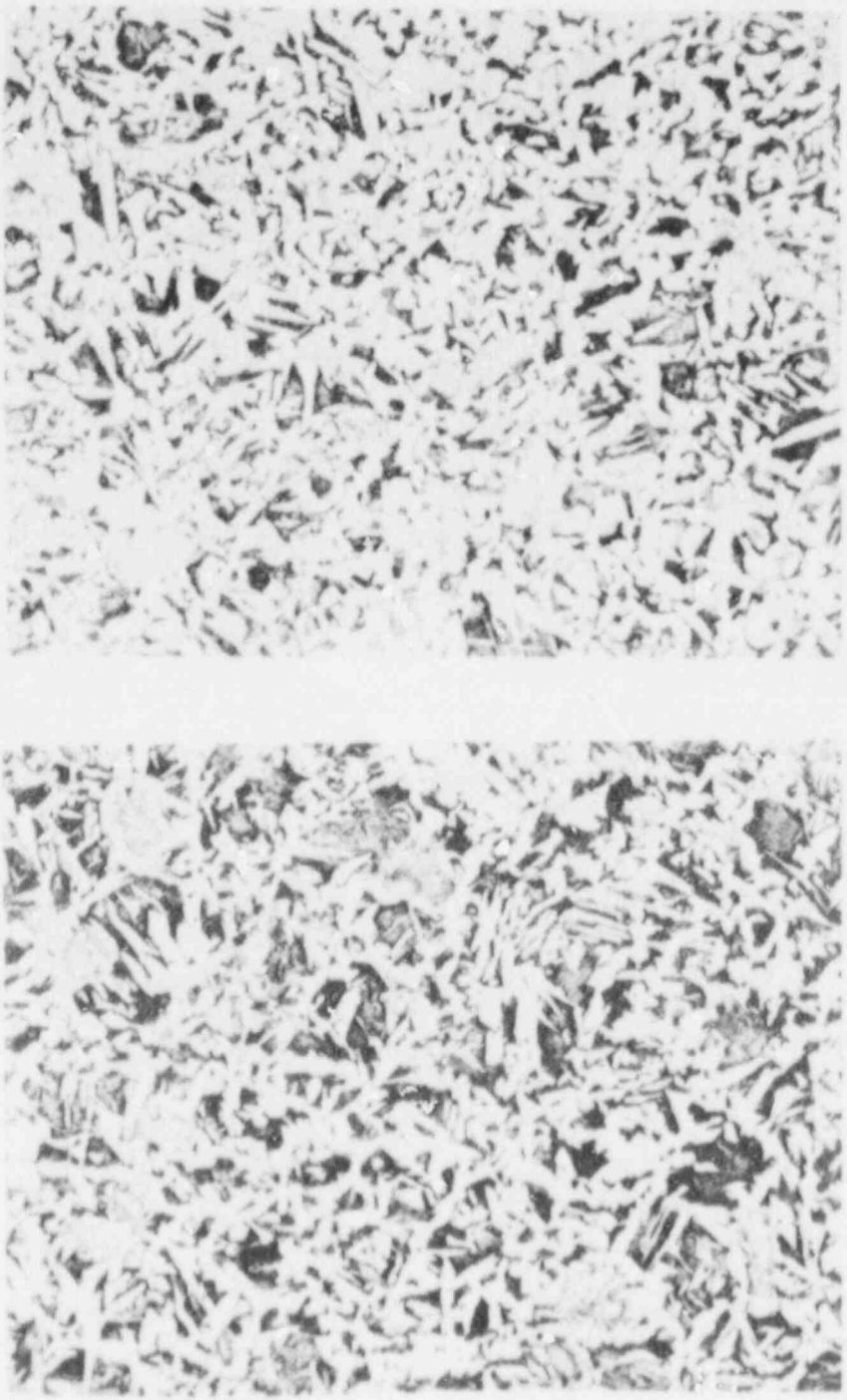

Fig. 8 Typical transverse (upper photo) and longitudinal (lower photo) cross-section microstructures of SA 106-B steel. 85x.

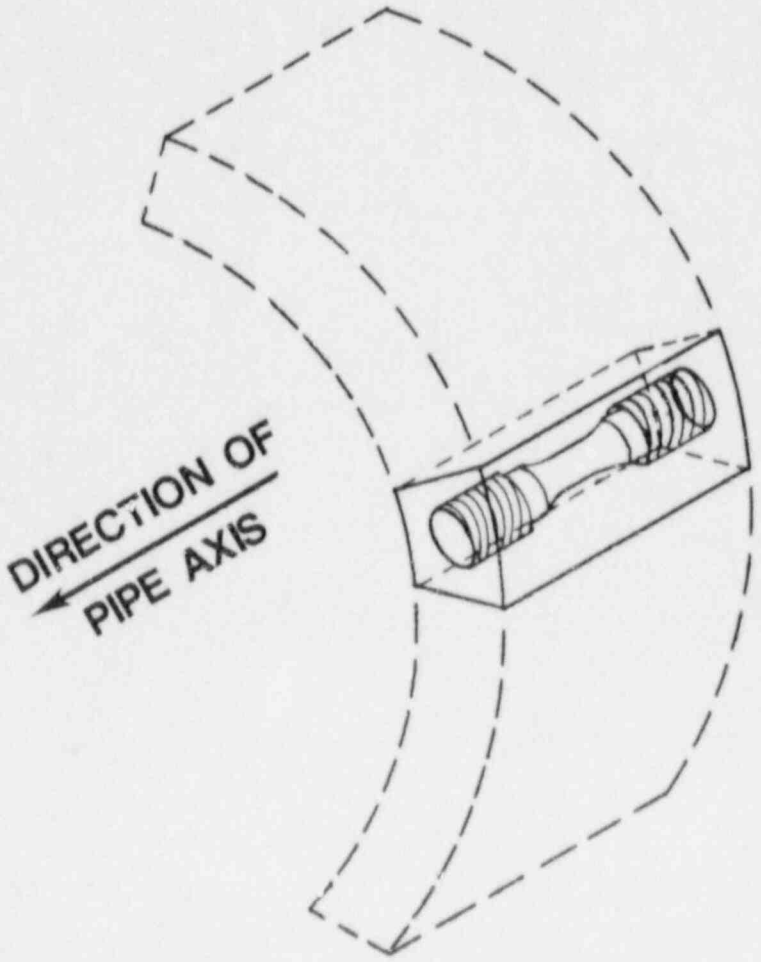

Fig. 9 Orientation of all specimens.

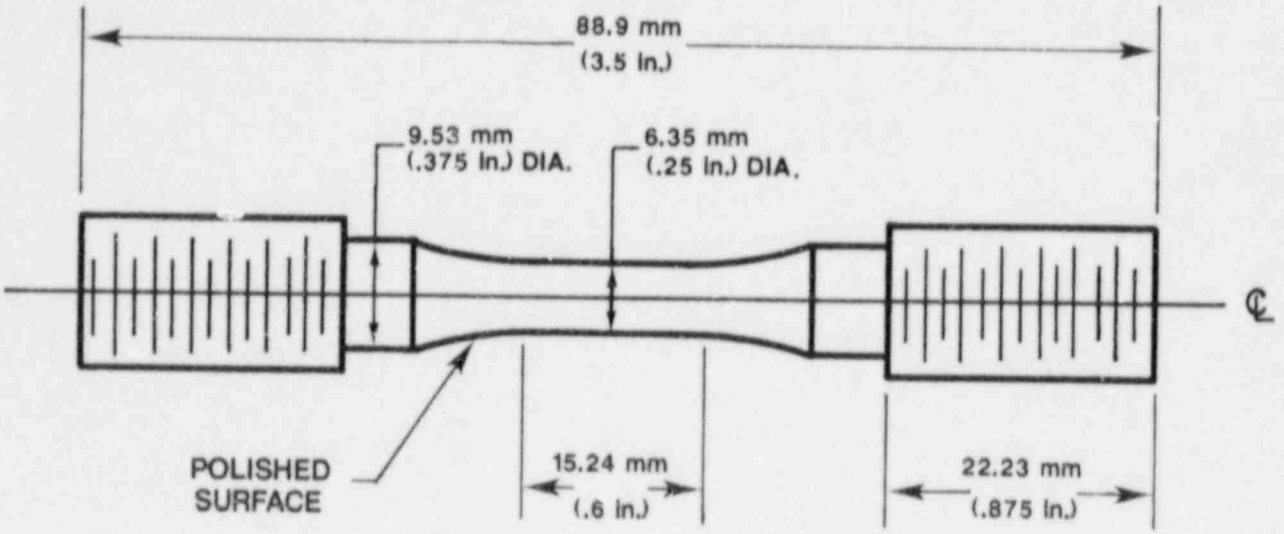

Fig. 10 Smooth specimen geometry.

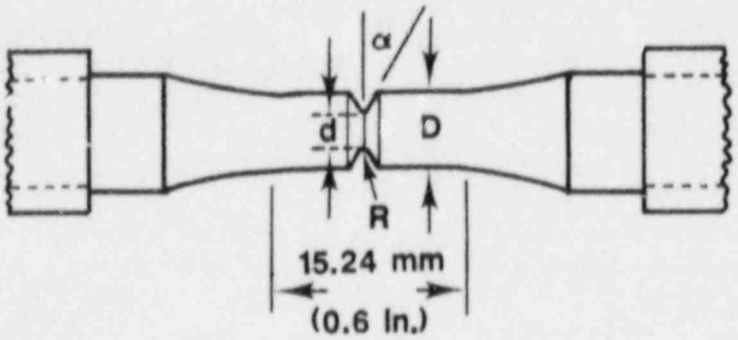

K_t	D	d	R	α (degrees)
2	8.10 mm (0.319 in.)	6.35 mm (0.250 in.)	.876 mm (0.0345 in.)	0
3	7.94 mm (0.3125 in.)	6.35 mm (0.250 in.)	.2845 mm (0.0112 in.)	0
6	9.53 mm (0.375 in.)	6.35 mm (0.250 in.)	.0711 mm (0.0028 in.)	30

Fig. 11 Notched specimen geometries.

3.1.2 Weld Metal Specimens

Weld metal specimens were obtained from girth-butt welded SA 106-B 203-mm (8-in.) diameter Schedule 100 pipe. The welds were prepared according to Section III, Division 1 of the ASME Boiler and Pressure Vessel Code for Class 1 piping (Ref. 1). The geometry of the weld groove consisted of a 75° included angle with a root land thickness of 1.27 mm (0.05 in.), and the pipe was counterbored over a length of 12.7 mm (0.5 in.) as measured from the root face (Fig. 12). The pipe was "fitted-up" with a root gap of 2.38 mm (0.0938 in.) before welding. The root pass was accomplished with the gas tungsten arc (GTA) process using 1.59-mm (0.0625-in.) diameter ER70S-3 filler metal. The subsequent fill passes were accomplished with the shielded metal arc (SMA) process using E7018 filler metal. The average chemical composition of the weld metal after deposition is given in Table 3. Metallographic studies showed that the heat-affected zone (HAZ) consisted of a mixture of fine-grained pearlite having an ASTM grain size of 10 and coarser-grained ferrite with a grain size of 8 (Fig. 13), whereas the center of the weld consisted of free ferrite with isolated patches of fine pearlite with a grain size of 9 (Fig. 14).

Table 3 Average Chemical Composition (in wt. %) of The Weld Metal After Deposition

C	S	Si	Mn	P	Cu
0.084	0.014	0.47	0.81	0.007	0.034

Specimen blanks were cut from the weld metal as shown in Fig. 12. Smooth specimens were machined so that the center of the gage section consisted of filler metal. The specimens were machined according to Fig. 10.

3.2 Test System and Control

The test system consisted of 50 kN (11,150 lb) and 100 kN (22,300 lb) servohydraulic test frames. The 50 kN machine consisted of a four-post design (Fig. 15) with a linear bearing and plate brace system which reinforced loading train components in the lateral direction so as to greatly reduce the incidence of compressive buckling of test specimens when large compressive cyclic loads were applied. The remainder of the loading train components are sufficiently thick so as to contribute negligibly to buckling. The 100 kN machine consisted of a more traditional two-post design and was not equipped with load train-stiffening hardware. Subsequently, tests which subjected the specimen to large compressive loads were restricted to the four-post machine.

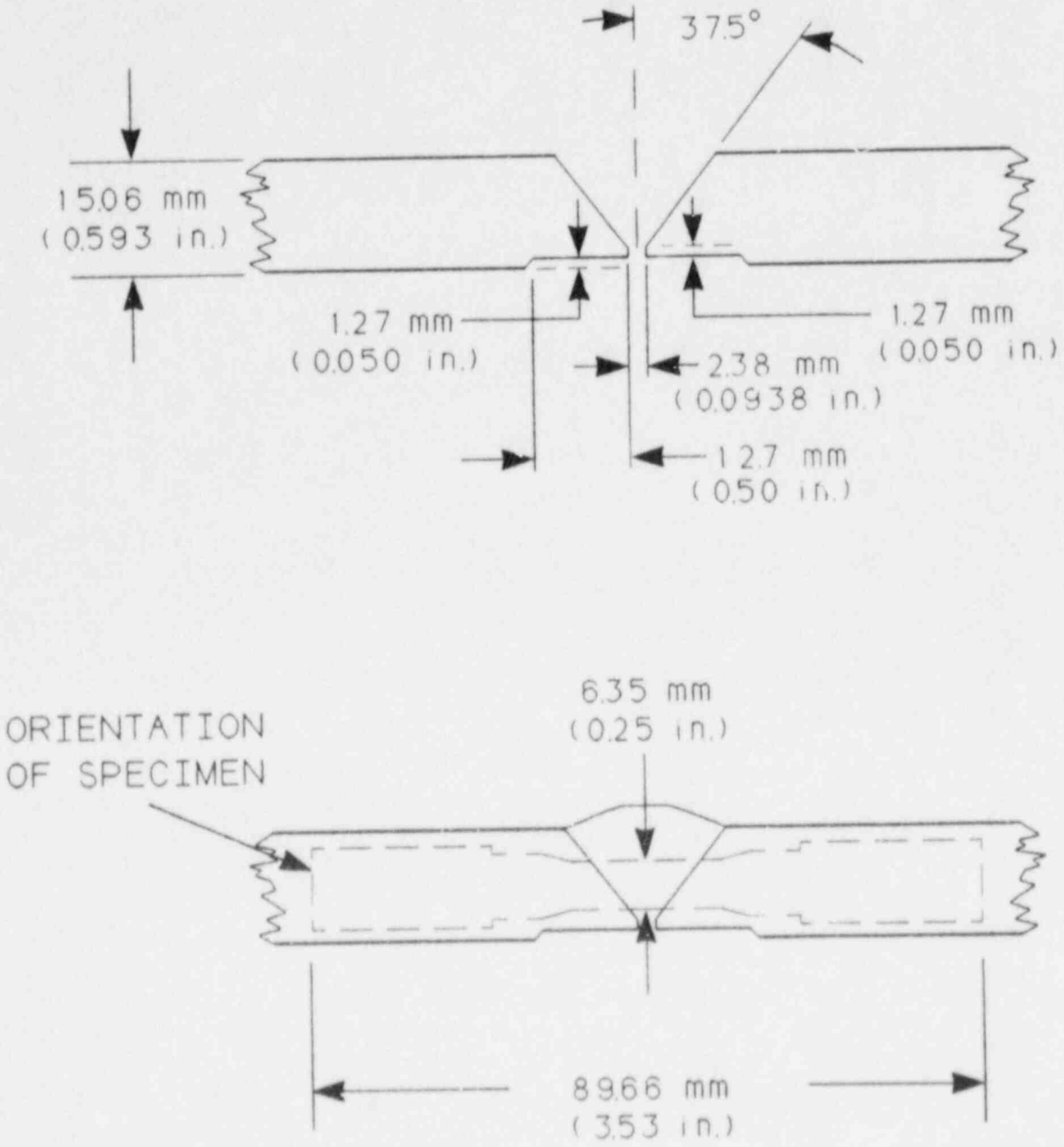

Fig. 12 Geometry of girth-butt welded SA 106-B 203 mm diameter steel pipe. The dotted silhouette shows the orientation of weld metal smooth specimens.

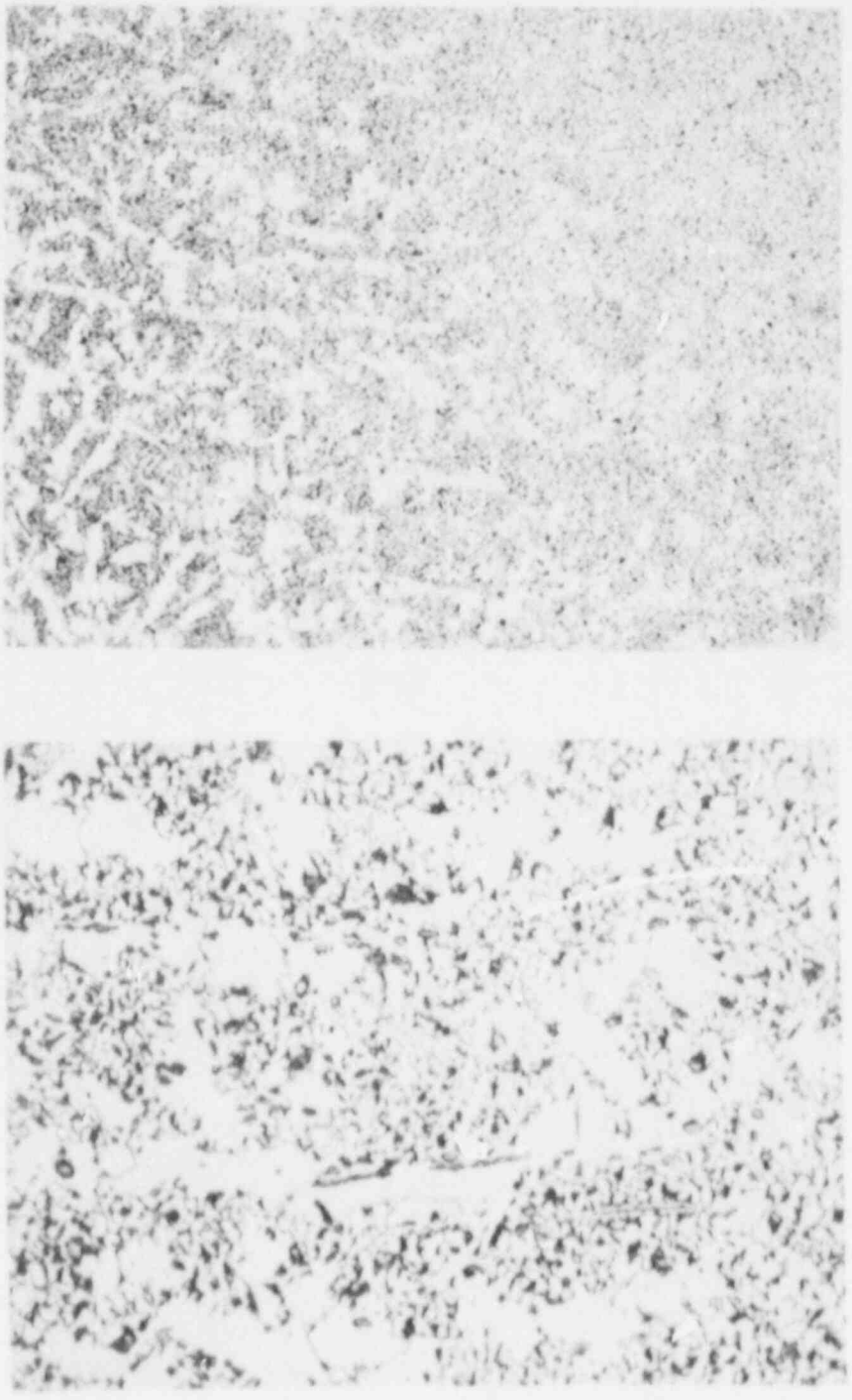

Fig. 13 Microstructure of SA 106-B steel girth-butt weld HAZ. 100x (upper photo) and 425x (lower photo).

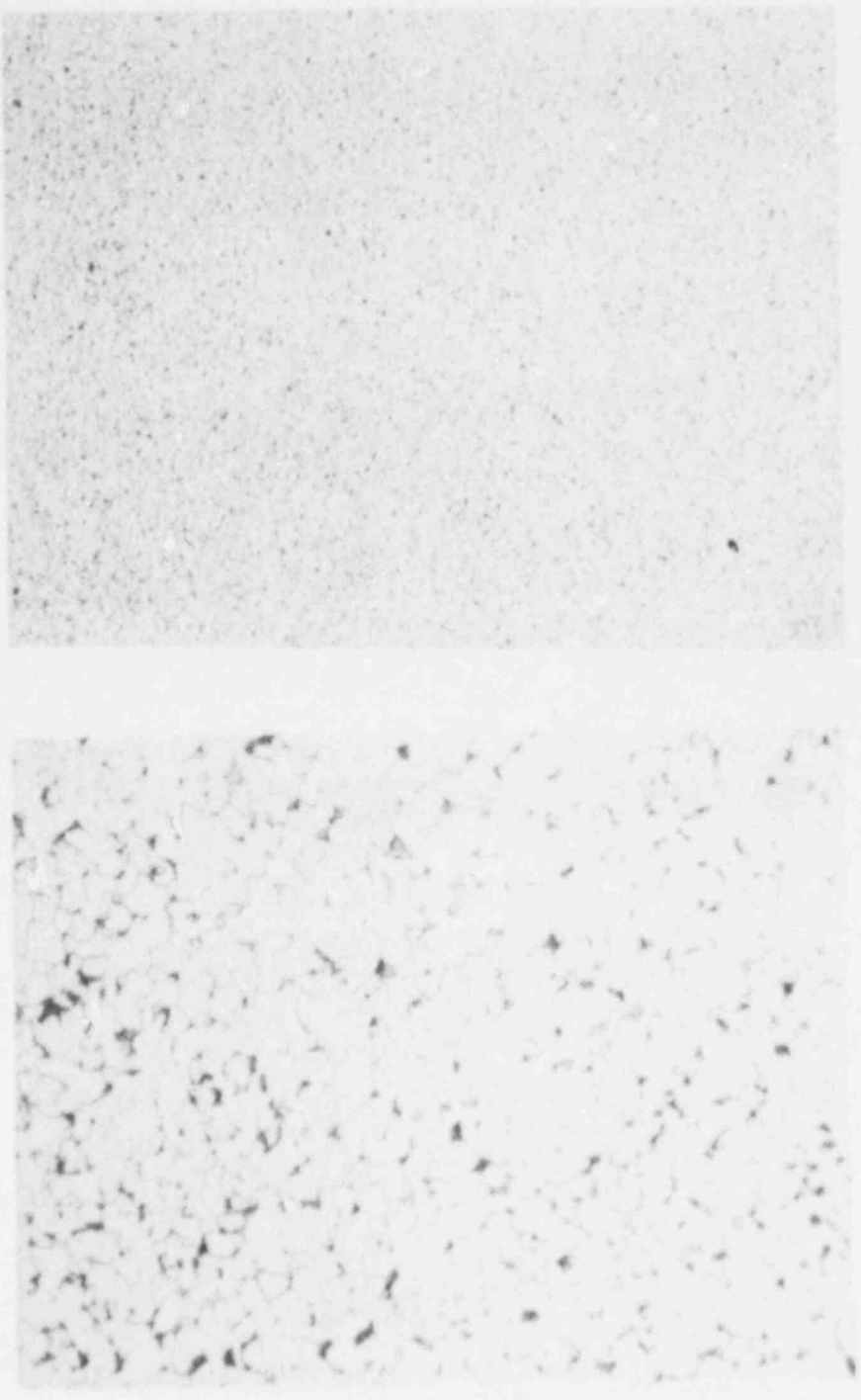

Fig. 14 Microstructure of SA 106-B steel girth-butt weld deposition metal. 100x (upper photo) and 425x (lower photo).

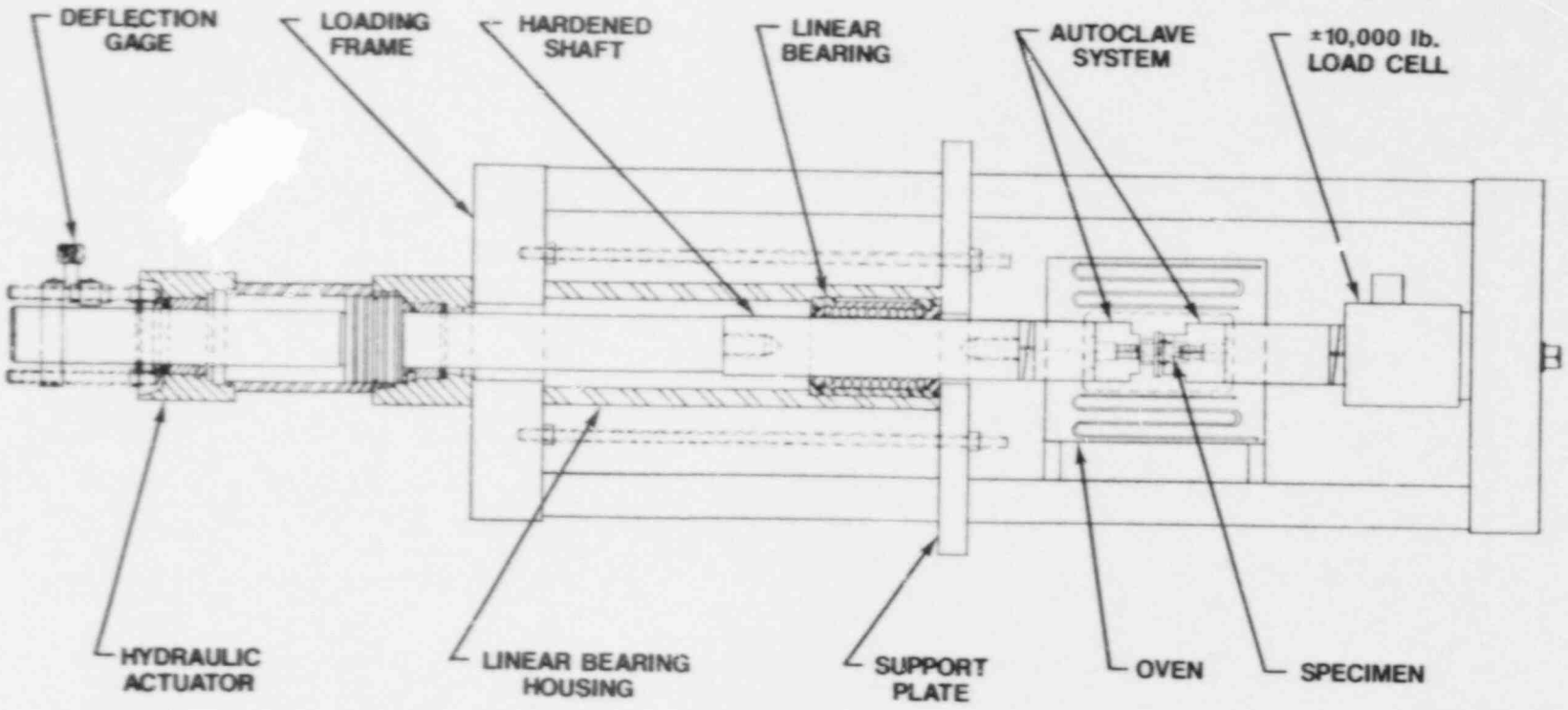

Fig. 15 Servohydraulic fatigue testing machine with detail of linear bearing and support plate used to stiffen the load train.

Two miniautoclave systems were designed and fabricated (Fig. 16) having a small environmental chamber which primarily surrounded the gage section of the specimen. A single seal design allowed for both easy test set-up and specimen displacement during the conduct of the test. The pressurized water environment was provided by a self-contained water console system which was also capable of monitoring the dissolved oxygen content, conductivity, pH, and water flow rate. Figure 17 shows a schematic of the water console system.

The water used for testing was drawn from the city water supply. The water was then passed through ion exchange columns into a mixing tank where boric acid and lithium hydroxide are added so that the water chemistry specifications would be satisfied (Table 4). The prepared water was then pumped into the testing system tank. Gaseous hydrogen was bubbled through the water before and during each test in order to reduce the dissolved oxygen level within specification limits. The water was pressurized and pumped into the miniautoclave using a diaphragm-type pressure pump. Flow rates through the miniautoclave were typically 0.5 L/hr (0.15 gal/hr). The water then passed out of the miniautoclave into a heat exchanger and pressure relief valve before being recirculated through the system. Water samples from the feedwater supply were periodically checked for chloride and fluoride content as well as pH. Additional information on PWR water supply systems at MEA can be found in Ref. 27.

Table 4 Water Chemistry Specifications

Boron (as boric acid)	1000 ± 200 ppm
Lithium (as lithium hydroxide)	1 ± 0.2 ppm
Chloride ions	< 0.15 ppm
Fluoride ions	< 0.10 ppm
Dissolved oxygen	< 10 ppb
Dissolved hydrogen (saturation)	30 to 40 cm^3/kg water

Sulfates, phosphates, and nitrates should be kept to minimum values. All other metallic or ionic species should be kept to trace levels. Some iron, both in solid and soluble form is the inevitable result of a corroding specimen.

An oven surrounding each of the miniautoclave/specimen assemblies was controlled by means of a thermocouple situated inside the miniautoclave chamber.

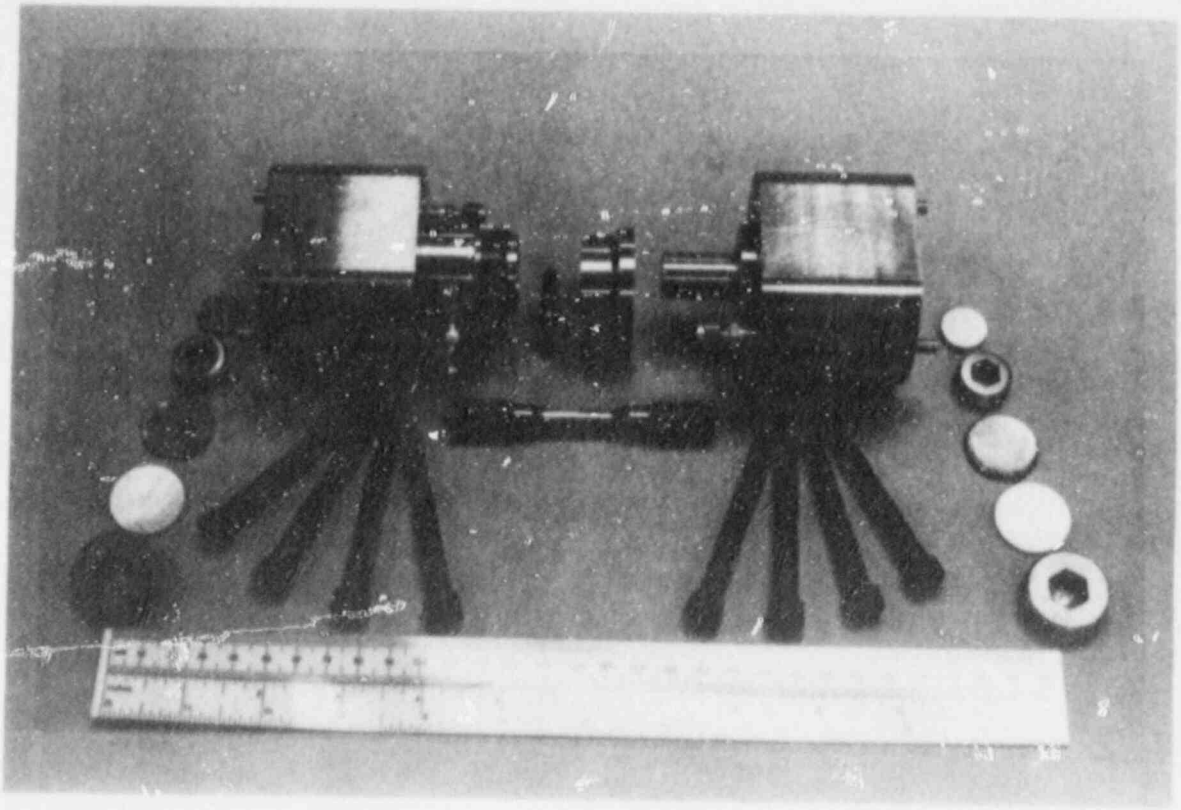

Fig. 16 Miniautoclave system components.

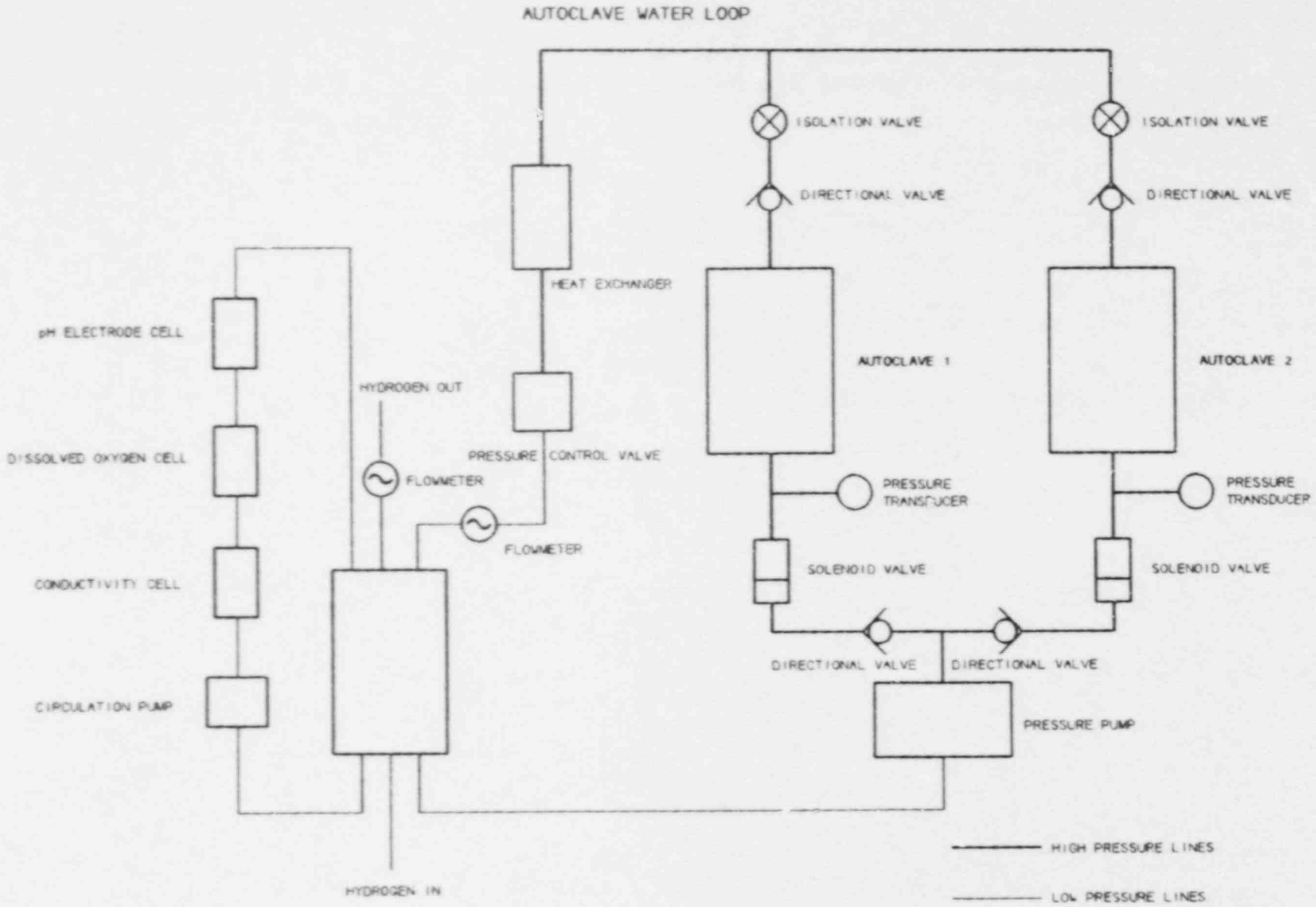

Fig. 17 Schematic of the PWR water supply.

3.3 Test Matrix

Table 5 contains the test matrix for the small specimen S-N tests conducted in both 24°C and 288°C air at atmospheric pressure and in 288°C PWR environments at 13.8 MPa. Entries marked with an asterisk were part of a frequency sensitivity study which defined the frequencies which would yield the most conservative test results in the fatigue life test matrix. Tests were usually started while in deflection control and were usually switched to load control once the plastic strains, if any, had stabilized. Failure was considered to be the point when the crack had progressed completely through the cross section of the specimen.

3.4 Data Acquisition and Analysis

Load histories were acquired by means of load cell signals. These signals were corrected for loading on the specimen due to water pressure and seal friction losses. Deflection histories were obtained in either of two ways. Axial strain feedback was acquired either through the use of a clip gage attached to the gage section of specimens tested at room temperature, or by means of a remotely-mounted clip gage for load train axial deflection data for specimens tested at elevated temperatures.

Load and deflection signals were fed into a chart recorder. Hysteresis loops were acquired for the first five cycles, as well as for the tenth, one-hundredth, and so forth until the approximate specimen half-life was reached. Data used in the construction of S-N curves were acquired from hysteresis loops taken approximately at the specimen half-life. Strain amplitudes were subsequently estimated by the following formula:

$$\epsilon_{ea} \approx e_{ea} = \frac{1}{2}\left(\frac{P_{max} - P_{min}}{AE}\right) \qquad (1)$$

where:

ϵ_{ea} is the elastic strain amplitude (which is strictly defined in terms of true strain quantities),

e_{ea} is the elastic engineering strain amplitude (where $\epsilon_{ea} \approx e_{ea}$ for the strain ranges employed in this investigation),

P_{max} and P_{min} are the maximum and minimum specimen loads, respectively,

A is the net cross-sectional area of the specimen, and

E is the elastic modulus for the specific temperature. The value for elastic modulus for this and other equations was determined by a temperature-dependent formula found in Reference 28.

Table 5 Test Matrix for Small S-N Specimens

Specimen Type	K_t	Strain Ratio	Test Frequency (Hz)	Environment	Number of Specimens Tested
Base Metal	1	-1.00	2-10	24°C Air	19
Base Metal	1	-1.00	2-10	288°C Air	16
Base Metal	1	0.05	2-10	288°C Air	3
Base Metal	1	0.50	2-10	288°C Air	3
Base Metal	2	-1.00	2-10	288°C Air	7
Base Metal	3	-1.00	2-10	288°C Air	8
Base Metal	6	-1.00	2-10	288°C Air	7
Weld Metal	1	-1.00	2-10	288°C Air	7
Base Metal	1	-1.00	1.0[a]	288°C PWR	9
Base Metal	1	-1.00	0.1[a]	288°C PWR	5
Base Metal	1	-1.00	0.017[a]	288°C PWR	4
Base Metal	1	0.05	1.0	288°C PWR	8
Base Metal	1	0.50	1.0	288°C PWR	7
Weld Metal	1	-1.00	1.0	288°C PWR	6
Weld Metal	1	0.05	1.0	288°C PWR	6
Weld Metal	1	0.50	1.0	288°C PWR	5
Base Metal	6	-1.00	1.0[a]	288°C PWR	6
Base Metal	6	-1.00	0.1[a]	288°C PWR	7
Base Metal	6	-1.00	0.017[a]	288°C PWR	5
Base Metal	6	0.05	0.017	288°C PWR	6
Base Metal	6	0.50	0.017	288°C PWR	1
Base Metal	3	-1.00	0.017	288°C PWR	2

[a] Part of the cyclic frequency sensitivity study.

Plastic strain amplitudes (ϵ_{pa}) at test temperature were estimated from an experimentally-established correlation between plastic strain measured on the specimen and specimen plastic deflection at room temperature as inferred on a remote measurement on the load frame. This method of strain measurement has been successfully been used by other investigators (Ref. 29). The correlation was made by simultaneously recording the displacement signals from clip gages mounted (a) on the test frame such that ram deflection was measured, and (b) on the gage length of a smooth axial specimen such that actual specimen strains were recorded (Fig. 18). Once ϵ_{pa} and ϵ_{ea} were estimated for each test, ϵ_a (total strain amplitude) was obtained by the following formula:

$$\epsilon_a = \epsilon_{ea} + \epsilon_{pa} \tag{2}$$

Notch strains were obtained using Neuber's rule. Fatigue test data obtained from test specimens having various notch acuities was analyzed using various interpretations of Neuber's rule, discussed in more detail in Ref. 30, showed that the use of K_f in Neuber's rule in conjunction with the uniaxial cyclic stress-strain curve provided the most accurate and simple means by which to assess notch stresses and strains for the purpose of fatigue life estimation. The use of K_f in the Neuber relation by other investigators (Refs. 31 - 38) has been successful. However, all Neuber-based methods of notch stress and strain assessment yield conservative results. The modified formula for Neuber's rule used in the analysis of this data is:

$$\sigma_a \epsilon_a = \frac{(K_f S_a)^2}{E} \tag{3}$$

where:

σ_a and ϵ_a are the true stress and strain amplitudes, respectively (which occur at the base of the notch, in this case),

K_f is the fatigue notch factor, and

S_a is the net section stress amplitude uncorrected for notch effects.

The equation for uniaxial cyclic stress-strain is:

$$\epsilon_a = \frac{\sigma_a}{E} + \left(\frac{\sigma_a}{A'}\right)^{1/n'} \tag{4}$$

where:

A' is the cyclic strength coefficient, and

n' is the cyclic strain hardening exponent.

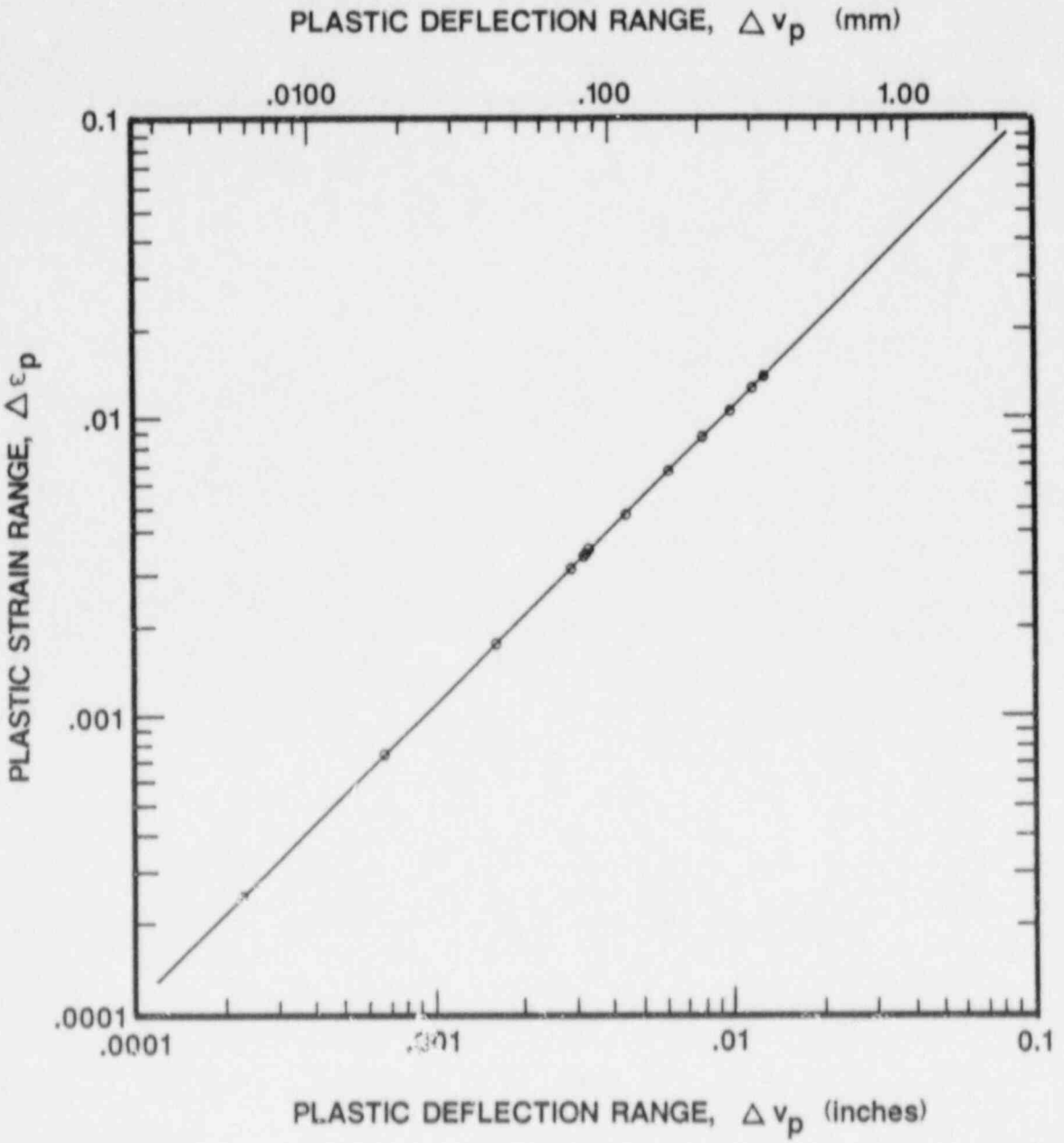

Fig. 18 Load train deflection range vs. specimen plastic strain range correlation used to determine specimen gage length total strain amplitude.

Knowing K_f, S_a, and E, Eqs. 3 and 4 can be simultaneously solved using a computerized iterative process to yield values for notch stresses and strains.

Scanning electron microscopy was also used to observe the fracture surfaces. Each surface was prepared for observation by using the ENDOX method to remove the high temperature oxide (Ref 39).

4. RESULTS AND DISCUSSION

4.1 Air Environment Tests

4.1.1 Smooth Specimens

Cyclic stress-strain tests were performed on base metal specimens at 24°C and 288°C and on weld metal specimens at 288°C by means of incremental step tests. The results are shown in Fig. 19. Cyclic strength coefficients and strain hardening exponents were fitted to Eq. 4 for all three curves. These constants, as well as other cyclic mechanical property data, are presented in Table 6.

Fatigue tests were performed on smooth base metal specimens at 24°C utilizing a strain ratio (R_ϵ) of -1.00. Tests utilizing smooth base metal specimens at 288°C were performed with R_ϵ values of 0.05, 0.50, and -1.00. Stress-life behavior for these materials is not a function of cyclic frequency when conducted in laboratory air, so the test frequencies for air tests were not considered to be a variable which would affect the outcome, and ranged from 1 to 10 Hz. Figures 20 and 21 contain strain-life and pseudostress-life plots, respectively, of base metal specimen data points from tests for both 24°C and 288°C. Tables 7 and 8 contain the data in tabular form. Coffin-Manson strain-life equations were fitted to the base metal specimen data for the R_ϵ = -1.00 results for both 24°C and 288°C air. The form of the equation is:

$$\epsilon_a = \frac{\sigma'_f}{E} (N_f)^b + \epsilon'_f (N_f)^c \qquad (5)$$

where:

σ'_f is the fatigue strength coefficient,

b is the fatigue strength exponent,

ϵ'_f is the fatigue ductility coefficient,

c is the fatigue ductility exponent, and

N_f is the number of cycles to failure.

Constants for the equations are found in Table 9.

Figures 20 and 21 show the effect of temperature on the fatigue behavior of base metal specimens varies according to strain amplitude magnitude. In the high cycle regime, the 288°C air tests result in enhanced fatigue strength over that of 24°C air tests when strain amplitudes are below 2×10^{-3} (pseudostress amplitudes below 344 MPa (50 ksi)), or when the number of cycles to failure are greater that 1.5×10^5 cycles. The fatigue limit at 10^7 cycles was determined by a least squares analysis of net section stress amplitude data and was determined to be 185 MPa (26.8 ksi) at 24°C, and 232 MPa (33.7 ksi) at 288°C. In the low cycle regime, however, 288°C air tests result in reduced fatigue strength when compared to 24°C air tests. This

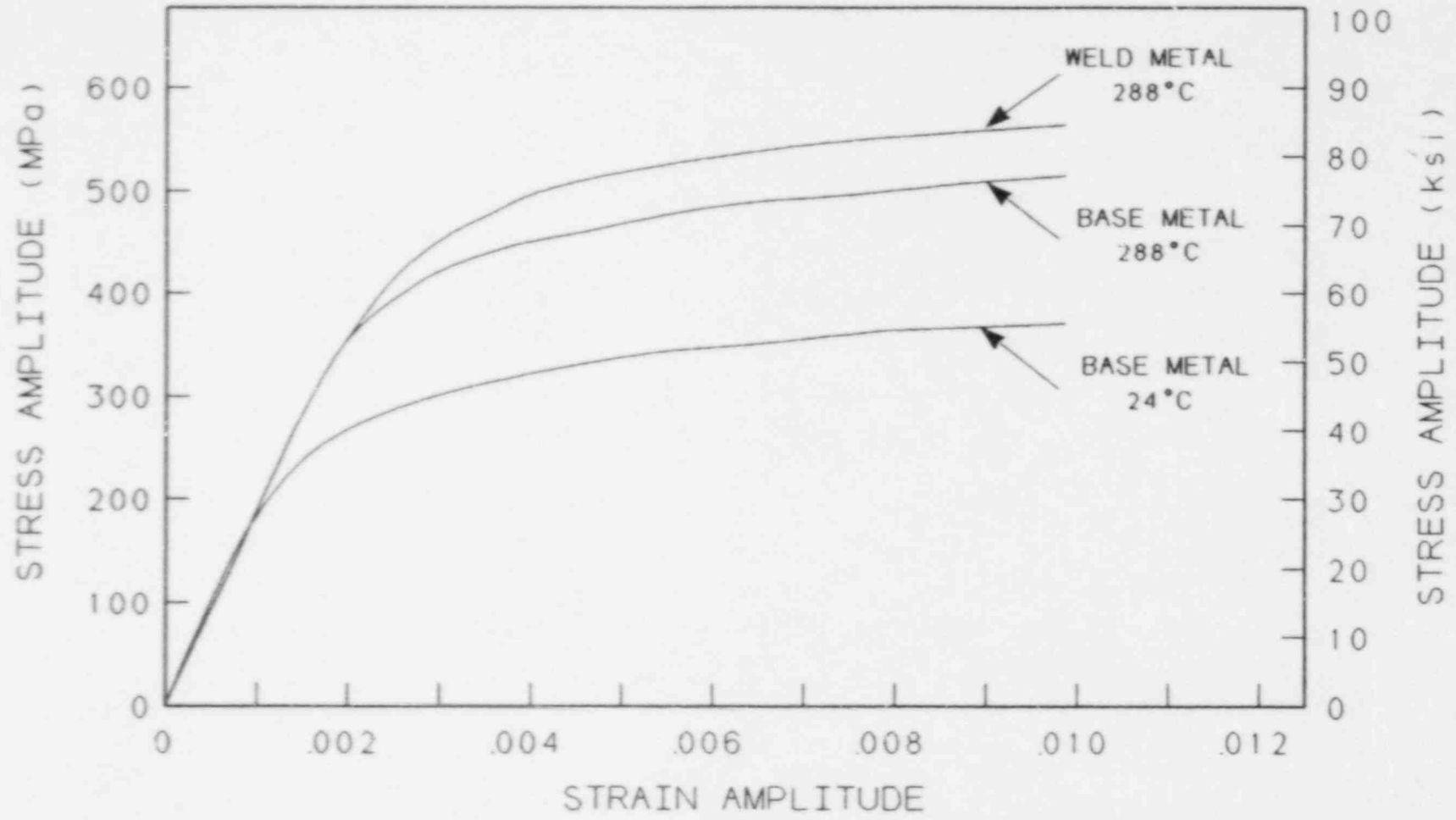

Fig. 19 Cyclic stress-strain curves of SA 106-B steel base metal at 24°C and 288°C, and weld metal at 288°C.

Table 6 Cyclic Stress-Strain Properties of SA 106-B Steel Base and Weld Metal.
Waveform: Triangular; R = 1.00; Frequency: 0.50 Hz

Material	Temperature		Elastic Modulus[a]		Cyclic Strength Coefficient		Strain Hardening Exponent	Yield Stress (0.002 Offset)		Stress at 0.010 Total Strain	
	(°C)	(°F)	(MPa)	(ksi)	(MPa)	(ksi)		(MPa)	(ksi)	(MPa)	(ksi)
Base Metal	24	76	205,810	29,850	689.7	105.4	0.13739	319.9	46.4	375.8	54.5
Base Metal	288	550	190,780	27,670	747.3	115.9	0.08661	462.0	67.0	522.0	75.7
Weld Metal	288	550	190,780	27,670	837.7	121.5	0.07600	375.8	54.5	575.0	83.4

[a] Estimated values from Ref. 28.

Note: Properties were measured at the approximate half-life of each specimen.

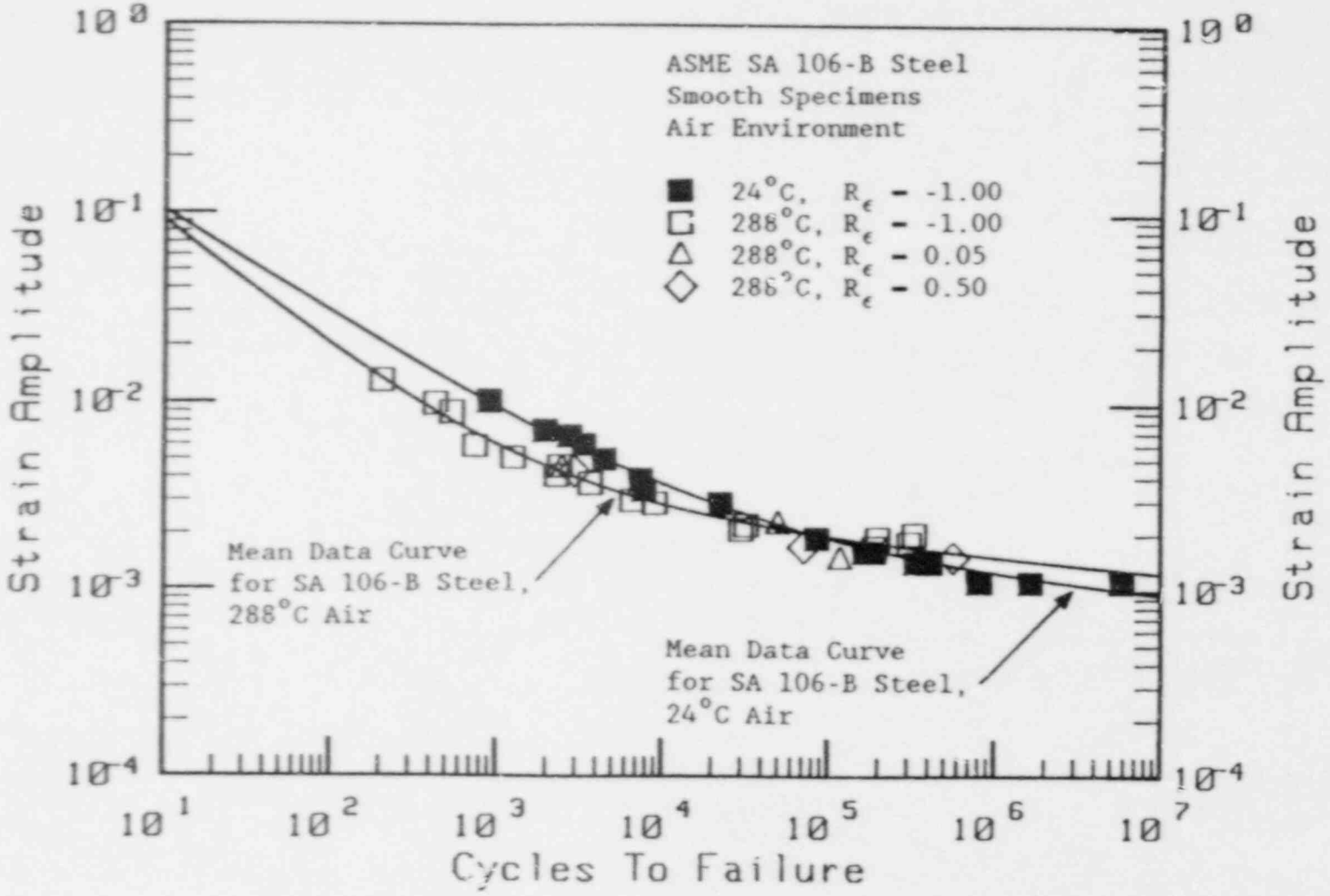

Fig. 20 Strain-life plot of SA 106-B steel smooth base metal specimens with R_e = -1.00, 0.05, and 0.50.

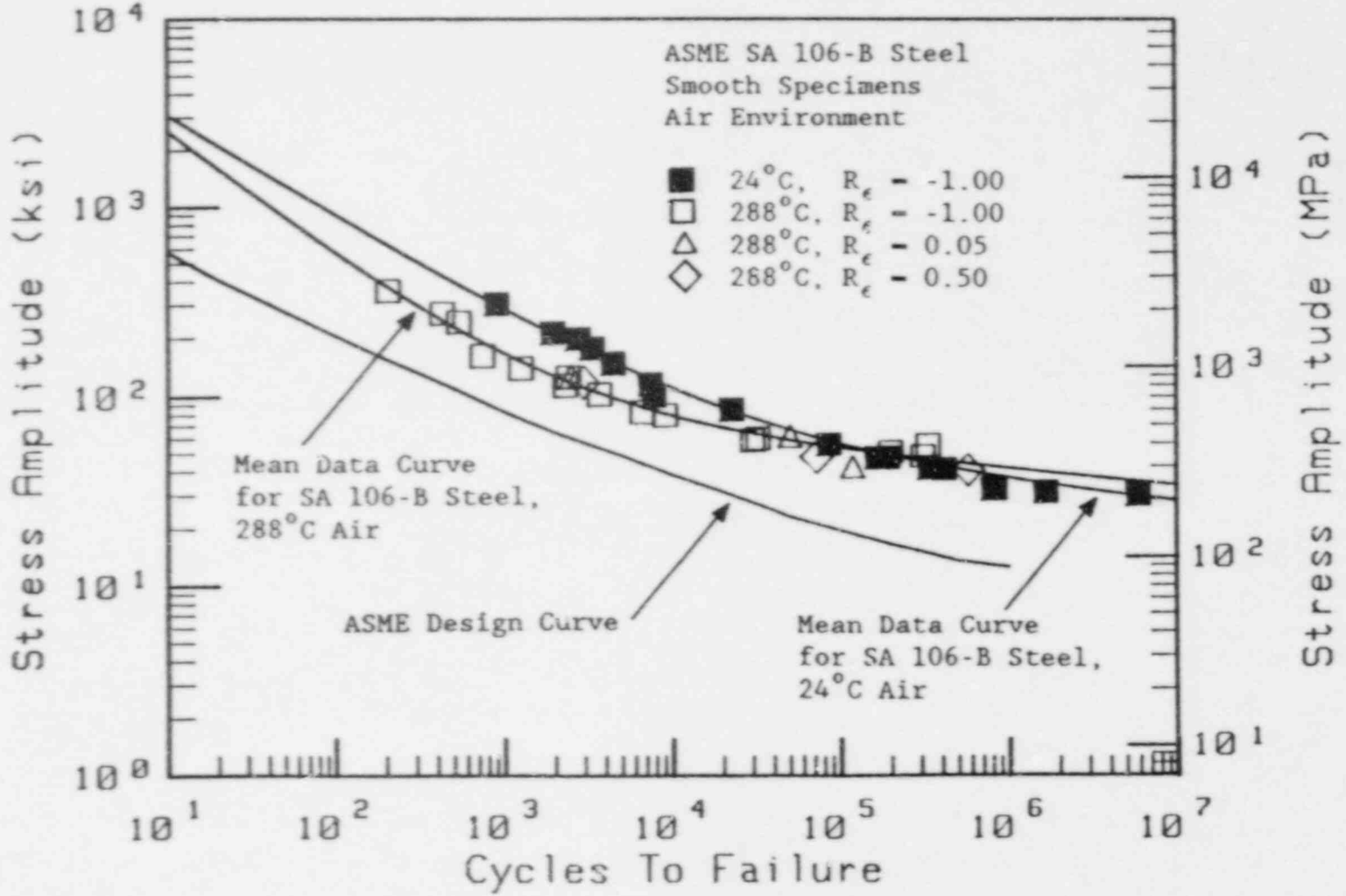

Fig. 21 Pseudostress-life plot of SA 106-B steel smooth base metal specimens with R_e = -1.00, 0.05, and 0.50.

Table 7 Fatigue Life Data For Smooth Base Metal Specimens of SA 106-B Steel Tested in 24°C (76°F) Air with R = -1.00; Elastic Modulus: 205.8×10^3 MPa (29.85×10^6 psi)

Specimen	Net Section Stress Amplitude (MPA)	(ksi)	Strain Amplitude	Pseudostress Amplitude (MPa)	(ksi)	Cycles to Failure
ZP11-48	365	52.9	0.0060	1235	179.1	3,315
ZP11-138	418	60.6	0.0102	2099	304.5	900
ZP11-13	305	44.3	0.0034	700	101.5	7,720
ZP11-145	380	55.1	0.0067	1389	201.4	2,740
ZP11-8	236	34.2	0.0014	288	41.8	337,040
ZP11-10	225	32.7	0.0011	225	32.7	824,190
ZP11-23	236	34.2	0.0014	288	41.8	411,780
ZP11-30	218	31.6	0.0011	218	31.6	1.656×10^6
ZP11-31	24	34.9	0.0019	391	56.7	85,200
ZP11-37	31	46.1	0.0039	803	116.4	7,370
ZP11-39	241	30.6	0.0011	211	30.6	5.88×10^6
ZP11-43	279	40.5	0.0029	597	86.6	22,470
ZP11-22	225	32.7	0.0011	225	32.7	806,060
ZP11-82	401	58.1	0.0072	1491	216.3	1,940
ZP11-4	246	35.7	0.0016	330	47.8	187,340
ZP11-15	246	35.7	0.0016	330	47.8	164,980
ZP11-51	309	44.8	0.0016	330	47.8	166,800

Table 8 Fatigue Life Data For Smooth Base Metal Specimens of SA 106-B Steel Tested in 288°C (550°F) Air; Elastic Modulus: 190.8×10^3 MPa (27.67×10^6 psi)

Specimen	Strain Ratio	Net Section Stress Amplitude (MPa)	(ksi)	Strain Amplitude	Pseudostress Amplitude (MPa)	(ksi)	Cycles to Failure
ZP11-17	-1.00	468	67.8	0.0041	782	113.4	2,300
ZP11-109	-1.00	538	78.1	0.0089	1698	246.3	540
ZP11-70	-1.00	443	64.3	0.0037	706	102.4	3,670
ZP11-40	-1.00	356	51.6	0.0021	401	58.1	30,200
ZP11-56	-1.00	424	61.5	0.0029	553	80.2	9,100
ZP11-28	-1.00	463	67.1	0.0046	878	127.3	2,400
ZP11-11	-1.00	427	62.0	0.0030	572	83.0	6,600
ZP11-21	-1.00	492	71.4	0.0059	1126	163.3	745
ZP11-60	-1.00	525	76.2	0.0051	973	141.1	1,260
ZP11-74	-1.00	375	54.4	0.0022	420	60.9	32,370
ZP11-9	-1.00	329	47.7	0.0018	343	49.8	308,806
ZP11-133	-1.00	536	77.7	0.0099	1888	273.9	430
ZP11-131	-1.00	591	85.7	0.0130	2480	359.7	205
ZP11-72	0.05	359	52.0	0.0023	439	63.6	50,195
ZP11-88	0.05	294	42.6	0.0015	286	41.5	118,300
ZP11-96	0.05	478	69.3	0.0046	878	127.3	2,480
ZP11-81	0.50	283	41.1	0.0015	286	41.5	570,500
ZP11-94	0.50	319	46.2	0.0017	324	47.0	71,800
ZP11-68	0.50	451	65.4	0.0043	820	119.0	2,940

Table 9 Coffin-Manson Constants for SA 106-B Steel Base and Weld Metal

Material	Temperature (°C)	Temperature (°F)	Fatigue Strength Coefficient (σ_f')	Fatigue Strength Exponent (b)	Fatigue Ductility Coefficient (ε_f')	Fatigue Dutility Exponent (c)
Base Metal	24	76	0.00339	-0.08242	0.37010	-0.56217
Base Metal	288	550	0.00477	-0.08450	0.45487	-0.71029
Weld Metal	288	550	0.00625	-0.10676	0.44322	-0.70961

temperature-dependent behavior of SA 106-B steel is believed to be due dynamic strain aging effects commonly found in many carbon steels. The test temperature of 288°C is within the range in which dynamic strain aging processes have been observed to occur (Refs. 40 - 45); thermally-enhanced diffusion and carbide formation kinetics tend to promote carbide formation in the persistant slip bands (PSB's) and within the rest of the metal matrix.

At high strain amplitudes, nucleating carbides, which have a lattice structure which is incoherent with the lattice structure of the matrix metal, are continuously sheared apart within the PSB's by high amplitude movement of screw dislocations, thereby forcing carbon back into solution. Carbides, having a lattice structure similar to that of the matrix metal, provide a "shear path" for the dislocations and offer little impediment to screw dislocation motion, and hence, restrict plastic cyclic deformation. Therefore, little or no fatigue strength enhancement of SA 106-B steel exists at 288°C. At low strain amplitudes, on the other hand, low amplitude movement of screw dislocations within the PSB's do not carry enough energy to shear apart the incoherent carbides, thereby restricting the movement of screw dislocations. The result is an increase in fatigue strength of SA 106-B steel in the high cycle regime at 288°C.

The effect of varying R_ϵ values can also be observed in Figs. 20 and 21. Virtually no difference in fatigue life was seen for R_ϵ values of 0.05, 0.50, and -1.00, especially in the low cycle fatigue range. The mean stress value is at a maximum after the first cycle of a test if R_ϵ is less than -1.00. Continued cycling will result in an exponential decrease in mean stress until a value of zero is approached. Figure 22 illustrates this point by showing a series of load-deflection hysteresis loops acquired from a smooth base metal specimen tested at 288°C having a strain ratio of 0.50 tested in low cycle fatigue, which failed after 605 cycles. Notice that the projected value of mean stress at failure is roughly 5 % of the stress amplitude.

High cycle tests, however, suggest a larger effect of mean stress on fatigue life. The results shown in Figs. 20 and 21 reveal a trend toward lowered fatigue life in the high cycle fatigue regime, but not enough high cycle fatigue data was generated, which would be necessary for a more complete quantification of this behavior. In this case, the mean stress value approaches a value greater than zero early in the life of the specimen. Figure 23 shows a set of hysteresis loops from a high cycle fatigue test at 288°C having a strain ratio of 0.50, and failing after 145,720 cycles. In this case, the projected value of mean stress at failure is roughly 12 % of the stress amplitude.

Empirical relationships used to predict mean stress effects on fatigue life incorporate material constants for the particular material. Some investigators (Ref. 46) have suggested the following equation as a method with which to account for mean stresses:

$$\sigma_{cr} = \frac{\sigma_a}{1 - \sigma_o/\sigma'_f} \qquad (6)$$

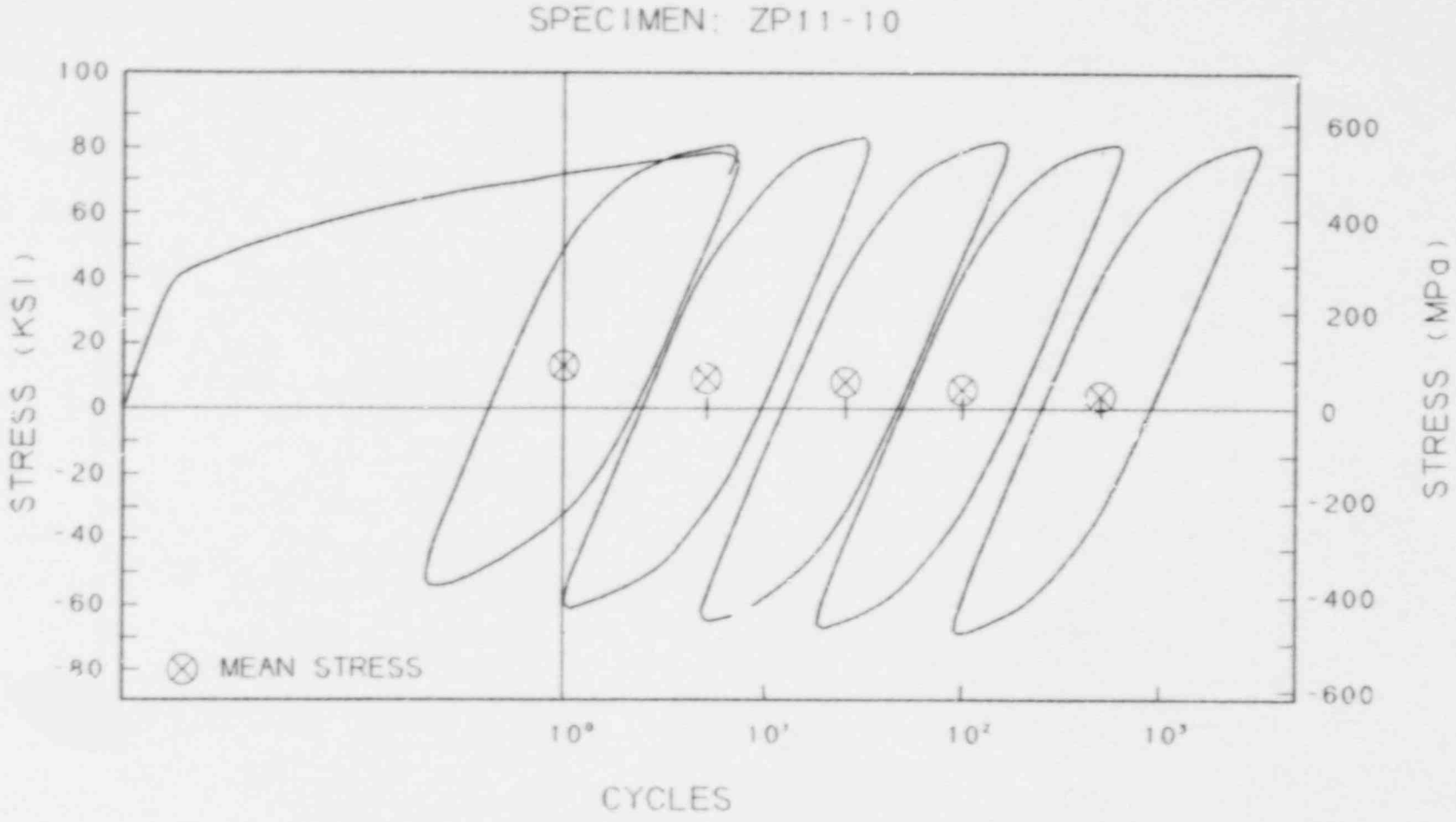

Fig. 22 Series of load-deflection hysteresis loops after progressive numbers of cycles in low cycle fatigue.

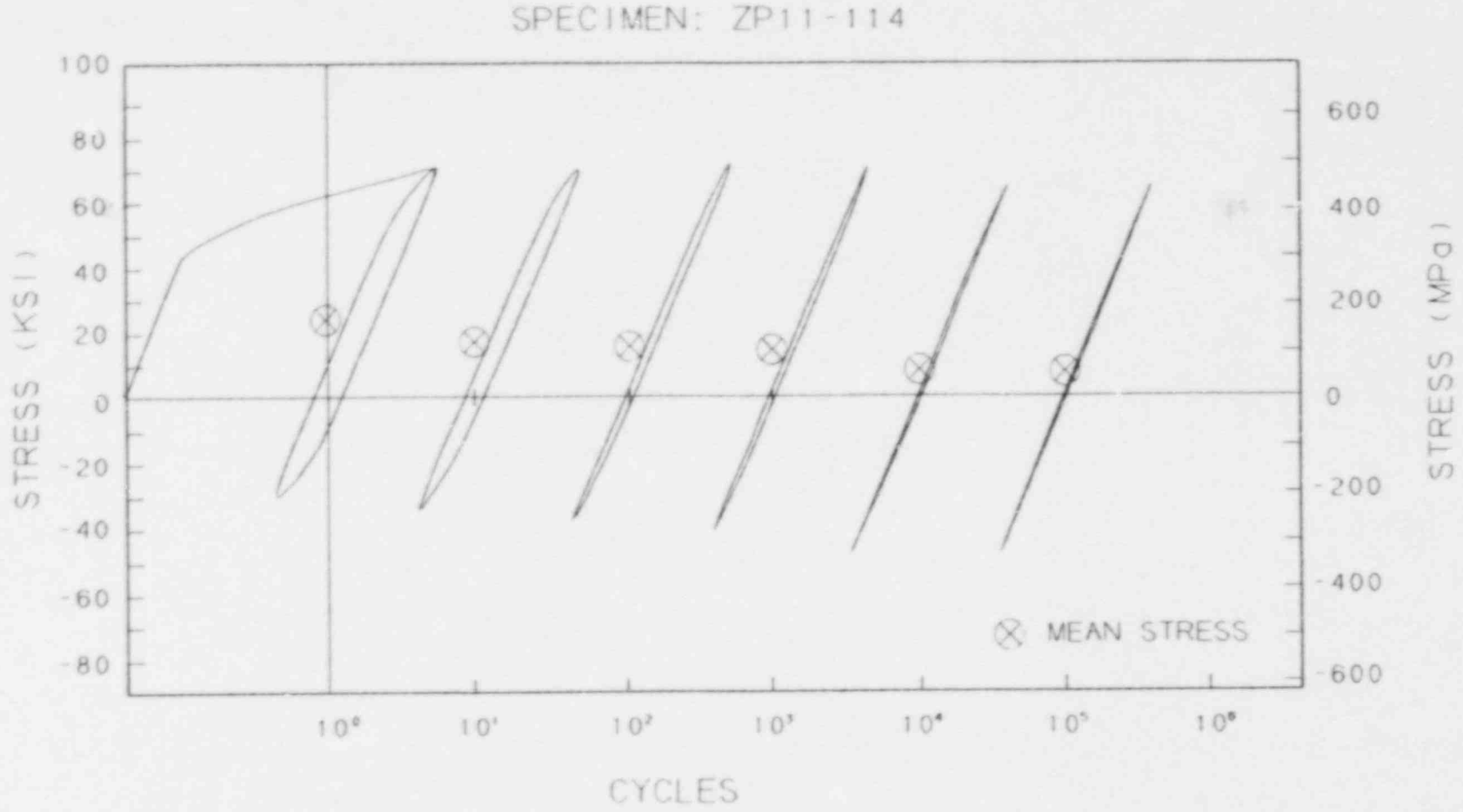

Fig. 23 Series of load-deflection hysteresis loops after progressive numbers of cycles in high cycle fatigue.

where:

σ_o is the mean stress, and

σ_{cr} is the completely-reversed stress amplitude expected to cause failure in the same number of cycles as the actual combination of σ_a and σ_o.

Combining Eq. 6 with the elastic component Eq. 5 yields:

$$\epsilon_a = \frac{\sigma_f' + \sigma_o}{E} (N_f)^b + \epsilon_f' (N_f)^c \qquad (7)$$

Inspection of Eq. 7 shows that, in the low cycle fatigue regime, the plastic component of strain amplitude dominates the value for total strain amplitude, thereby minimizing the effect of the mean stress correction. Conversely, in the high cycle fatigue regime, the elastic component of the equation dominates the value of total strain amplitude.

The results of the smooth weld metal specimens were obtained from S-N tests conducted at 288°C with R_ϵ = -1.00, and are compared with base metal S-N results in Figs. 24 and 25. Table 10 shows the weld metal test results in tabular form. Coffin-Manson constants were fitted to the curve and are given in Table 9. Tests were not performed at other strain ratios since virtually no strain ratio effect was observed for smooth specimen tests. The results indicate that these specimens fabricated from SA 106-B weldments exhibit slightly enhanced fatigue strength properties over that of the base metal. This underscores the fact that proper materials selection and welding procedures ensure that, exclusive of geometric stress raisers almost always found associated with conventional weldments, weld deposition and HAZ metal enhance the fatigue strength of the weld joint. This point is further supported by the cyclic stress-strain curves (Fig. 19) and the fatigue life plots (Figs. 24 and 25) which show higher cyclic and fatigue strengths for the smooth weld metal specimens.

4.1.2 Notched Specimen Tests

The results for notched specimen tests are expressed in three forms: (1) net section stress amplitude, (2) local (notch) strain amplitude, and (3) pseudostress amplitude. Figure 26 shows the results in terms of net section stress amplitude vs. cycles to failure. Table 11 shows the notched specimen test results in tabular form.

Below 10^3 cycles, fatigue life is not affected by the presence of the notch. This phenomenon has been observed previously in ductile steels (Ref. 47). Increasing the cycles to failure from 10^3, increases the notch effect until the maximum effect is reached at 10^7 cycles. The mean data line, and hence, K_f factors at 10^7 cycles, was obtained for each data set by linear regression analysis. K_f is simply defined as the ratio of smooth specimen stress amplitude to net section stress amplitude of a notched specimen at equal lives to failure. Table 11 also shows the empirically-determined values for K_f.

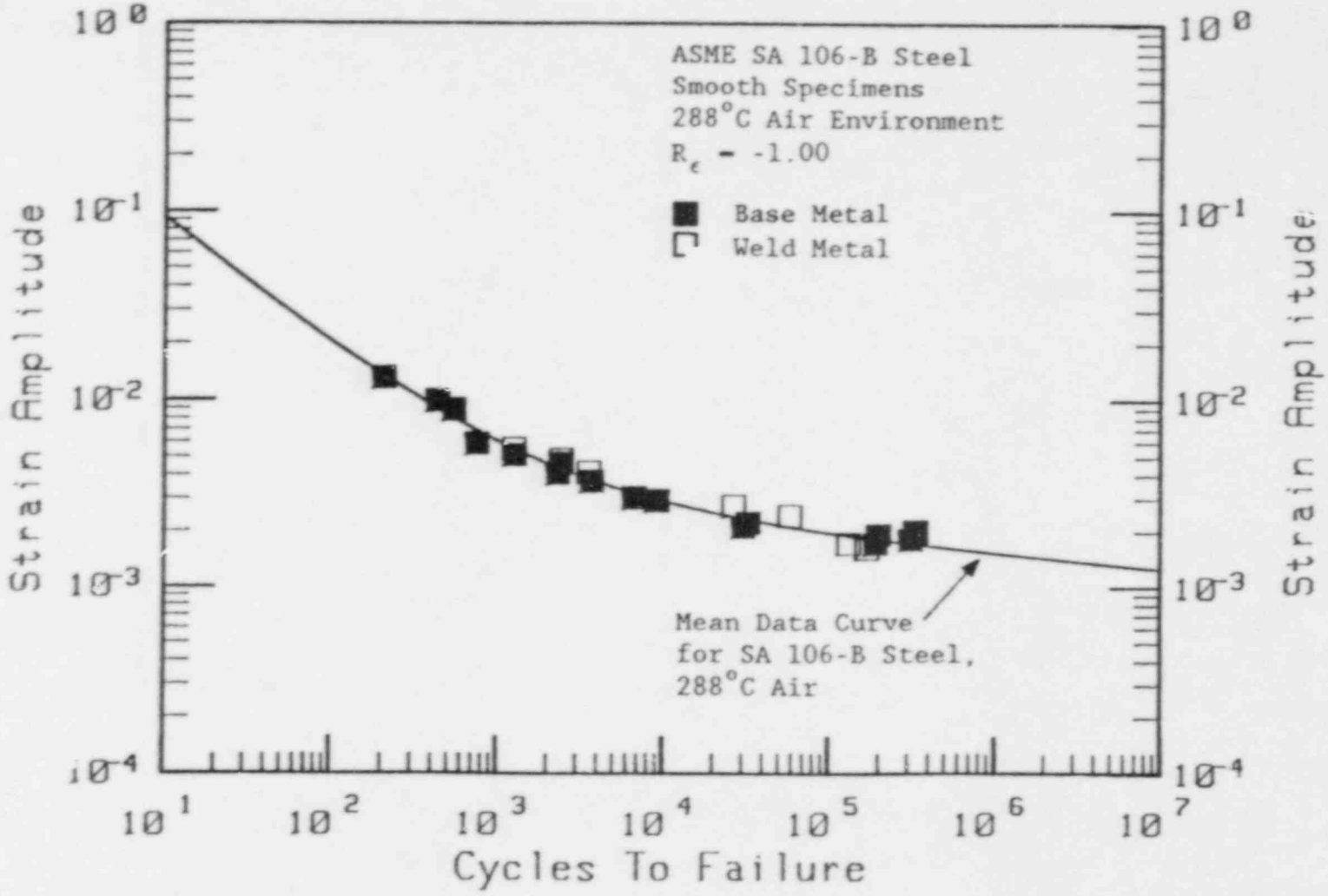

Fig. 24 Strain-life plot of SA 106-B steel smooth weld metal specimens tested in 288°C air.

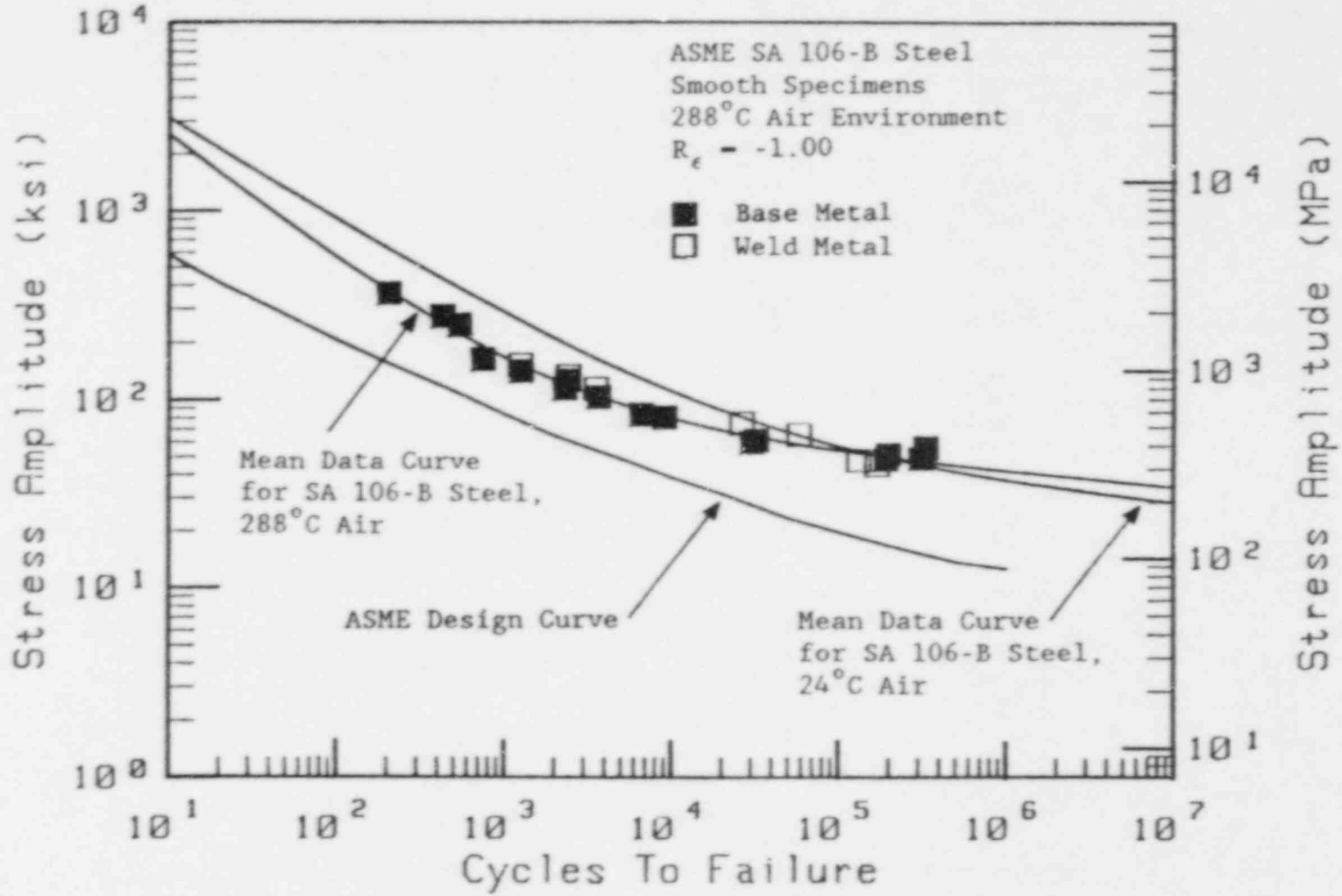

Fig. 25 Pseudostress-life plot of SA 106-B steel smooth weld metal specimens tested in 288°C air.

Table 10 Fatigue Life Data for Smooth Weld Metal [illegible] of SA 106-B Steel Tested in 288°C (550°F) Air with R = -1.00

Specimen	Net Section Stress Amplitude (MPa)	(ksi)	Strain Amplitude	Pseudostress Amplitude (MPa)	(ksi)	Cycles to Failure
11W-65	494.4	71.7	0.0040	763	110.7	3,560
11W-66	406.1	58.9	0.0023	439	63.6	58,310
11W-68	446.8	64.8	0.0026	496	71.9	26,535
11W-69	329.6	47.8	0.0018	343	49.8	132,240
11W-71	540.6	78.4	0.0056	1,066	154.6	1,260
11W-81	520.6	75.5	0.0044	839	121.7	2,425
11W-89	309.6	44.9	0.0016	305	44.3	170,000

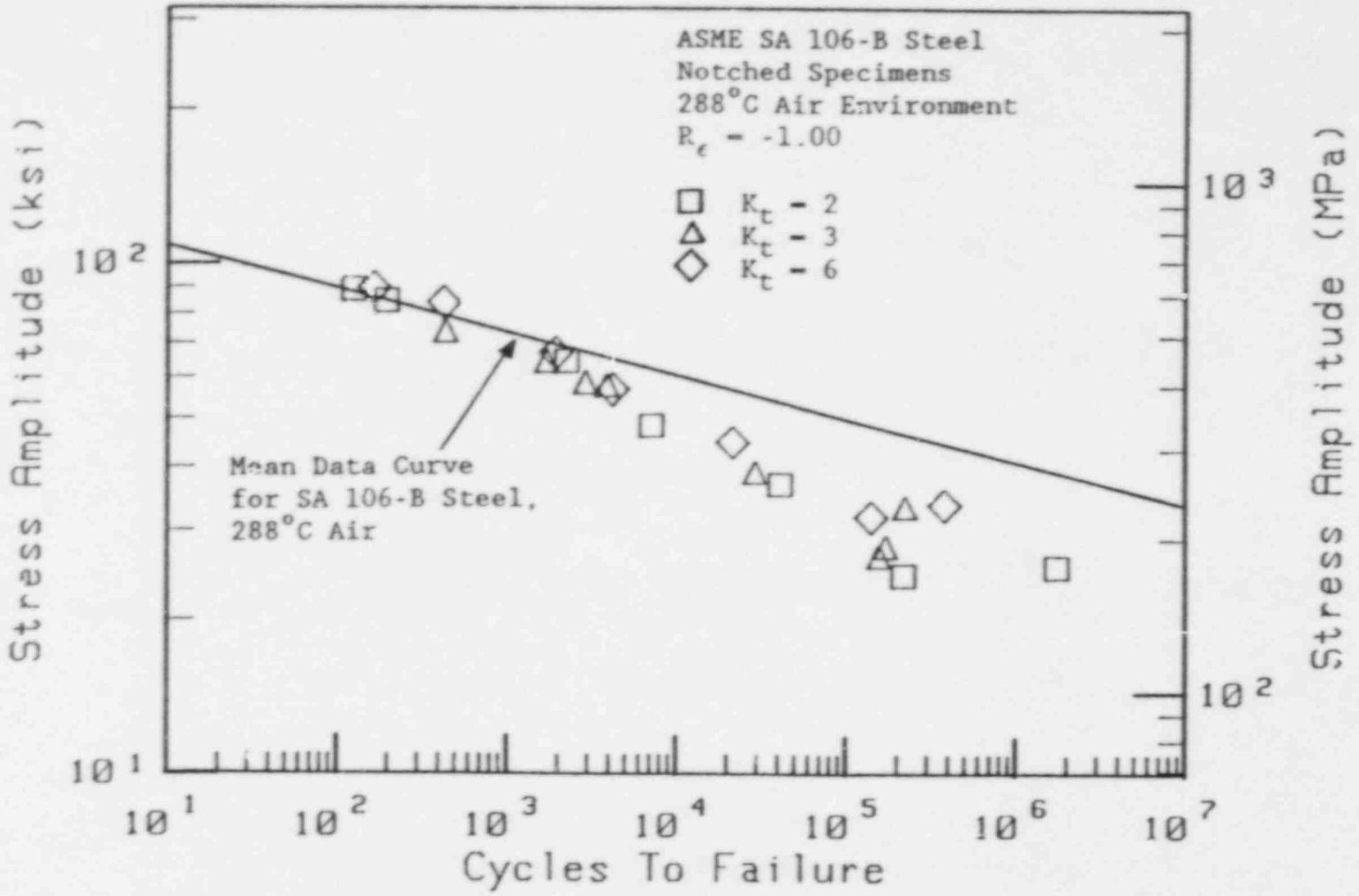

Fig. 26 Net section stress-life plot of SA 106-B steel notched (K_t = 2, 3, and 6) base metal specimens tested in 288°C air.

Table 11 Notched Specimen Life Data For SA 106-B Steel Tested in 288°C (550°F) Air at a Load Ratio of -1.00; Net Section Stress Amplitude Values

Specimen	K_t	K_f	Net Section Stress Amplitude (MPa)	(ksi)	Cycles to Failure
K2-1	2	1.75	462	67.0	1,930
K2-2	2	1.75	577	83.7	425
K2-3	2	1.75	614	89.1	165
K2-4	2	1.75	307	44.5	21,510
K2-5	2	1.75	392	56.9	4,170
K2-7	2	1.75	232	33.6	380,970
K2-9	2	1.75	219	31.8	140,380
K3-1	3	2.29	193	28.0	171,010
K3-2	3	2.29	268	38.8	29,200
K3-3	3	2.29	400	58.0	3,860
K3-5	3	2.29	445	64.5	1,695
K3-22	3	2.29	411	59.6	2,880
K3-7	3	2.29	230	33.3	222,550
K3-10	3	2.29	510	74.0	435
K3-15	3	2.29	184	26.7	156,610
K6-1	6	1.98	254	36.9	40,825
K6-3	6	1.98	170	24.7	218,300
K6-2	6	1.98	334	48.4	7,070
K6-5	6	1.98	445	64.6	2,220
K6-6	6	1.98	613	88.9	125
K6-14	6	1.98	176	25.5	1,740,500
K6-18	6	1.98	580	84.1	195

Notched specimen results, expressed in terms of local strain and pseudostress amplitudes obtained from a modified Neuber's rule, are shown in Figs. 27 and 28, respectively. Table 12 shows the notched specimen test results in tabular form. It can be seen from both these results and from finite element analysis investigations (Ref. 48) that the use of Neuber's rule results in conservative estimates of notch stresses and strains, which makes direct comparisons of fatigue data from smooth and notched specimens difficult. However, it is clear that the inherent conservativeness of Neuber's rule offers an added degree of safety from a design standpoint, after accounting for structural discontinuities. The use of K_f instead of K_t offers a more realistic assessment of notch stresses and strains when used in notched specimen total life schemes.

4.2 PWR Environment Tests

4.2.1 Frequency Sensitivity Study

The effect of cyclic frequency on the fatigue life of smooth and sharply-notched (K_t = 6) specimens was determined by the results of a frequency sensitivity study (Ref. 9) which incorporated 1.0, 0.1, and 0.017 Hz testing in PWR environments with an R_ϵ value of -1.00. Linear regression analysis results, reproduced in Fig. 29 from net section stress amplitude data, best shows the frequency effect trends in the data. Tables 13 and 14 show the PWR environment test results in tabular form. The results from smooth specimen testing indicated that virtually no frequency sensitivity effect on fatigue life was observed. Tests conducted on sharply-notched specimens indicated that 0.017 Hz appeared to be the most detrimental frequency. These results are consistent with the concept presented earlier which suggests that since fatigue crack growth overwhelmingly dominates the fatigue life of sharply-notched components, then a cyclic frequency effect, which has been observed to occur during fatigue crack growth (Refs. 19 and 20), would be more evident with sharply-notched specimens than with smooth specimens tested in PWR environments. These results dictate that smooth and notched specimen tests in PWR environments should be tested at 1.0 Hz and 0.017 Hz, respectively.

4.2.2 Smooth Specimen Tests

Comparison between the results obtained with smooth specimens tested in 288°C air and PWR environments with R_ϵ values of 0.05, 0.5, and -1.00 shows that low dissolved oxygen levels do not critically affect crack initiation in SA 106-B piping steel (Figs. 30 and 31); Table 15 shows the PWR environment test results in tabular form. However, as a result of PWR operating temperatures, a reduction of fatigue life exists for carbon piping steels in the low cycle regime, and an improvement in fatigue strength properties in the high cycle regime, as discussed in Section 4.1.1. Again, this phenomenon can be explained in terms of dynamic strain aging phenomena in carbon steels. Comparison of these results with the ASME Section III design curve shows that the margins of safety of 2 on stress and 20 on cycles incorporated into the design curve are not properly based on the fatigue life behavior of SA 106-B (or possible other steels) at 288°C.

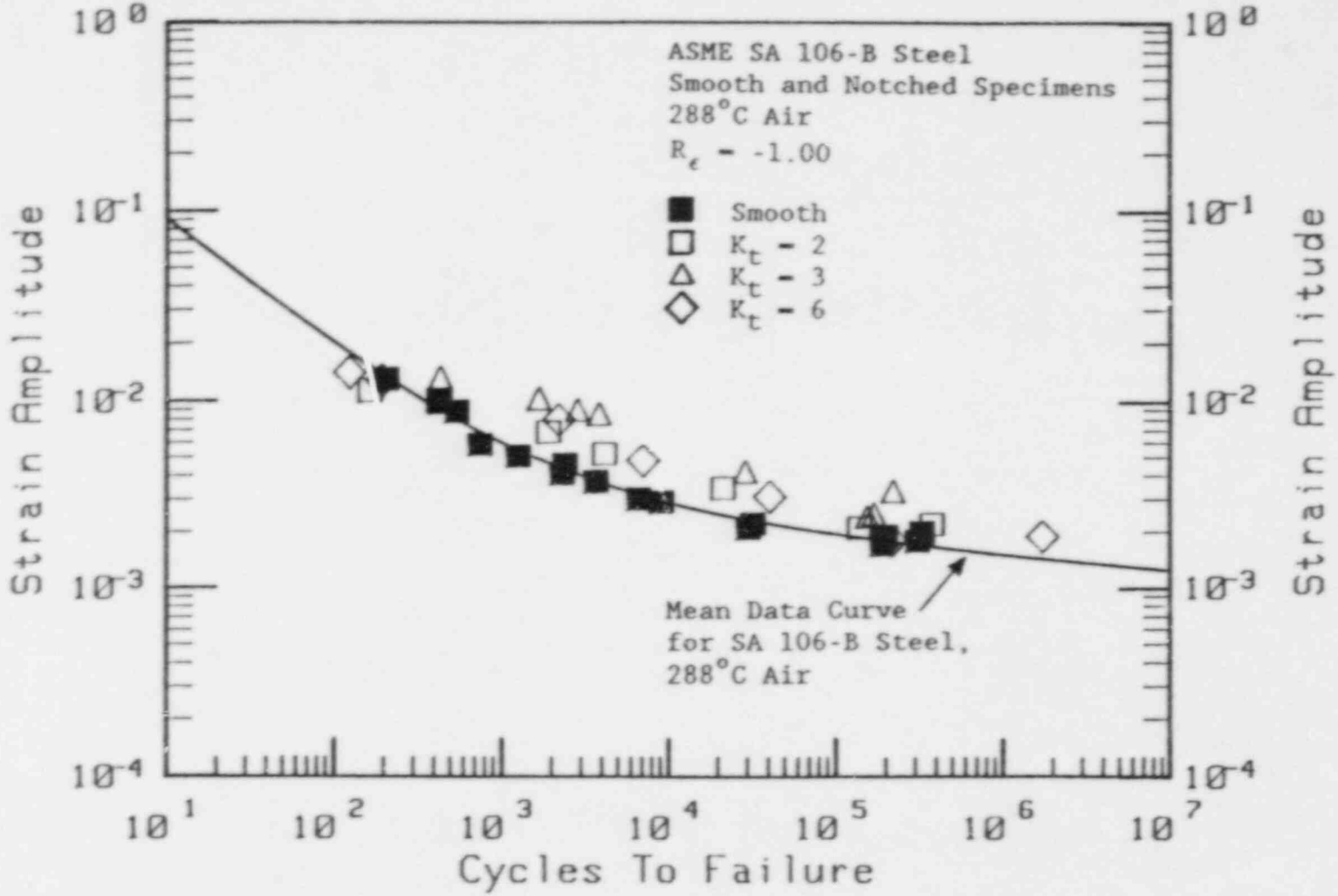

Fig. 27 Strain-life plot of SA 106-B steel notched (K_t = 2, 3, and 6) base metal specimens tested in 288°C air.

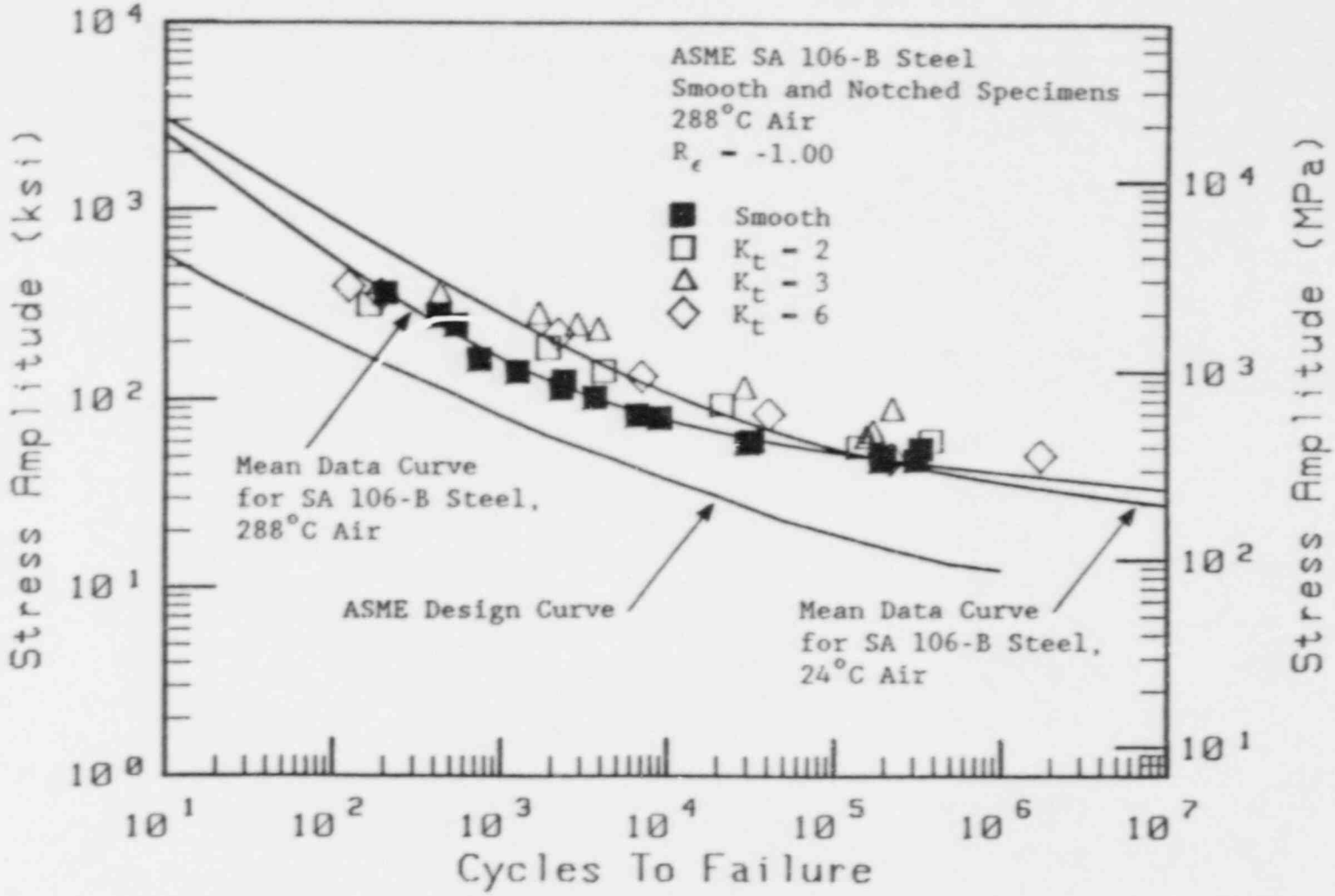

Fig. 28 Pseudostress-life plot of SA 106-B steel notched (K_t = 2, 3, and 6) base metal specimens tested in 288°C air.

Table 12 Fatigue Analysis of Notched Base Metal Specimen Data For SA 106-B Steel (see Table 4). Notch Analysis Was Accomplished by Using K_f in Neuber's Rule in Conjunction With the Uniaxial Cyclic Stress-Strain Curve; R = -1.00

Specimen	K_t	K_f	Notch Stress Amplitude (MPa)	Notch Stress Amplitude (ksi)	Notch Strain Amplitude	Pseudostress Amplitude (MPa)	Pseudostress Amplitude (ksi)	Cycles to Failure
K2-1	2	1.75	498	72.3	0.0069	1,311	190.2	1,930
K2-2	2	1.75	523	75.9	0.0102	1,950	282.8	425
K2-3	2	1.75	530	76.8	0.0114	2,182	316.4	165
K2-4	2	1.75	443	64.2	0.0034	651	94.4	21,510
K2-5	2	1.75	478	69.4	0.0052	981	142.3	4,170
K2-7	2	1.75	385	55.9	0.0022	426	61.8	380,970
K2-9	2	1.75	371	53.8	0.0021	397	57.6	140,380
K3-1	3	2.29	406	58.9	0.0025	482	69.9	171,010
K3-2	3	2.29	463	67.1	0.0042	811	117.6	29,200
K3-3	3	2.29	512	74.3	0.0086	1,636	237.3	3,860
K3-5	3	2.29	524	76.0	0.0104	1,960	287.0	1,695
K3-22	3	2.29	516	74.8	0.0090	1,717	249.1	2,880
K3-7	3	2.29	439	63.7	0.0033	629	91.3	222,550
K3-10	3	2.29	538	78.1	0.0133	2,534	367.5	435
K3-15	3	2.29	395	57.3	0.0024	450	65.3	156,610
K6-1	6	1.98	432	62.6	0.0031	589	85.2	40,825
K6-3	6	1.98	333	48.3	0.0018	341	49.5	218,300
K6-2	6	1.98	474	68.7	0.0048	923	133.8	7,070
K6-5	6	1.98	508	73.7	0.0080	1,531	222.0	2,220
K6-6	6	1.98	543	78.7	0.0142	2,715	393.8	125
K6-14	6	1.98	343	49.7	0.0019	354	51.3	1,740,500
K6-18	6	1.98	543	78.8	0.0129	2,455	356.1	195

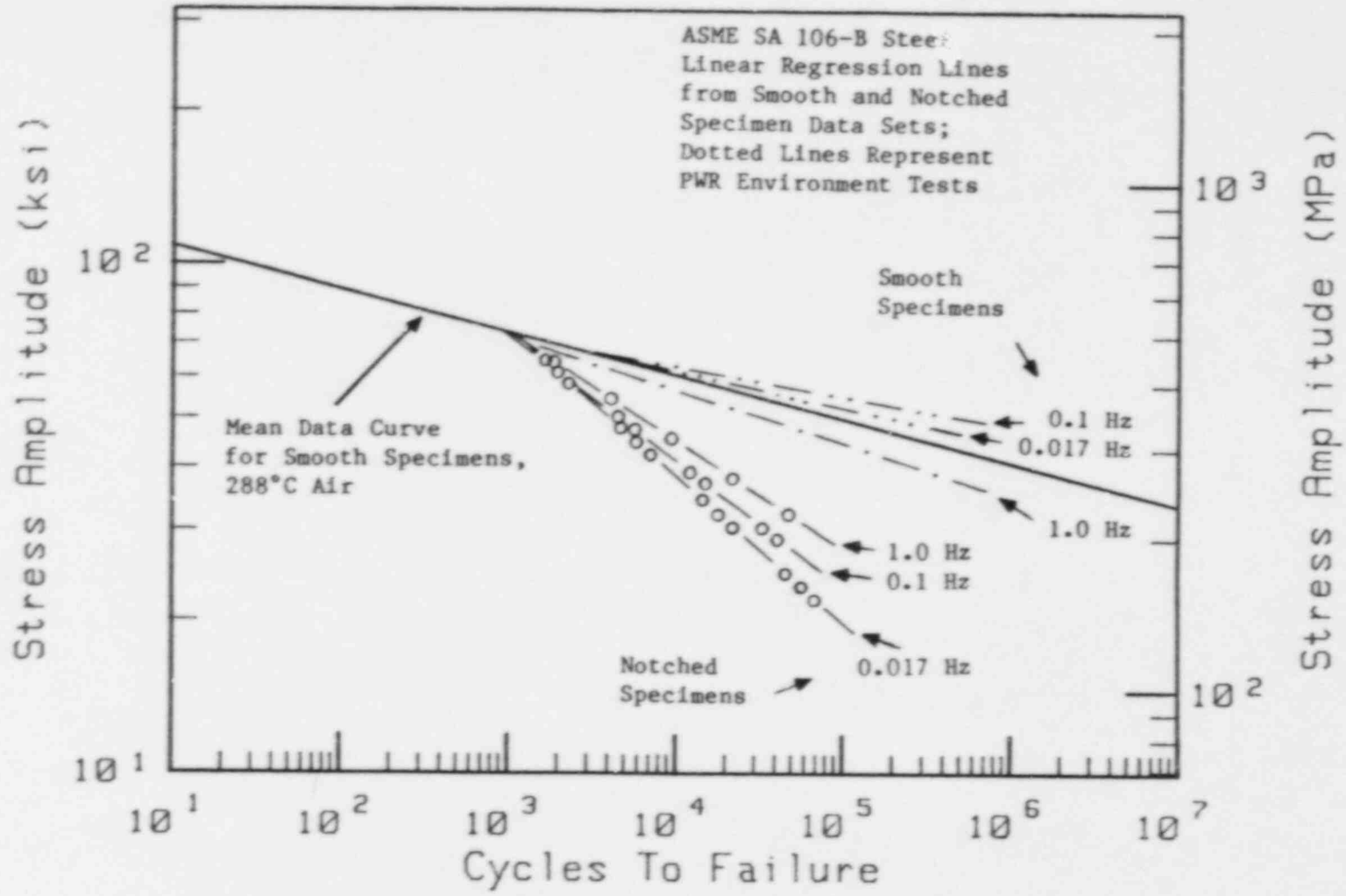

Fig. 29 Net section stress-life results of SA 106-B steel smooth and sharply-notched (K_t = 6) base metal specimen cyclic frequency sensitivity study. Linear regression analysis was used to determine the slopes of the mean data lines.

Table 13 Cyclic Frequency Sensitivity Study Fatigue Life Data For Smooth Base Metal Specimens of SA 106-B Steel Tested in 288°C PWR Environments at Three Frequencies

Specimen	Frequency	Net Section Stress Amplitude (MPa)	Net Section Stress Amplitude (ksi)	Notch Strain Amplitude	Pseudostress Amplitude (MPa)	Pseudostress Amplitude (ksi)	Cycles To Failure
ZP11-148	1.0	410.9	59.6	0.0031	517	75.0	8820
ZP11-112	1.0	486.1	70.5	0.0063	1041	151.0	1320
ZP11-73	1.0	495.7	71.9	0.0064	1067	154.7	1360
ZP11-107	1.0	401.3	58.2	0.0031	513	74.4	12,500
ZP11-150	1.0	316.5	45.9	0.0020	323	46.8	85,885
ZP11-105	1.0	339.2	49.2	0.0021	349	50.6	34,320
ZP11-146	1.0	497.8	72.2	0.0044	1209	175.2	975
ZP11-119	1.0	319.9	46.4	0.0020	325	47.2	46,700
ZP11-118	1.0	526.1	76.3	0.0080	1324	192.0	730
ZP11-122	0.1	501.2	72.7	0.0067	1105	160.3	1225
ZP11-129	0.1	505.4	73.3	0.0069	1134	164.5	1185
ZP11-134	0.1	424.7	61.6	0.0032	521	75.6	10,575
ZP11-139	0.1	419.9	60.9	0.0034	556	80.6	26,130
ZP11-116	0.1	419.9	60.9	0.0034	563	81.6	27,275
ZP11-140	0.017	502.6	72.9	0.0055	908	131.7	1595
ZP11-149	0.017	433.0	62.8	0.0028	455	66.0	13,055
ZP11-106	0.017	405.4	58.8	0.0028	463	67.2	24,920
ZP11-103	0.017	527.4	76.5	0.0071	1175	170.4	1220

Table 14 Cyclic Frequency Sensitivity Study. Fatigue Life Data for Notched (K_t = 6, K_f = 1.98) Base Metal Specimens of SA 106-B Steel Tested in 288°C PWR Environments at Three Frequencies

Specimen	Frequency	Net Section Stress Amplitude (MPa)	(ksi)	Notch Strain Amplitude	Pseudostress Amplitude (MPa)	(ksi)	Cycles To Failure
K6-15	1.0	515.7	74.8	0.0122	2023	293.4	515
K6-22	1.0	532.3	77.2	0.0130	2144	310.9	495
K6-34	1.0	281.3	40.8	0.0042	687	99.7	12,955
K6-47	1.0	308.2	44.7	0.0049	803	116.5	13,670
K6-55	1.0	277.9	40.3	0.0041	674	97.7	14,895
K6-12	1.0	530.2	76.9	0.0129	2128	308.7	475
K6-23	0.1	529.5	76.8	0.0128	2123	307.9	345
K6-24	0.1	533.0	77.3	0.0130	2148	311.6	1160
K6-7	0.1	514.3	74.6	0.0122	2013	291.9	725
K6-8	0.1	532.3	77.2	0.0130	2144	310.9	845
K6-21	0.1	280.6	40.7	0.0041	685	99.3	11,165
K6-53	0.1	288.2	41.8	0.0043	716	103.9	8960
K6-20	0.1	276.5	40.1	0.0400	668	96.9	12,090
K6-58	0.017	273.7	39.7	0.0040	656	95.2	8760
K6-14	0.017	541.9	78.6	0.0134	2215	321.3	590
K6-25	0.017	548.8	79.6	0.0137	2268	328.9	440
K6-11	0.017	561.2	81.4	0.0143	2362	342.6	570
K6-41	0.017	273.0	39.6	0.0040	654	94.8	9990

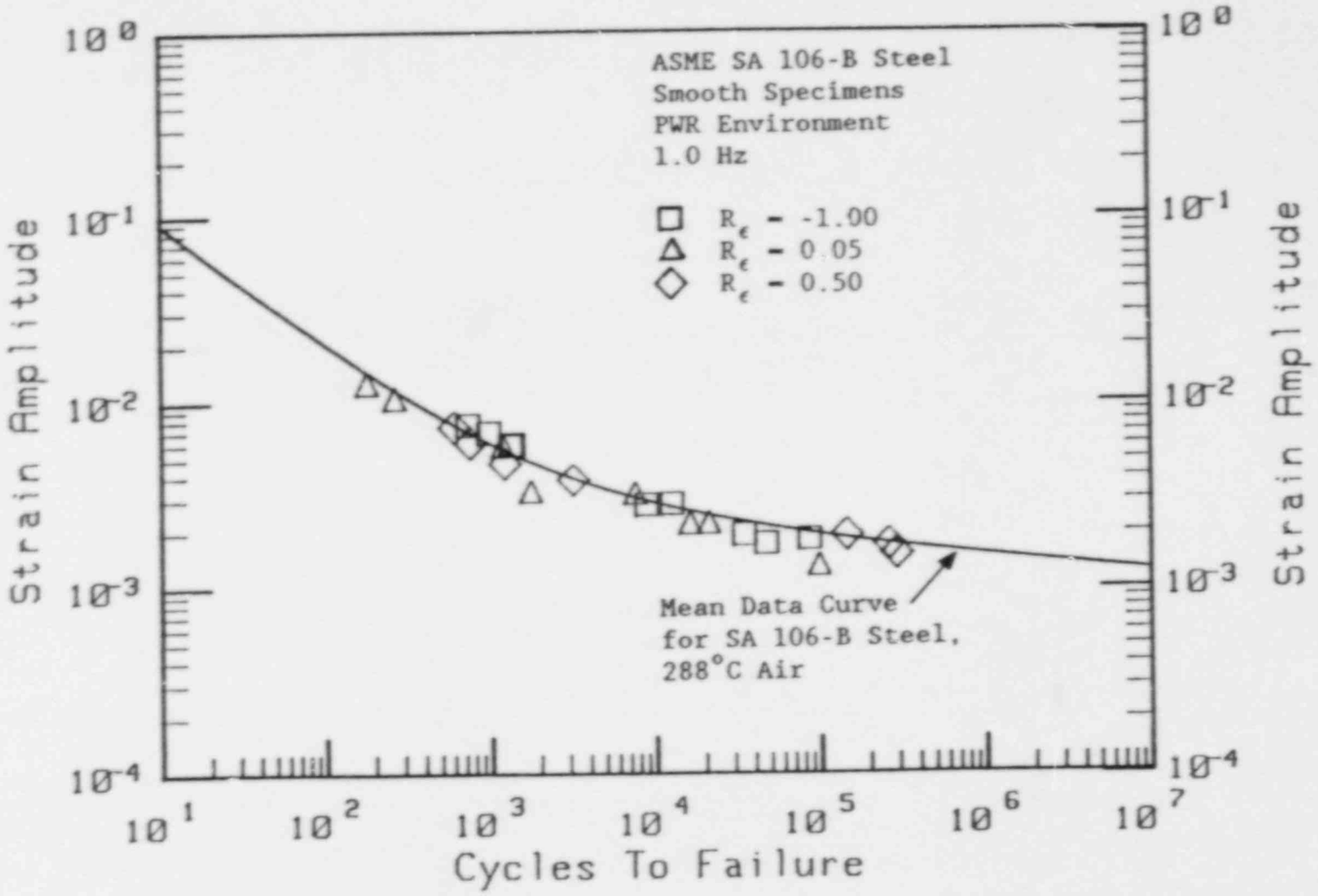

Fig. 30 Strain-life plot of SA 106-B steel smooth base metal specimens in 288°C PWR environments.

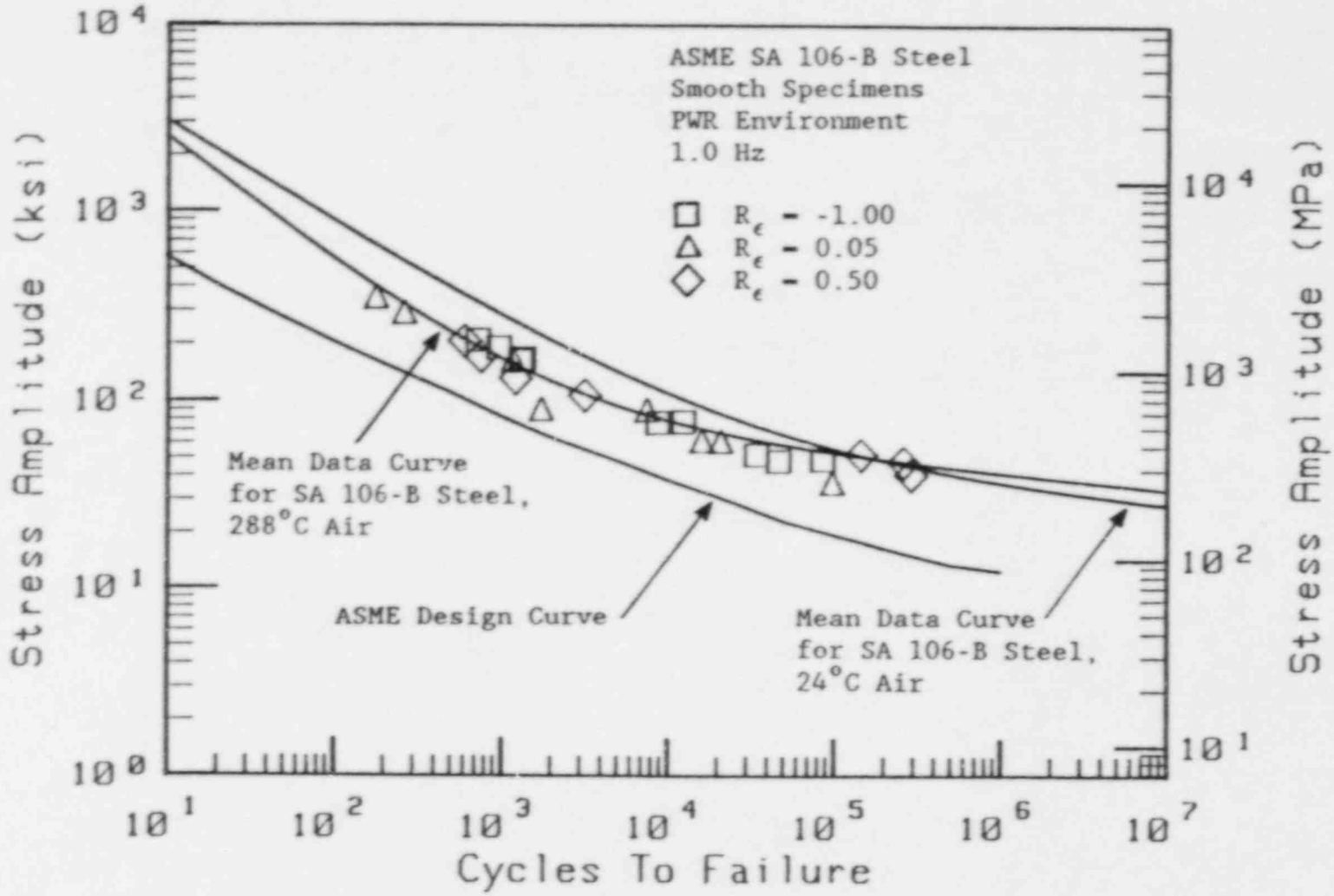

Fig. 31 Pseudostress-life plot of SA 106-B steel smooth base metal specimens in 288°C PWR environments.

Table 15 Fatigue Life Data For Smooth Base Metal Specimens of SA 106-B Steel Tested in 288°C PWR Environments at 1.0 Hz

Specimen	Strain Ratio	Net Section Stress Amplitude (MPa)	(ksi)	Strain Amplitude	Pseudostress Amplitude (MPa)	(ksi)	Cycles to Failure
ZP11-148	-1.00	411	59.6	0.0028	534	77.5	8,820
ZP11-112	-1.00	486	70.5	0.0059	1,126	163.3	1,320
ZP11-73	-1.00	496	71.9	0.0060	1,145	166.0	1,360
ZP11-107	-1.00	401	58.2	0.0028	534	77.5	12,500
ZP11-150	-1.00	316	45.9	0.0018	343	49.8	85,885
ZP11-105	-1.00	339	49.2	0.0019	362	52.6	34,320
ZP11-146	-1.00	498	72.2	0.0069	1,316	190.9	975
ZP11-119	-1.00	320	46.4	0.0017	324	47.0	46,700
ZP11-118	-1.00	526	76.3	0.0076	1,450	210.3	730
ZP11-102	0.05	418	60.6	0.0032	611	88.5	7,570
ZP11-132	0.05	379	54.9	0.0033	630	91.3	1,750
ZP11-143	0.05	390	56.6	0.0022	420	60.9	16,195
ZP11-128	0.05	485	70.3	0.0059	1,126	163.3	1,185
ZP11-108	0.05	236	34.2	0.0013	248	36.0	98,400
ZP11-147	0.05	566	82.1	0.0106	2,022	293.3	265
ZP11-141	0.05	320	46.4	0.0022	420	60.9	21,025
ZP11-136	0.05	561	81.3	0.0127	2,423	351.4	180
ZP11-110	0.50	505	73.2	0.0074	1,412	204.8	605
ZP11-127	0.50	485	70.4	0.0061	1,164	168.8	755
ZP11-124	0.50	445	64.5	0.0047	897	130.0	1,220
ZP11-123	0.50	429	62.2	0.0038	725	105.1	3,190
ZP11-120	0.50	276	40.1	0.0015	286	41.5	290,460
ZP11-114	0.50	339	49.2	0.0019	362	52.6	145,720
ZP11-142	0.50	324	47.0	0.0017	324	47.0	262,160

This effect appears to be primarily attributed more to the effects of temperature than to the PWR environment, at least within the scope of this work. What these results show, however, is that 1.0 ppb dissolved oxygen does not critically affect fatigue crack initiation in carbon piping steels as a result of test conditions within the current test matrix. It is not unlikely, however, that other adverse testing conditions, such as prolonged exposure and subsequent pitting, lower cyclic frequencies, mechanical underloads, water chemistry excursions, residual and mean stresses, or variations in material composition can result in more severe fatigue life degradation to carbon piping steels. Virtually all of these conditions have occurred in PWR reactor piping systems at one time or another.

Smooth weld metal specimens were tested under PWR conditions with R_ϵ values of 0.05, 0.50, and -1.00 (Figs. 32 and 33; Table 16 shows the PWR environment test results in tabular form). Again, the results show that SA 106-B weldments exhibit enhanced fatigue strength properties greater than that of base metal specimens, and that high temperature, low dissolved oxygen water exhibits a minimal effect on fatigue life behavior.

4.2.3 Notched Specimen Tests

Notched specimens having a K_t factor of either 3 or 6 were tested in PWR environments at a frequency of 0.017 Hz and R_ϵ ratios of 0.05, 0.5, and -1.00 (Figs. 34 thru 36). Table 17 shows PWR environment test data in tabular form. The results are expressed in terms of net section stress amplitude, notch strain amplitude, and pseudostress amplitude, respectively. The margin of safety offered by the factors of 2 and 20 are almost completely used up, even though Neuber's rule estimations of notch stress amplitude (and hence, pseudostress amplitude) are inherently conservative. A reduction in cycles to failure resulted for notched specimens of SA 106-B steel tested in high temperature, low dissolved oxygen environments, probably as a result of accelerated crack growth rates. This is consistent with the argument presented earlier, which suggests that since: (1) notched specimens can undergo crack initiation almost immediately after cycling, and (2) PWR environments have been shown to accelerate crack growth of precracked specimens, it logically follows that notched S-N specimens would exhibit shorter lives to failure than comparable unnotched S-N specimens. The plot of net section stress amplitude vs. cycles to failure more dramatically expresses the degradation due to the environment when compared to the other plots of notch strain amplitude or pseudostress amplitude vs. cycles to failure, since Neuber's rule tends to be conservative in estimating notch base stress and strains.

The degree of notch acuity does not appear to affect the degree of degradation which may result from the environment.

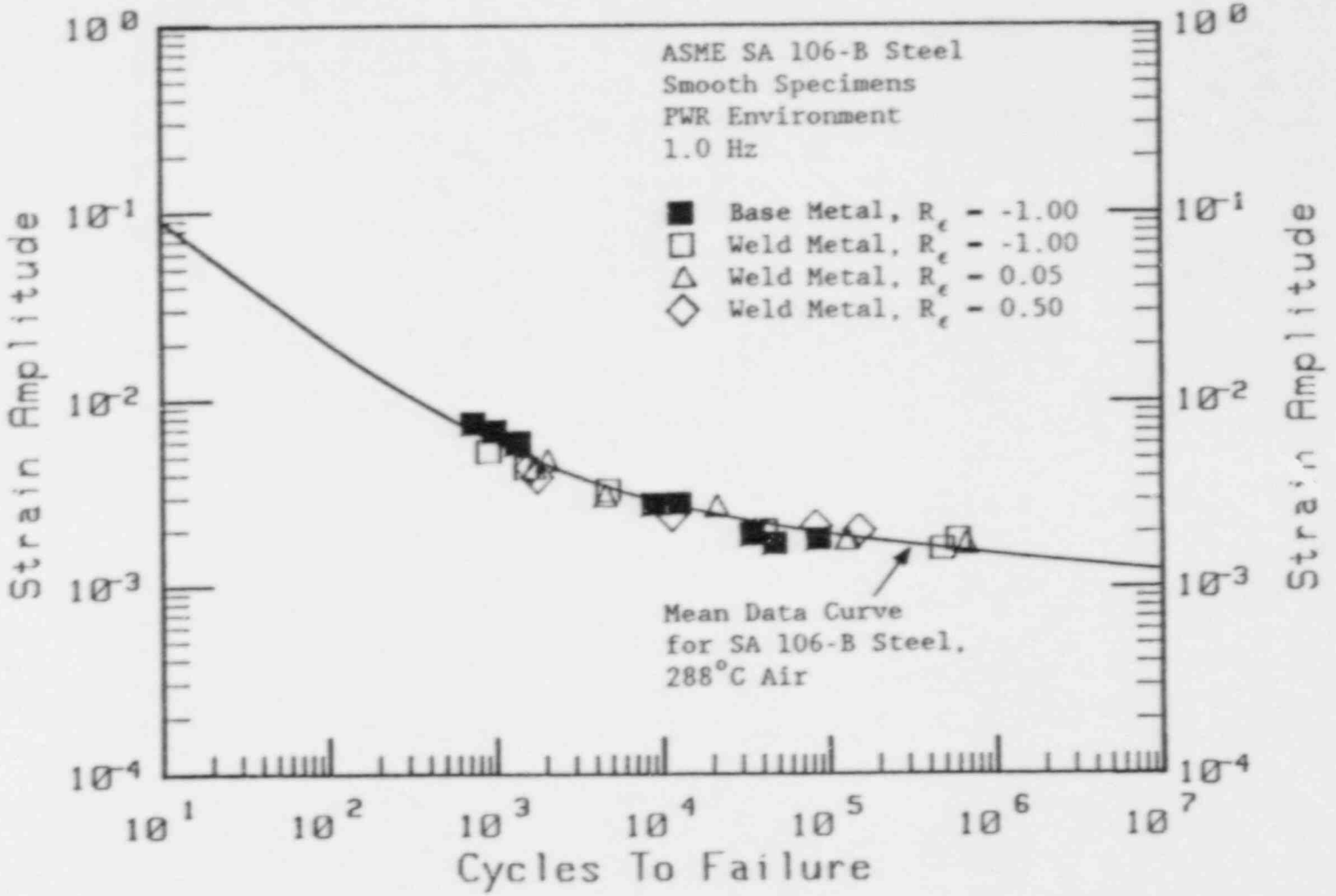

Fig. 32 Strain-life plot of SA 106-B steel smooth weld metal specimens in 288°C PWR environments.

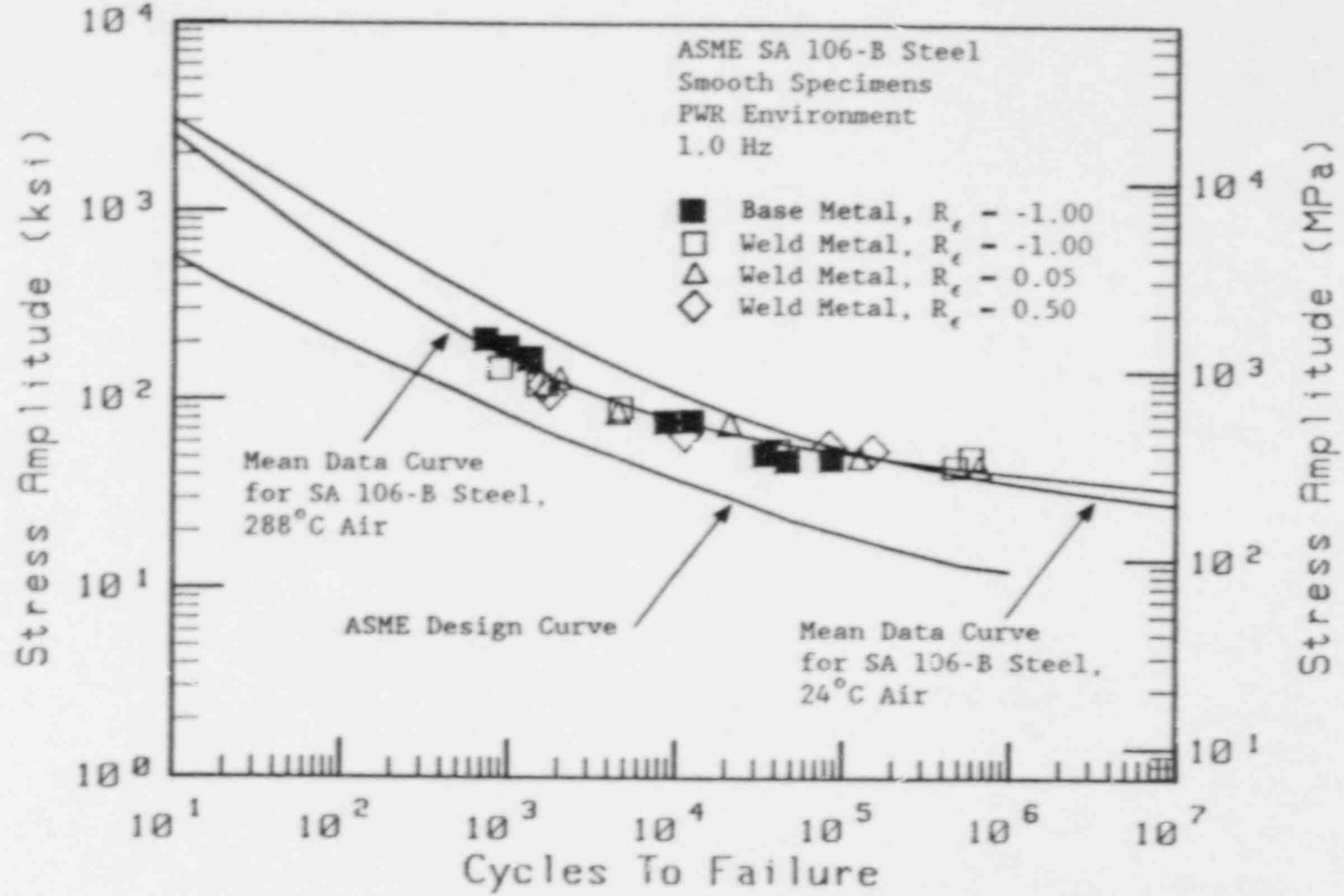

Fig. 33 Pseudostress-life plot of SA 106-B steel smooth weld metal specimens in 288°C PWR environments.

Table 16 Fatigue Life Data For Smooth Weld Metal Specimens of SA 106-B Steel Tested in 288°C PWR Environments at 1.0 Hz

Specimen	Strain Ratio	Net Section Stress Amplitude (MPa)	(ksi)	Strain Amplitude	Pseudostress Amplitude (MPa)	(ksi)	Cycles to Failure
11W-93	-1.00	307	49.5	0.0016	305	44.3	473,790
11W-72	-1.00	344	49.8	0.0018	343	49.8	592,460
11W-87	-1.00	376	54.5	0.0020	382	55.3	41,290
11W-79	-1.00	549	79.6	0.0044	839	121.7	1,530
11W-33	-1.00	547	79.4	0.0054	1,030	149.4	905
11W-85	-1.00	494	71.7	0.0033	630	91.3	4,740
11W-70	0.05	340	49.3	0.0018	343	49.8	128,760
11W-67	0.05	519	75.2	0.0044	839	121.7	1705
11W-92	0.05	466	67.6	0.0031	591	85.8	4,595
11W-78	0.05	375	54.4	0.0027	515	74.7	21,340
11W-82	0.05	545	79.0	0.0048	916	132.8	2,050
11W-74	0.05	310	44.9	0.0017	324	47.0	663,470
11W-73	0.50	500	72.5	0.0044	839	121.7	1,610
11W-86	0.50	497	72.1	0.0039	744	107.9	1,775
11W-64	0.50	415	60.2	0.0024	458	66.4	11,490
11W-63	0.50	374	54.3	0.0021	401	58.1	84,240
11W-88	0.50	360	52.2	0.0020	382	55.3	153,000

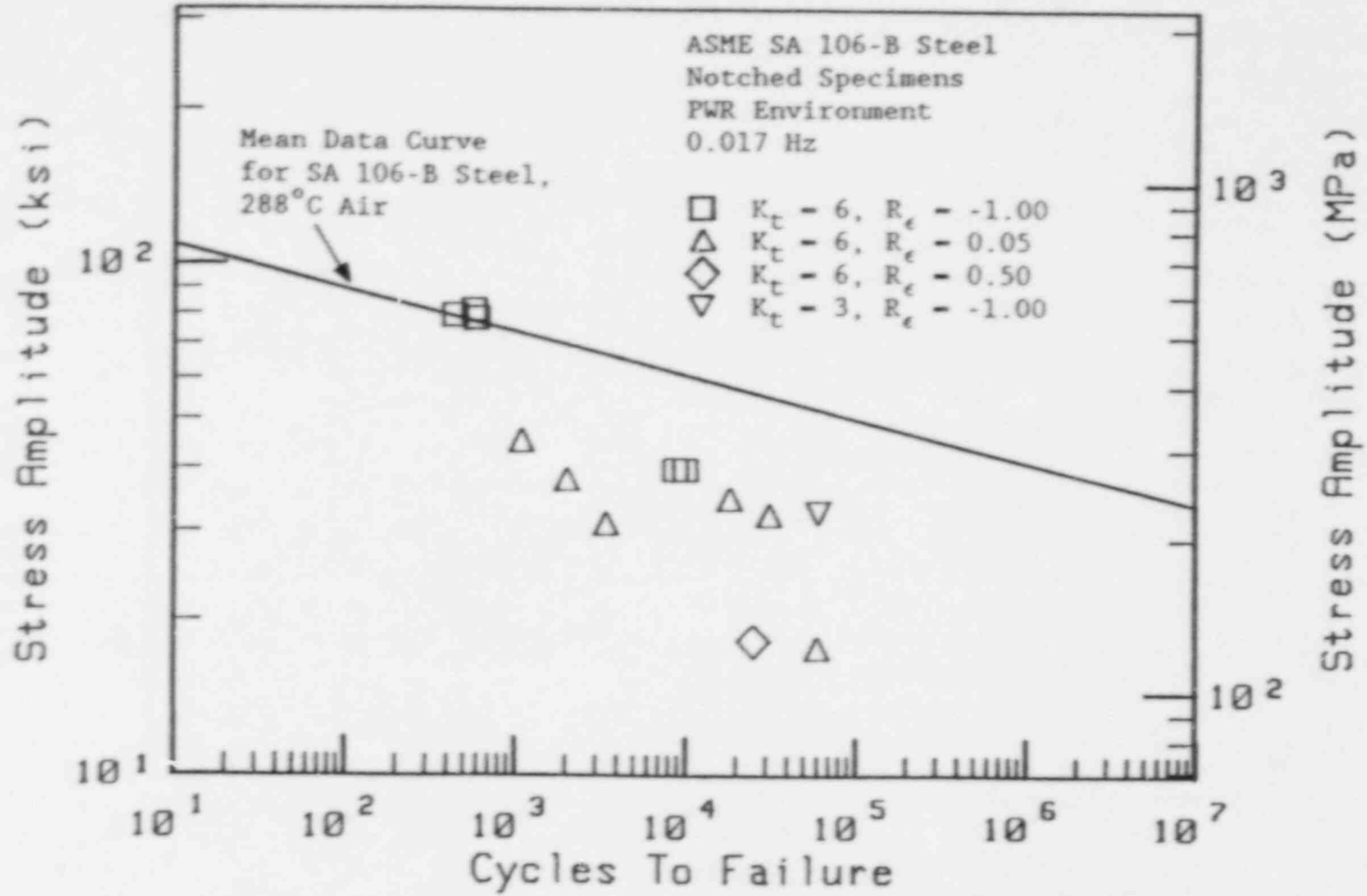

Fig. 34 Net section stress-life plot of SA 106-B steel notched (K_t = 2, 3, and 6) base metal specimens in 288°C PWR environments.

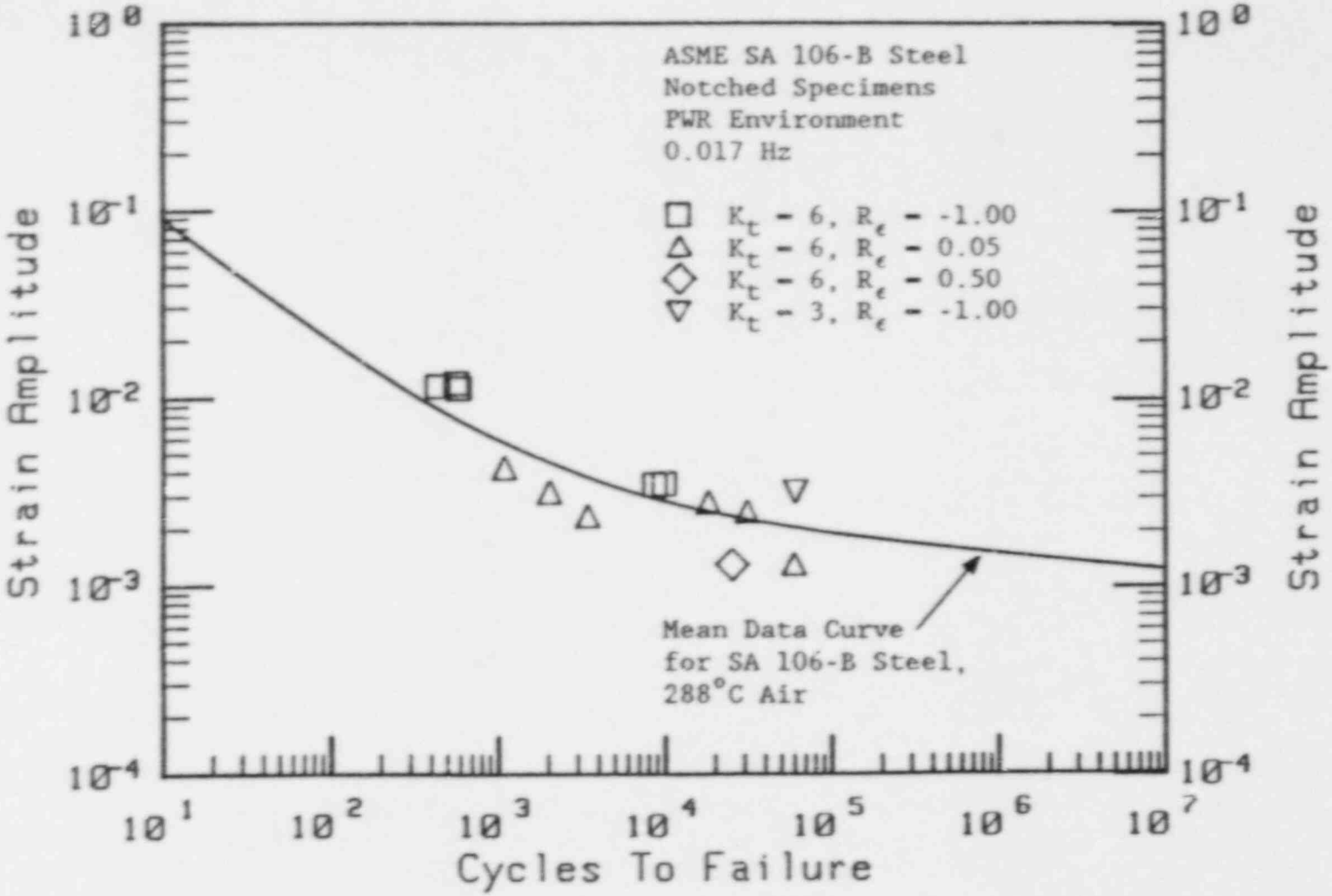

Fig. 35 Strain-life plot of SA 106-B steel notched (K_t = 2, 3, and 6) base metal specimens in 288°C PWR environments.

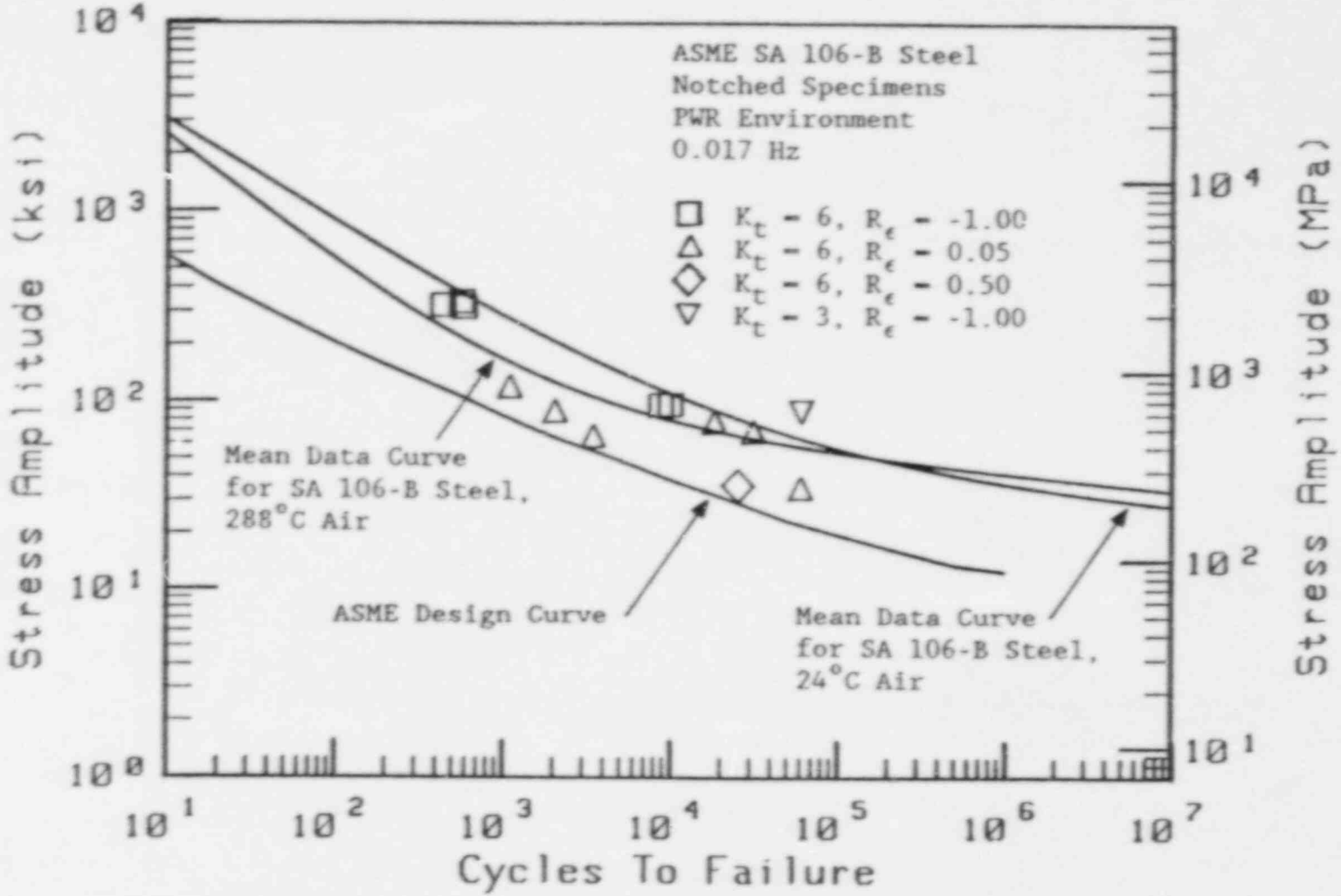

Fig. 36 Pseudostress-life plot of SA 106-B steel notched (K_t = 2, 3, and 6) base metal specimens in 288°C PWR environments.

Table 17 Fatigue Life Data For Notched Base Metal Specimens of SA 106-B Steel Tested in 288°C PWR Environments at 0.017 Hz

Specimen	K_t	Strain Ratio	Net Section Stress Amplitude (MPa)	(ksi)	Strain Amplitude	Pseudostress Amplitude (MPa)	(ksi)	Cycles to Failure
K6-58	6.0	-1.00	274	39.7	0.0035	668	96.8	8,760
K6-14	6.0	-1.00	542	78.6	0.0114	2,175	315.4	590
K6-25	6.0	-1.00	549	79.6	0.0117	2,232	323.8	440
K6-11	6.0	-1.00	561	81.4	0.0121	2,308	334.8	570
K6-41	6.0	-1.00	273	39.6	0.0035	668	96.8	9,990
K6-42	6.0	0.05	214	31.0	0.0024	458	66.4	3,455
K6-36	6.0	0.05	222	32.2	0.0025	477	69.2	31,290
K6-61	6.0	0.05	261	37.9	0.0032	611	88.5	2,040
K6-39	6.0	0.05	312	45.3	0.0043	820	119.0	1,100
K6-36	6.0	0.05	239	34.7	0.0028	534	77.5	18,350
K6-50	6.0	0.05	121	17.6	0.0013	248	36.0	60,125
K6-59	6.0	0.50	125	18.2	0.0013	248	36.0	25,390
K3-11	3.0	-1.00	225	32.7	0.0032	611	88.5	60,680

4.3 Fractography

Scanning electron fractographs of fracture surfaces formed by fatigue crack growth were taken of smooth specimens tested in air at 24°C and 288°C, and of smooth and sharply-notched specimens tested in 288°C PWR environments. In all specimens, crack growth was oriented normal to the axial direction in the pipe from which they were machined.

Figure 37 was obtained from a specimen tested in 24°C air, and cracking tended to be transgranular in nature. Figure 38 was obtained from a specimen tested in 288°C air. Again, cracking tended to be transgranular. Some evidence of environmentally-assisted fatigue can be observed on fracture surfaces of base metal notched specimens tested at 0.017 Hz in 288°C PWR environments (Figs. 39 and 40), and on the fracture surfaces of base metal smooth specimens tested at 1.0 Hz (Fig. 41). Figures 39 and 40 show areas of transgranular fracture over slip planes. Dissolved manganese sulfide inclusions left behind a series of cavities which can be observed in Figs. 39 and 40. A tendency for more faceted, or planar, fracture was observed in specimens tested in PWR environments. Figure 41 shows a transgranular surface from a smooth specimen tested at 1.0 Hz which did not form along slip planes as prominently as in the notched specimens tested at 0.017 Hz. However, striations can be observed in some areas, indicating environmentally-assisted cracking. Widespread brittle fracture was not observed in any of these specimens, possibly because the manganese sulfide inclusions are oriented parallel to the axis of the pipe, which is perpendicular to the plane of the advancing fatigue crack. Therefore, the crack grows in a direction which is most resistant to fatigue crack growth.

Fractography of weld metal specimens tested at 1.0 Hz in PWR environments is shown in Figure 42. This figure shows a tendency for fatigue fracture which alternated between transgranular and intergranular cleavage within the fine-grained weld metal. This observation suggests that segregation of an impurity element, such as sulfur, occurred at the grain boundaries and promoted intergranular separation within the weld metal. Other weld metal specimens experienced crack initiation at the surface with the crack propagating through the base metal adjacent to the heat-affected zone, and resembled the fracture surfaces found associated with base metal specimens.

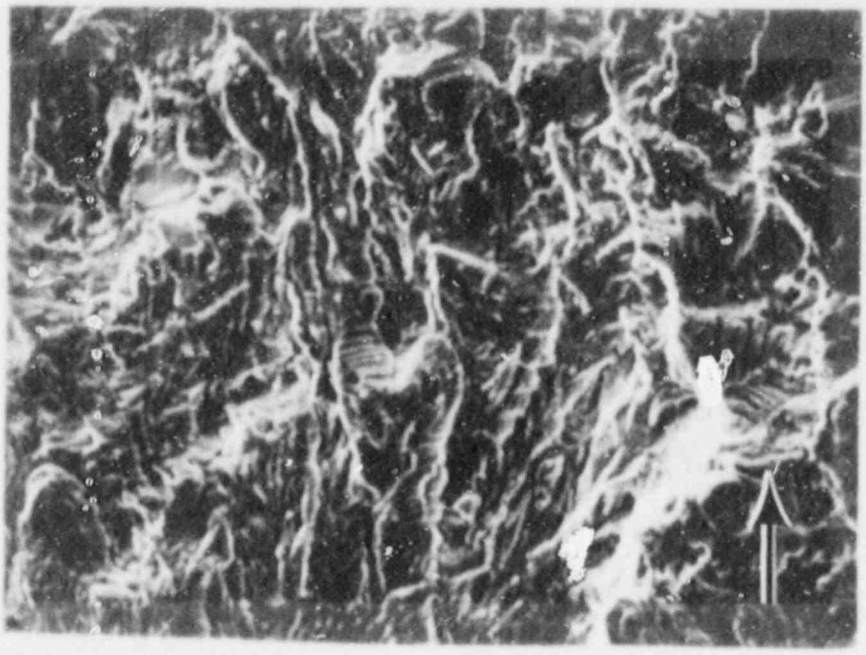

Fig. 37 Fractograph of base metal smooth specimen ZP11-10, which failed after 824,190 cycles tested in 24°C air. The arrow shows the direction of crack growth. 700x.

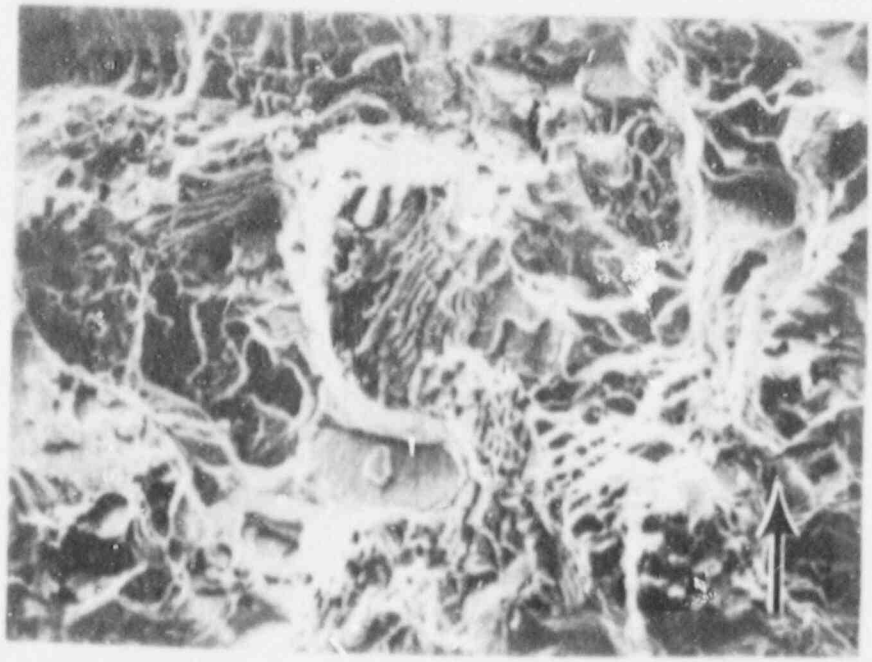

Fig. 38 Fractograph of base metal smooth specimen ZP11-9, which failed after 308,800 cycles tested in 288°C air. The arrow shows the direction of crack growth. 700x.

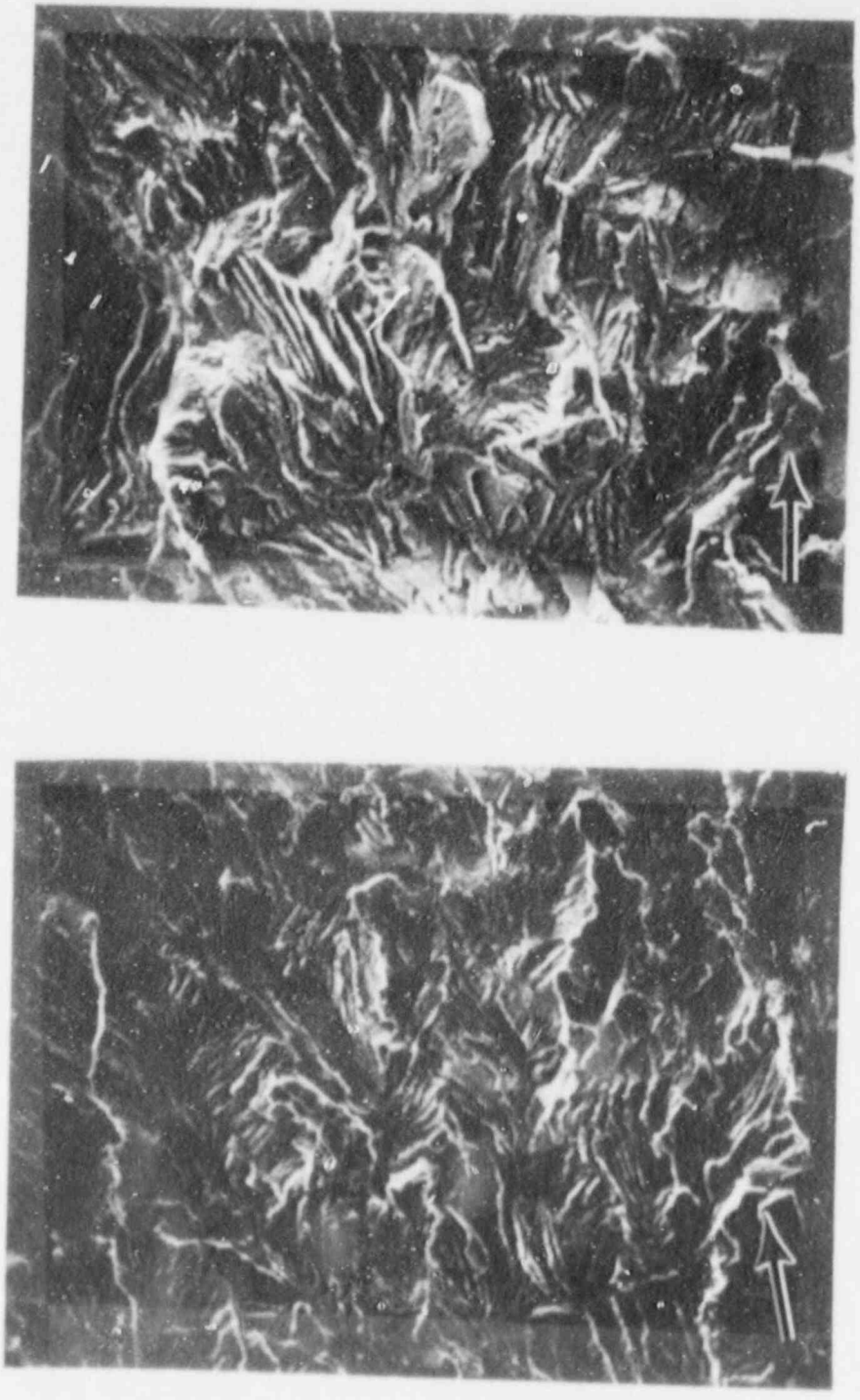

Fig. 39 Fractographs of base metal notched specimen K6-36, which failed after 31,290 cycles tested in a 288°C PWR environment at a frequency of 0.017 Hz. Cracking is predominantly by means of transgranular cleavage along slip planes. The arrow shows the direction of crack growth. 500x.

Fig. 40 Fractographs of base metal notched specimen K6-50, which failed after 60,125 cycles tested in a 288°C PWR environment at a frequency of 0.017 Hz. Cracking is predominantly by means of transgranular cleavage. The arrow shows the direction of crack growth. 500x.

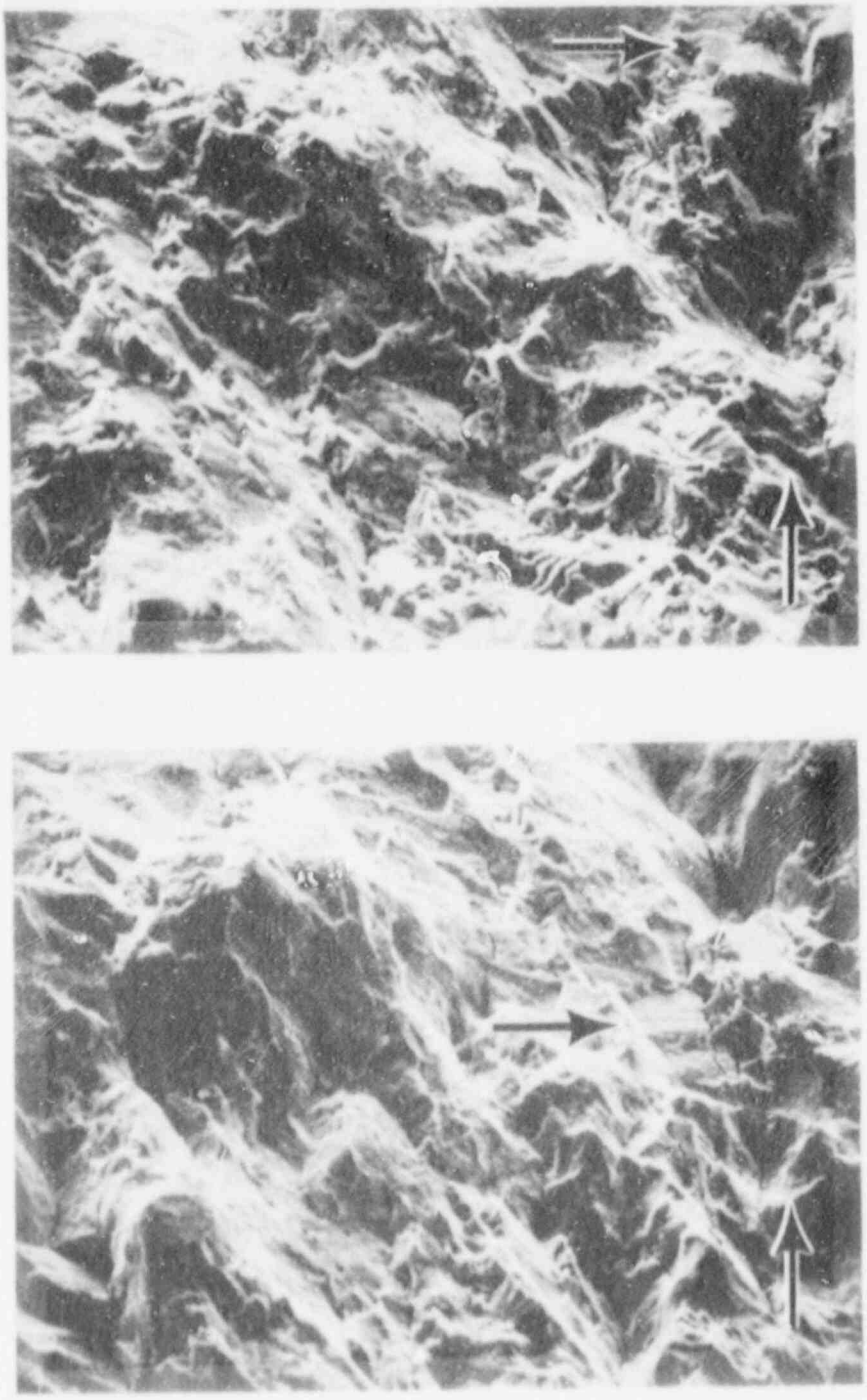

Fig. 41 Fractographs of base metal smooth specimen ZP11-142, which failed after 262,160 cycles tested in a 288°C PWR environment at a frequency of 1.0 Hz. Some striations characteristic of environmentally-assisted cracking can be observed, and are denoted by the horizontal arrows. The the vertical arrow shows the direction of crack growth. 500x.

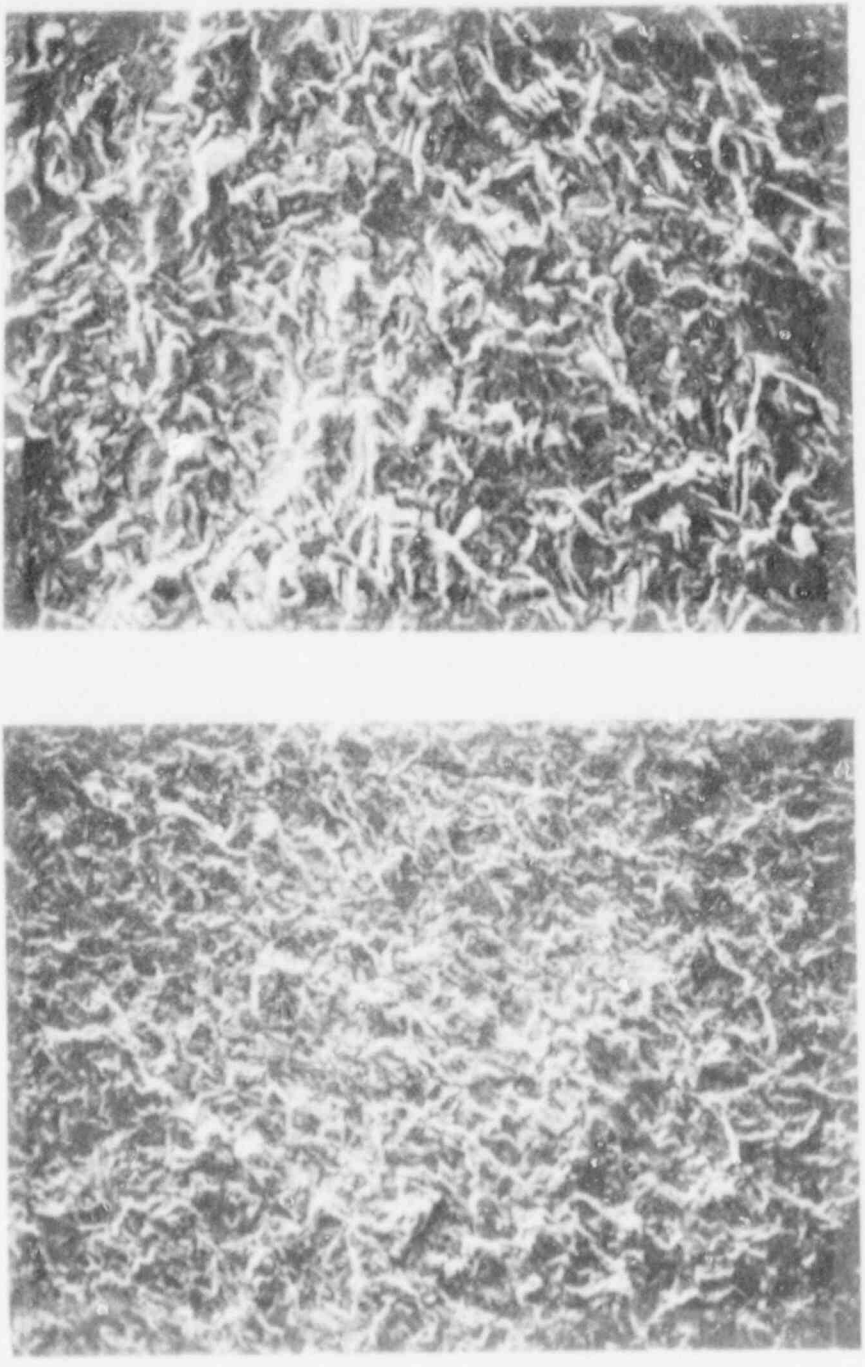

Fig. 42 Fractographs of weld metal smooth specimen 11W-93, which failed after 473,790 cycles tested in a 288°C PWR environment at a frequency of 1.0 Hz. Fracture surface details are indicative of the fine-grained weld metal microstructure. 500x.

5. RELEVANCE TO ASME SECTION III

The results of this investigation include the creation of the first known data base of fatigue life data for SA 106-B piping steel small specimens in simulated PWR environments. The data suggest that the ASME Section III design curve for carbon and low alloy steels having an ultimate strength not greater than 551.6 MPa (80 ksi) is not based on a mean data curve which accurately reflects the material's response to temperature within the temperature range for which the curve is assumed to be valid, and does not accurately reflect the aggressive nature of aqueous PWR environments on fatigue behavior. Fatigue life tests of notched SA 106-B specimens are degraded by PWR conditions to such a degree that the margin of safety offered by the design curve is almost completely used up, albeit not to the degree caused by BWR environments. Nevertheless, it should be clear to vendors and regulatory bodies associated with the nuclear power generation industry that Section III should be revised before plant life extension activities are carried through.

Re-certification of pressure-retaining components for operation beyond their original 40 year design lives will require that utilities must recalculate, with greater precision, the stress analysis of pressure vessel and piping components, and new fatigue usage factors, based on a revised Section III methodology which properly takes into account all of the known variables which degrade fatigue life. However, the ASME Subcommittee on Fatigue Strength has not decided upon the optimum approach by which to account for environmental effects within the framework of Section III. One approach which addresses the degradation of pressure-retaining components involves the incorporation of a set of revised design rules which would require a set of correction factors which account for variables such as environment, mean stress, local notch yielding, etc. Such an approach would allow designers to "tailor" their analyses, based on the specific conditions which a component may encounter. However, such an approach would allow for unintentional ommission of variables, or may not allow for unforseen transient conditions which may unknowingly increase cumulative usage. Another approach dictates that all variables known to affect fatigue life be built into the design curve itself. Such an approach is inherently more conservative, and analysis would be more straight-forward since fewer correction factors would be involved. However, such conservatism is almost always more expensive because of inherent shorter design lives and higher materials costs.

Regardless of the approach which will eventually be chosen, both PWR and BWR environment fatigue life data bases are not large and comprehensive enough to proceed with Section III revisions. These data bases must be enlarged to account for additional reactor-typical critical variables, such as high cycle fatigue, material variability, fabrication-related material changes, notch effects, prestrains, and residual stresses. Equally as important is experimental repeatability, which in itself helps to establish validity of observed trends in material behavior in aggressive environments.

6. CONCLUSIONS

This investigation characterized the cyclic stress-strain and fatigue life behavior of SA 106-B piping steel base and weld metal in 24°C and 288°C air environments and 288°C PWR environments containing 1.0 ppb dissolved oxygen. The variables which were investigated included: (1) stress (strain) amplitude, (2) temperature, (3) cyclic frequency, (4) notch acuity, and (5) strain ratio. The results of this experimental program have shown that the fatigue response of smooth and notched specimens is affected by conditions found associated with PWR environments, although to a lesser degree than that found with BWR environments. In addition to the conclusions found in Ref. 30 regarding the air environment test results, the following conclusions can be drawn regarding the PWR environment test results:

1. Little or no cyclic frequency sensitivity of fatigue life was observed for smooth base metal specimens, whereas 0.017 Hz appeared to be the most detrimental frequency for notched specimens. This is consistent with the argument which suggests that since (a) notched specimens can undergo crack initiation almost immediately after cycling, and (b) PWR environments have been shown to accelerate crack growth of precracked specimens, then notched S-N specimens should exhibit shorter lives to failure than comparable unnotched S-N specimens.

2. Fatigue of notched base metal specimens in low dissolved oxygen 288°C PWR environments nearly used up the margins of safety incorporated into the ASME design curve for carbon steels, based on laboratory tests of smooth specimens in air, partly because the Neuber-generated values of notch strain used in this investigation were conservative. These results for notched specimen tests are consistent with the argument in (1) above. Fatigue of smooth base and weld metal specimens showed virtually no effect of the PWR environment, which implies that crack initiation is not significantly affected by 1.0 ppb dissolved oxygen within the range of variables in this work.

3. Fatigue life of specimens tested in the low cycle regime do not appear to be affected by strain ratios of 0.05 and 0.50 since the mean stress approaches a value which is small in comparison to the stress amplitude. Similar tests in the high cycle regime show a trend toward lower fatigue life for strain ratios of 0.05 and 0.50 since mean stress is a more significant proportion of the stress amplitude.

4. The data suggest that the ASME Section III methodology, which takes into account PWR environment variables which degrade the fatigue life of pressure-retaining components, should be revised. Before this takes place, however, Code writers must decide which approach should be used in order

to better address plant life extension issues without compromising public safety. These approaches include: (a) the correction factor approach, and (b) the design curve modification approach.

5. PWR and BWR environment fatigue life data bases are not large and comprehensive enough to proceed with Section III revisions. Expansion of both data bases under a variety of reactor-typical conditions must be enlarged to account for additional critical variables, such as prolonged exposure, high cycle fatigue, ultra-low frequency cycling, material variability, fabrication-related material changes, notch effects, prestrains, and residual stresses.

REFERENCES

1. ASME Boiler and Pressure Vessel Code, Nuclear Power Plant Components, Section III, Division 1, Subsection NB, Class 1 Components, American Society of Mechanical Engineers, New York, issued annually.

2. W. H. Tuppeny, Jr., "Criteria for Pressure Vessel Design in the U.S.A., Design Criteria of Boilers and Pressure Vessels, American Society of Mechanical Engineers, New York, 1970, pp. 37-52.

3. L. F. Coffin, Jr. and J. F. Tavernelli, "The Cyclic Straining and Fatigue of Metals," Trans. Met Soc., Trans. ASME, Vol. 215, 1959, pp. 794-807.

4. B. F. Langer, "Design Values for Thermal Stress in Ductile Materials," Welding Institute Research Supplement, Vol. 37, Sept. 1958, pp. 411s-417s.

5. B. F. Langer, "Design of Pressure Vessels for Low Cycle Fatigue," Journal of Basic Engineering, Vol. 84(3), Sept. 1962, pp. 389-402.

6. L. F. Kooistra and M. M. Lemcoe, "Low Cycle Fatigue Research on Full-Size Pressure Vessels," Welding Research Journal Supplement, July 1962, p. 297s.

7. L. F. Kooistra, E. A. Lange, and A. G. Pickett, "Full Size Pressure Vessel Testing and Its Application and Design," Journal of Engineering for Power, Trans. ASME, Vol. 86, 1964, pp. 419-428.

8. "BWR Environmental Cracking Margins for Carbon Steel Piping", D. Weinstein, P. I., General Electric Company, Electric Power Research Institute Report EPRI NP-2406, May 1982.

9. J. B. Terrell, "Effect of Cyclic Frequency on the Fatigue Life of ASME SA 106-B Piping Steel in PWR Environments," submitted to Journal of Materials Engineering.

10. "Residual Life Assessment of Major Light Water Reactor Components (Draft)," V. N. Shah and P. E. MacDonald, Eds., Idaho National Engineering Laboratory, USNRC Report NUREG/CR-4731, Aug. 1986.

11. T. A. Prater and L. F. Coffin, "The Use of Notched Compact-Type Specimens for Crack Initiation Design Rules in High-Temperature Water Environments," Corrosion Fatigue: Mechanics, Metallurgy, Electrochemistry, and Engineering, ASTM STP 801, T. W. Crooker and B. N. Leis, Eds., American Society for Testing and Materials, Philadelphia, PA, 1983, pp. 423-444.

12. T. A. Prater and L. F. Coffin, "Notch Fatigue Crack Initiation in High Temperature Water Environments: Experiments and Life Prediction," Journal of Pressure Vessel Technology, Trans. ASME, Vol. 109, Feb. 1987, pp. 124-134.

13. K. Iida, H. Kobayashi, and M. Higuchi, "Predictive Method of Low Cycle Fatigue Life of Carbon and Low Alloy Steels in High Temperature Water Environments," Proceedings of the Second International Atomic Energy Agency Specialists' Meeting on Subcritical Crack Growth, W. H. Cullen, Ed., USNRC Conference Proceeding NUREG/CP-0067, Vol. 2, Apr. 1986, pp. 385-409.

14. W. J. Shack, T. F. Kassner, P. S. Maiya, J. Y. Park, W. Ruther, T. Kusay, E. F. Rybicki, and R. B. Stonesifer, "BWR Pipe Crack Remedies Evaluation," Fifteenth Water Reactor Safety Information Meeting, USNRC Report NUREG/CP-0091, Vol. 2, 1988, pp. 381-405.

15. M. P. B. Allery and G. Birbeck, "Effect Of Notch Root Radius on the Initiation and Propagation of Fatigue Cracks," Engineering Fracture Mechanics, Vol. 4, 1972, pp. 325-331.

16. R. G. Forman, "Study of Fatigue Crack Initiation from Flaws Using Fracture Mechanics Theory," Engineering Fracture Mechanics, Vol. 4, 1972, pp. 333-345.

17. A. Baus, H. P. Lieurade, G. Sanz, and M. Truchon, "Correlation Between the Fatigue-Crack Initiation at the Root of a Notch and Low-Cycle Fatigue Data," Flaw Growth and Fracture, ASTM STP 631, American Society for Testing and Materials, Philadelphia, PA, 1977, pp. 96-111.

18. N. E. Dowling, "Notched Member Fatigue Life Predictions Combining Crack Initiation and Propagation," Fatigue of Engineering Materials and Structures, Vol. 2, 1979, pp. 129-138.

19. P. S. Maiya, "Effects of Notches on Crack Initiation in Low Cycle Fatigue," Materials Science and Engineering, Vol. 38, 1979, pp. 289-294.

20. K. Saanouni and C. Bathias, "Study of Fatigue Crack Initiation in the Vicinity of Notches," Engineering Fracture Mechanics, Vol. 16(5), 1982, pp. 695-706.

21. D. F. Socie, N. E. Dowling, and P. Kurath, "Fatigue Life Estimation of Notched Members," Fracture Mechanics: Fifteenth Symposiun, ASTM STP 833, American Society for Testing and Materials, Philadelphia, PA, 1984, pp. 284-299.

22. P. Kurath, ?. Kahn and D. F. Socie, "Fatigue Life Estimates for a Notched Member in a Corrosive Environment," Journal of Pressure Vessel Technology, Trans. ASME, Vol 109, Feb. 1987, pp. 135-141.

23. W. A. Van Der Sluys and R. Emanuelson, "Overview of Data Trends in Cyclic Crack Growth Results in LWR Environments," Proceedings of the Second International Atomic Energy Agency Specialists' Meeting on Subcritical Crack Growth, W. H. Cullen, Ed., USNRC Conference Proceeding NUREG/CP-0067, Vol. I, Apr. 1986, pp. 199-218.

24. W. H. Cullen, "Fatigue Crack Growth Rates in Pressure Vessel and Piping Steels in LWR Environments," USNRC Report NUREG/CR-4724, Mar. 1987.

25. "Standard Recommended Practice For Constant-Amplitude Low-Cycle Fatigue Testing," Designation E 606-80, Annual Book of ASTM Standards, Metals - - Mechanical Testing, Vol. 03.01, revised annually, American Society for Testing and Materials, Philadelphia, PA, 1985, pp. 681-698.

26. R. E. Peterson, Stress Concentration Factors, John Wiley and Sons, New York, 1974.

27. W. H. Cullen, et al., "Fatigue Crack Growth of A 508 Steel in High-Temperature, Pressurized Reactor Grade Water," USNRC Report NUREG/CR-0969, 1979.

28. D. R. Ireland, W. L. Server, and R. A. Wullert, "Procedures for Testing and Data Analysis, Task A - Topical Report," Effects Technology, Inc., ETI Technical Report 75-43, Oct. 1975, pp. 5-46.

29. N. E. Dowling, "Crack Growth During Low-Cycle Fatigue of Smooth Axial Specimens," Cyclic Stress-Strain and Plastic Deformation Aspects of Fatigue Crack Growth, ASTM STP 637, American Society for Testing and Materials, Philadelphia, PA, 1977, pp. 97-121.

30. J. B. Terrell, "Fatigue Life Characterization of Smooth and Notched Piping Steel Specimens in 288°C Air Environments," USNRC Report NUREG/CR-5013, May 1988.

31. R. M. Wetzel, "Smooth Specimen Simulation of Fatigue Behavior of Notches," Journal of Materials, JMLSA, Vol. 3(2), Sept. 1968, pp. 646-657.

32. T. H. Topper, R. M. Wetzel, and J. Morrow, "Neuber's Rule Applied to Fatigue of Notched Specimens," Journal of Materials, JMLSA, Vol. 4(1), Mar. 1969, pp. 200-209.

33. T. H. Topper, B. I. Sandor, and J. Morrow, "Cumulative Damage Under Cyclic Strain Control," Journal of Materials, JMLSA, Vol. 4(1), Mar. 1969, pp. 189-199.

34. D. F. Socie, "Fatigue-life Prediction Using Local Stress-Strain Concepts," Experimental Mechanics, Vol. 17(2), Feb. 1977, pp. 50-56.

35. A. Baus, H. P. Lieurade, G. Sanz, and M. Truchon, "Correlation Between the Fatigue-Crack Initiation at the Root of a Notch and Low Cycle Fatigue Data," Flaw Growth and Fracture, ASTM STP 631, American Society for Testing and Materials, Philadelphia, PA, 1977, pp. 96-111.

36. P. S. Maiya, "Effects of Notches on Crack Initiation in Low Cycle Fatigue," Materials Science and Engineering, Vol. 38, 1979, pp. 289-294.

37. K. Saanouni and C. Bathias, "Study of Fatigue Crack Initiation in the Vicinity of Notches," Engineering Fracture Mechanics, Vol. 16(5), 1982, pp. 695-706.

38. B. N. Leis, C. V. B. Gowda, and T. H. Topper, "Cyclic Inelastic Deformation and the Fatigue Notch Factor," Cyclic Stress-Strain Behavior - Analysis, Experimentation, and Failure Predictions, ASTM STP 519, American Society for Testing and Materials, Philadelphia, PA, 1973, pp. 133-150.

39. P. M. Yuzawich and C. W. Hughes, "An Improved Technique for Removal of Oxide Scale From Fractured Surfaces of Ferrous Materials," Practical Metallography, Vol. 15, 1978 pp. 184-195.

40. L. F. Coffin, "The Effect of Quench Aging and Cyclic-Strain Aging on Low Carbon Steel," Journal of Basic Engineering, Trans. ASME, Vol. 87, Jun. 1965, pp. 351-362.

41. D. V. Wilson and J. K. Tromans, "Effects of Strain Ageing on Fatigue Damage in Low-Carbon Steel," Acta Metallurgica, Vol. 18, Nov. 1970, pp. 1197-1208.

42. D. V. Wilson, "Precipitation and Growth of Carbide Particles in a Cyclically Strained Low Carbon Steel," Acta Metallurgica, Vol. 21, May 1973, pp. 673-682.

43. D. V. Wilson, "Effects of Microstructure and Strain Ageing on Fatigue Crack Initiation in Steel," Metal Science, Vol. 11, Aug./Sep. 1977, pp. 321-331.

44. D. V. Wilson and B. Mintz, "Effects of Microstructural Instability on the Fatigue Behavior of Quenched and Quench-Aged Steels," Acta Metallurgica, Vol. 20, Jul. 1972, pp. 985-995.

45. C. C. Li and W. C. Leslie, "Effects of Dynamic Strain Aging on the Subsequent Mechanical Properties of Carbon Steels," Metallurgical Transactions A, ASM-AIME, Vol. 9A, Dec. 1978, pp. 1765-1775.

46. N E. Dowling, W. R. Brose, and W. K. Wilson, "Notched Member Fatigue Life Predictions by the Local Strain Approach," Fatigue Under Complex Loading - Analysis and Experiments, Society of Automotive Engineers, 1977, pp. 57-84.

47. H. O. Fuchs and R. I. Stephens, Metal Fatigue in Engineering, Wiley-Interscience, New York, 1980, p. 159.

48. W. K. Wilson, "Elastic-Plastic Analysis of Blunt Notched CT Specimens and Applications," Journal of Pressure Vessel Technology, Vol. 96(4), Nov. 1974, pp. 544-550.

NRC FORM 335 (11-81)

U.S. NUCLEAR REGULATORY COMMISSION

BIBLIOGRAPHIC DATA SHEET

1. REPORT NUMBER (Assigned by DDC)
NUREG/CR-5136
MEA-2289

4. TITLE AND SUBTITLE (Add Volume No., if appropriate)
FATIGUE STRENGH OF SMOOTH AND NOTCHED SPECIMENS OF ASME SA 106-B STEEL IN PWR ENVIRONMENTS

2. (Leave blank)

3. RECIPIENT'S ACCESSION NO.

7. AUTHOR(S)
J. B. Terrell

5. DATE REPORT COMPLETED
MONTH: August | YEAR: 1988

9. PERFORMING ORGANIZATION NAME AND MAILING ADDRESS (Include Zip Code)
MATERIALS ENGINEERING ASSOCIATES, INC.
9700-B MARTIN LUTHER KING, JR HIGHWAY
LANHAM, MARYLAND 20706-1837

DATE REPORT ISSUED
MONTH: September | YEAR: 1988

6. (Leave blank)

8. (Leave blank)

12. SPONSORING ORGANIZATION NAME AND MAILING ADDRESS (Include Zip Code)
DIVISION OF ENGINEERING
OFFICE OF NUCLEAR REGULATORY RESEARCH
U.S. NUCLEAR REGULATORY COMMISSION
WASHINGTON, D.C. 20555

10. PROJECT/TASK/WORK UNIT NO.

11. FIN NO.
B8900

13. TYPE OF REPORT
Technical Report

PERIOD COVERED (Inclusive dates)

15. SUPPLEMENTARY NOTES

14. (Leave blank)

16. ABSTRACT (200 words or less)

Fatigue strain-life tests were conducted on ASME SA 106-B piping steel base metal and weld metal specimens in 288°C (550°F) pressurized water reactor (PWR) environments as a function of strain amplitude, strain ratio, notch acuity, and cyclic frequency. Notched base metal specimens tested at 0.017 Hz in 1.0 part per billion (ppb) dissolved oxygen environments nearly completely used up the margins of safety of 2 on stress and 20 on cycles incorporated into the ASME Section III design curve for carbon steels. Tests conducted with specimens having theoretical notch concentration (K_t) values ranging from 2 to 6 showed virtually no effect of notch acuity on fatigue life. Tests conducted with smooth base and weld metal specimens at 1.0 Hz showed virtually no degradation in cycles to failure when compared to 288°C air test results. In all cases, however, the effect of temperature alone reduces the margin of safety offered by the design curve in the low cycle regime for the test specimens. Comparison between the fatigue life results of smooth and notched specimens suggests that fatigue crack initiation is not significantly affected by 1.0 ppb dissolved oxygen, and that most of the observed degradation may be attributed to crack growth acceleration. These results suggest that the ASME Section III methodology should be revised to account for PWR environment variables which degrade fatigue life of pressure-retaining components.

17. KEY WORDS AND DOCUMENT ANALYSIS

17a. DESCRIPTORS

Fatigue
Stress-life
Piping steels
SA 106-B steel
Welds
PWR environment
Dissolved oxygen
Neuber's rule
ASME Code Section III
Plant life extension

17b. IDENTIFIERS/OPEN-ENDED TERMS

18. AVAILABILITY STATEMENT
Unlimited

19. SECURITY CLASS (This report)
Unclassified

21. NO OF PAGES

20. SECURITY CLASS (This page)
Unclassified

22. PRICE
$